Using Machine Learning to Understand the Hydrologic Impacts of Permafrost Thaw-Driven Land Cover Change

by

Shaghayegh Akbarpour

A thesis
presented to the University of Waterloo
in fulfillment of the
thesis requirement for the degree of
Doctor of Philosophy
in
Civil Engineering (Water)

Waterloo, Ontario, Canada, 2023

Examining Committee Membership

The following served on the Examining Committee for this thesis. The decision of the Examining Committee is by majority vote.

External Examiner:	Gregory J. McDermid Professor Department of Geography University of Calgary
Supervisor(s):	James R. Craig Associate Professor Dept. of Civil and Environmental Engineering University of Waterloo
Internal Member:	John Quilty Assistant Professor Dept. of Civil and Environmental Engineering University of Waterloo
Internal Member:	Nandita Basu Professor Dept. of Civil and Environmental Engineering University of Waterloo

Internal-External Member: Derek T. Robinson
Associate Professor
Dept. of Geography and Environmental Management
University of Waterloo

Internal-External Member: William L. Quinton
Professor
Dept. of Geography and Environmental Studies
University of Laurier

Author's Declaration

This thesis consists of material all of which I authored or co-authored: see Statement of Contributions included in the thesis. This is a true copy of the thesis, including any required final revisions, as accepted by my examiners.

I understand that my thesis may be made electronically available to the public.

Statement of contribution

Shaghayegh Akbarpour was the sole author of Chapter 1 and 2, and 6 which were written under the supervision of Dr. James R. Craig. Chapters 3, Chapters 4 and 5 were written with the intent to publish. Exceptions to sole authorship of material are as follows:

- **Research presented in 3:** Chapter 3 of this thesis contains an unpublished paper submitted to the International Journal of Applied Earth Observation and Geoinformation [3], where Shaghayegh Akbarpour designed and developed a python-based model for land cover classification, tested the algorithm on 10 study sites in the Northwest Territories (NWT), and wrote the manuscript. Dr. Craig provided input during model development, introduced an innovative method for categorizing wetlands of discontinuous permafrost zones of the NWT based on their geometrical differences, and provided guidance during manuscript editing. Dr. Chasmer provided further guidance during the editing process.

  Citation:

  Shaghayegh Akbarpour, Laura Chasmer, and James R. Craig."Hydrological classification of isolated wetlands in discontinuous permafrost regions using RGB imagery." Under review in the International Journal of Applied Earth Observation and Geoinformation.

- **Research presented in 4:** This work was published in Remote Sensing Applications: Society and Environment (2022) [4]. In this study, Shaghayegh Akbarpour investigated the performance of machine learning-based algorithms for modeling land cover change. She developed a land cover change model using R and conducted data analysis while contributing to the manuscript preparation. Dr. Craig provided valuable contributions to the project by offering guidance on mathematical formulations, reviewing and revising the manuscript, and suggesting ideas such as devising the data generative model.

  Citation:

  Shaghayegh Akbarpour, and James R. Craig."Simulating thaw-induced land cover change in discontinuous permafrost landscapes." Remote Sensing Applications: Society and Environment 28 (2022): 100829.

- **Research presented in 5:** Chapter 5 of this thesis will be converted into a manuscript. The hydrological model was developed by Mahkameh Taheri, with collaborative input from Shaghayegh Akbarpour on the model's design, and under the

supervision of Dr. Craig. Mahkameh Taheri also developed the Upscaled Wetland Fill-and-Spill (UWFS) algorithm used in the hydrological modeling process [120]. Additionally, both Mahkameh Taheri and Shaghayegh Akbarpour contributed to the generation of climate data. Shaghayegh Akbarpour provided support by generating historical land cover change data [3] and future climate-related data for the coupling framework [4], and by modeling the land cover evolution for future climate scenarios. Dr. Craig provided guidance and supervision throughout the project, including the development of the Time Series Land Cover Change model (TSLCM), the Taiga Wetland Identification Neural Network (TWINN) solution, and the UWFS algorithm.

Abstract

Discontinuous permafrost regions are experiencing a change in land cover distribution as a result of permafrost thaw. In wetlands interspersed with discontinuous permafrost, climate change is particularly problematic because temperature increases can result in significant permafrost thaw, thaw-driven landscape changes, and resultant changes in watershed hydrologic responses.

The influence of land cover change on the short- and long-term hydrological responses of wetland-peatland complexes is poorly understood. A better understanding of the impacts of climate-related land cover evolution on the hydrology of wetland-covered watersheds requires information about the distribution of hydrologically important lands, their pattern, and the rate at which they change over time. Here, we first developed a machine learning-based land cover evolution model (TSLCM) to estimate the long-term evolution of dominant land covers for application to the discontinuous permafrost regions of Northern Canada. This model is applied to replicate historical land cover and estimate future land cover scenarios at the Scotty Creek Research Basin in the Northwest Territories, Canada.

A significant challenge when analyzing land cover change effects on hydrological properties is generating time-dependent classified maps of the region of interest, and the challenges associated with preprocessing remotely sensed data for discriminating between wetlands and forest-covered regions. In this work, we focus on two important objectives supporting the improved classification of wetlands in discontinuous permafrost regions: the exclusive use of only RGB imagery, and the use of an image segmentation method to accelerate the automatic classification of land cover. A semantic segmentation neural network, a multilayer perceptron (MLP), and watershed function algorithms are applied to develop the taiga wetland identification neural network (TWINN) for the hydrological classification of wetlands. TWINN is here demonstrated to accurately classify high-resolution imagery of discontinuous permafrost regions within the Northwest Territories into the water, forest, and wetlands, and also able to delineate the runoff area of wetlands.

To study the effect of land cover evolution on runoff generation in the Scotty Creek basin, the products of TWINN and TSLCM are used to inform a process-based hydrological model where land cover change is represented explicitly. According to simulation results, land cover transitions can modify annual mean streamflow by as much as 7%, in addition to influences due to changing precipitation regimes alone.

Acknowledgements

Completing this Ph.D. thesis has been a journey filled with challenges and opportunities for growth, and I am beyond grateful for the support and encouragement of so many incredible people along the way.

I would like to begin by expressing my heartfelt thanks to my supervisor, Dr. James Craig, for keeping me on track when my research was going off the rails, for his impeccable guidance, and for always having my back through thick and thin in my academic path.

I also want to thank my thesis committee members, Professor Nandita Basu, Dr. John Quilty, Dr. Derek T. Robinson, and Professor Gregory J. McDermid, for their time, effort, and invaluable feedbacks.

I am also indebted to Professor William L. Quinton and the Scotty Creek research group for their remarkable contributions, insights, and feedback during the past four years.

I would also like to express my gratitude to my hydrological research group for their friendships, support, and shared experiences, particularly Mahkameh Taheri, for being my co-conspirator and fellow sufferer in the world of Ph.D. woes.

Moving on to my family back in Iran, I owe my dad a huge thank you for his support and insistence that I pursue my graduate studies. His constant encouragement and guilt trips were instrumental in helping me finish this thesis. And my brother Komeil, who's been my very own cheerleader, always rooting for me even when I thought I couldn't do it. I'm so lucky to have you as my brother!

And of course, I couldn't have done any of this without my amazing mom. I'm forever grateful for everything she's done for me.

A big thanks to my partner, Hossein, for always being there (and also not being there, when I needed space). Your love, patience, and support have been my saving grace.

And finally, I want to give a massive shoutout to my fluffy and hungry forever buddy, Gil, for being the cutest stress-reliever with his endless cuddles and tail-wagging antics.

Dedication

To my mom.

To the voices silenced by discrimination.

To the extraordinarily courageous women of Iran.

To the strong indigenous women of the Northwest Territories.

To WOMEN, LIFE, FREEDOM

Table of Contents

List of Figures

List of Tables

List of Abbreviations

CNN Convolutional Neural Network 24–29, 31–33, 48, 50, 104

GCM Global Climate Model 87, 88, 90, 93, 100

MLR Multinomial Logistic Regression 7, 61–67, 69–73, 80, 81, 103

NWT Northwest Territories v, 2, 9, 10, 12, 14, 18, 19, 22, 27, 36, 38, 44, 46, 55, 77, 78, 80, 105, 106, 108

RCP Representative Concentration Pathway 87, 90, 92–94, 97, 99, 100

SCRS Scotty Creek Research Station 4, 11–13, 28, 29, 49, 53–55, 58, 62, 63, 72, 74, 103, 106

TSLCM Time Series Land Cover Change model vi, 5, 7, 53, 54, 56–58, 60, 63, 74, 75, 78, 80–82, 84, 85, 87–90, 92, 99–101, 103–106

TWINN Taiga Wetland Identification Neural Network vi, 5, 24, 25, 28–30, 34, 36–38, 41, 44, 46–50, 78, 84–86, 104–107

UWFS Upscaled Wetland Fill-and-Spill vi, 5, 7, 78, 81, 82, 84, 85, 88, 97, 99, 100, 104, 105

Chapter 1

Introduction

1.1 Introduction

Climate change has yielded numerous environmental changes in the northern hemisphere, especially in permafrost regions [117]. Rapid warming in permafrost regions is increasing the output of greenhouse gases [29] and leading to thaw-induced changes to regional hydrology [30]. Recent studies in the Arctic and subarctic regions reflect a growing awareness of changes in permafrost regions; these studies focus on vegetation, wildlife, hydrological changes in aquatic ecosystems, land use and land cover, and geophysical and geomorphological changes of the permafrost underlain regions [128].

In the Northwest Territories (NWT), Canada, and elsewhere, the outcome of permafrost degradation can be observed as land cover and hydrologic change in discontinuous permafrost regions. Lateral permafrost thaw in these discontinuous permafrost regions is influencing permafrost's distribution and extent, and intensifying the fragmentation rate of peat plateaus. The increased permafrost thaw affects the spatial distribution of three key land cover types (permafrost plateaus, bogs, and fens), and consequently, their hydrological responses [105]. Historical remote sensing products report a noticeable transformation of forest-covered land (permafrost plateaus) into wetland (fens and bogs) [105, 104]. This transformation is causing restrictions in hydrological interactions between groundwater and surface water, altering water storage, increasing summer streamflow, and changing the hydrological role of permafrost [105]. Connon et al. 2014 [30] illustrated that climate-related changes in hydraulic connectivity are increasing streamflow in the NWT due to degradation in the lateral extent of permafrost plateaus. Many local factors may influence vertical and lateral permafrost thaw, including thermal gradient, air temperature, incoming radiation, canopy cover, the lateral movement of groundwater, and the geometry of the thawing permafrost.

A variety of permafrost models are used in cryosphere science to assess the influence of permafrost evolution and the rate of vertical permafrost thaw. However, models for simulating lateral thaw are limited to complex 3D models [63, 101, 78]. These models are generally too computationally expensive to deploy at large scales. Other means are therefore needed in order to predict local rates of lateral permafrost loss and corresponding land cover change. Such predictions of land cover change can then be input into hydrologic models to determine the potential for hydrologic change at watershed scales. To date, there is no available predictive model for simulating this spatio-temporal land cover evolution and its corresponding hydrological impact in discontinuous permafrost zones characteristic of those found in the NWT. The absence of a predictive model for spatio-temporal land cover evolution and its corresponding hydrological impact may be due to a number of reasons, including the complexity of the process, the lack of reliable long-term historical remote

sensing data sets (particularly classified maps showing the distribution of hydrologically relevant land cover), and resource constraints. The challenging and time-consuming process of data processing is another concern when analyzing long-term changes in dominant land covers in discontinuous permafrost zones.

To analyze the long-term effects of land cover evolution on hydrological properties of a basin, track the pattern and pace of change, and reduce prediction uncertainties, a spatio-temporal land cover change model trained by historical observations of land cover evolution in discontinuous permafrost regions of the taiga plains is needed. There are many alternative methods available for addressing this need; recent improvements in machine learning, deep learning, and advanced computer vision techniques have shown a potential to solve contemporary problems in land cover classification, simulating long-term land cover evolution, and coupling hydrological models and land cover change models in other geographic locations [142, 126].

1.2 Aims and Objectives

Permafrost thaw drives the erosion of peat plateaus, leads to the merging of bogs and fens, influences the wetting-drying cycles of the ground, and changes the primary runoff characteristics of landscapes. The overarching goal of this research is to study these thaw-induced land cover change effects on the hydrological properties of systems comprised of permafrost plateaus, fens, and bogs such as those depicted in Figure 1.1. The research described herein addresses this goal by:

1. Developing an automatic method for the classification of wetlands and permafrost plateau from remote sensing products.
2. Developing, training, and testing a machine-learning-based land cover change model for simulating both long-term and short-term land cover evolution due to lateral permafrost thaw.
3. Creating a simple wetland runoff contributing area delineation method.
4. Coupling a hydrological model and land cover change model predictions to analyze the hydrological effects of land cover change and assess the magnitude of land cover change influence relative to the influence of changing meteorological forcing.

In this research, a general machine learning-based land cover change model and a deep learning-based automatic solution were developed to analyze the effects of remotely observable variables on spatial and temporal patterns of historical change in lowland discontinuous permafrost zones and generate long-term land cover change scenarios for further analysis. Challenges associated with developing a spatio-temporal land cover change model include extrapolating the time series change of land cover when the training data set is limited and the portability of model results to other regions. The temporal extrapolation and transferability issue can be tackled by implementing and testing machine learning and data generative methods. An additional concern regarding the application of the developed land cover change model is the time-consuming and complex input data preparation step, which can be addressed by developing an automated method for land cover classification. The final portion of this thesis is focused on using the output of the developed land cover change model as input to a hydrological model to illustrate the hydrological effects of land cover evolution in lowland discontinuous permafrost zones. Coupling hydrological models to land cover change models can help to quantify the contribution of land cover changes to the watershed properties such as flood potential, soil water availability, or groundwater recharge. Here, the land cover change model and the Raven [32] hydrological model were coupled in a data coupling framework, where the results of the land cover change model were used to inform the hydrological model. Specifically, the simulated land cover predicted by the land cover change model was used to delineate the primary and secondary contributing (bog contributing areas) areas by the devised runoff area delineation method in this research. Discretizing the primary and secondary contributing areas helps to understand how isolated bogs connect over time and how the conversion from isolated bogs to connected bogs alters the hydrological function of the landscape. The delineated primary and secondary runoff areas were employed as an input in the Raven hydrological framework [32] to simulate the likely future hydrological impacts of the landscape changes and investigate the effects of this parameter on the hydrological responses.

The explicit objectives of this research are to:

1. Iteratively develop and test a machine learning geospatial model that can estimate the conversion between the three primary land cover types at SCRS and in other similar discontinuous permafrost regions of the discontinuous permafrost zones in the taiga plains (Chapter 4).

2. Use historical remote sensing imagery products to evaluate long-term changes to the land cover characteristics of discontinuous permafrost zone's wetlands by incorporating deep learning-based algorithms (Chapter 3 and Chapter 4).

3. Simulate the likely future hydrological impacts of thaw-induced landscape changes based on the predicted land cover evolution from the machine learning-based model using a hydrological model (UWFS method) implemented in the Raven hydrological framework (Chapter 3, Chapter 4, and Chapter 5).

Figure 1.1 portrays the flowchart of this thesis.

1.3 Thesis structure

This thesis is organized as follows:

Chapter 2 examines the impacts of permafrost thaw on land cover and hydrological processes in discontinuous permafrost regions. It also discusses the use of machine learning and deep learning algorithms to detect thaw-induced changes and evaluates the dynamic feedback between land cover change models and hydrologic models for more accurate quantification of catchment ecosystems in permafrost regions. The overall goal of the chapter is to provide a comprehensive understanding of the complex interactions between permafrost thaw, land cover change, and hydrological processes in discontinuous permafrost regions.

Chapter 3 includes a paper submitted to the International Journal of Applied Earth Observation and Geoinformation [3], co-authored by myself, Dr. Laura Chasmer, and my supervisor, Dr. James R. Craig, with author efforts noted in the statement of contributions. In this paper, we applied a semantic segmentation-deep learning model and a Multi Layer Perceptron (MLP) method to develop the TWINN for the classification of isolated wetlands. In order to improve upon other methods used for identifying wetlands in discontinuous permafrost regions, we focused on two important objectives: using only RGB images and using a method of image segmentation to speed up the processing of data for the classification of wetlands and permafrost plateaus.

Chapter 4 corresponds to a paper published in Remote Sensing Applications: Society and Environment (2022) [4], co-authored by myself and my supervisor, Dr. James R. Craig. In this paper, we discussed the development of a machine learning-based model to estimate the evolution of the key hydrologically-important land cover types in discontinuous permafrost regions of the taiga plains. The model was derived, trained, and tested against historical observations of landscape change. Simulating land cover transitions and patterns using the TSLCM was demonstrated to be effective against historical observations. This study concluded that ensemble learning models are weak in forecasting time series changes

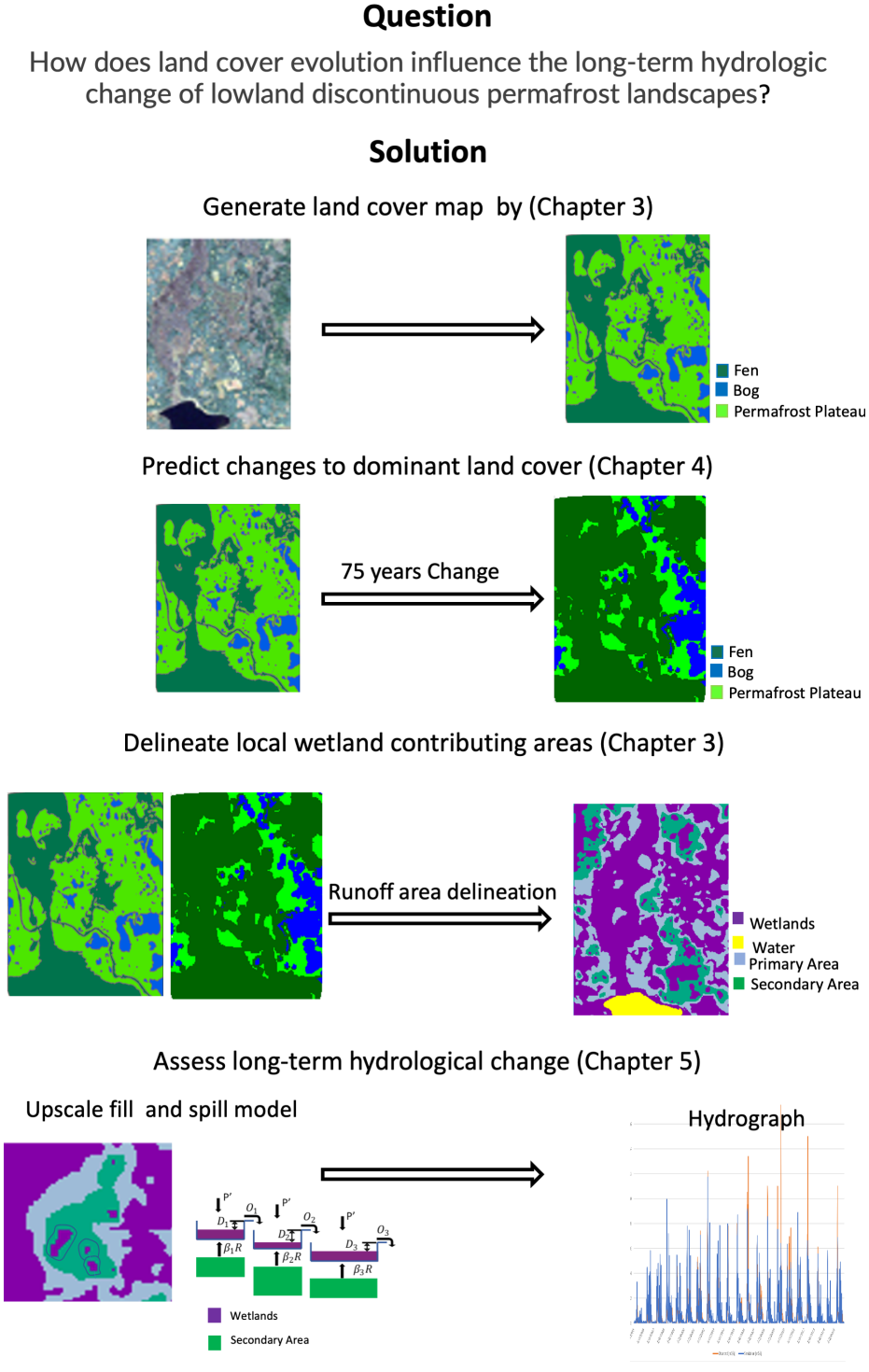

Figure 1.1: Flow chart representing the objectives of this thesis.

and capturing spatial-temporal correlations, but still produce better results than MLR methods in replicating historical land cover changes.

In Chapter 5, we examined the potential long-term impacts of thaw-driven land cover evolution on the hydrological response of the gauged Scotty Creek basin in the Northwest territories. To do this, we used reasonable estimates of future land cover generated by the TSLCM and a hydrological model which captures the key runoff characteristics of the landscape. We quantified the effects of land cover change on runoff from the basin by employing an UWFS method which can simulate the runoff response of hundreds to thousands of wetlands.

Chapter 6 summarizes the conclusions of the research conducted in this dissertation.

Chapter 2

Background and literature review

A discussion of discontinuous permafrost land covers is presented here in a way that emphasizes the land cover alterations and considers potential hydrological trends caused by thaw processes. The first two sections examine discontinuous permafrost land cover types and their interactions. The chapter also reviews studies that focus on the impacts of the permafrost thaw on the distribution of the dominant land covers especially wetlands, machine learning-based and deep learning algorithms for improving the accuracy of remote sensing products and the dynamic feedback between land cover change model and hydrologic models.

2.1 Land Cover: Permafrost

Permafrost refers to the ground that remains below 0 °C temperature for at least two consecutive years [133]. The surface layer of soil above permafrost, which freezes and thaws in a cycle, is referred to as the active layer, which may be underlain by perennially frozen or unfrozen ground. Each year, climate change brings noticeable seasonality to discontinuous permafrost regions, with distinctive changes in land cover and hydrological conditions occurring during each season [133].

Zhang et al. (1999) [139] reported that about 50% of the exposed land in the Northern Hemisphere is in a seasonal freezing-thawing state during winter. The seasonal freezing and thawing of permafrost have a strong impact on the hydrologic functions of the landscape, the land surface energy budget, and the biological processes involved [39].

2.2 Land Cover: Discontinuous Permafrost Lands

Permafrost zones occupy about 22% of the Northern Hemisphere [139]. The distribution pattern of permafrost in discontinuous permafrost regions is influenced by various factors, including topography, hydrology, as well as local surfaces and subsurface characteristics, such as vegetation cover and soil texture [39, 111].

Some areas in the NWT are characterized by permafrost-underlain peat plateaus, also known as permafrost plateaus, which are formed by the accumulation of dead plants [133]. The extent of the permafrost plateaus varies from tens of meters to kilometers; the surface of this type of land is dry, and their surroundings are typically waterlogged. Permafrost plateaus are elevated features; this type of land is known as a runoff generator in the representative discontinuous permafrost region of Scotty Creek [30, 106] (Figure 2.1). The

occurrence of wetlands in the discontinuous permafrost regions depends on the balance between gains and losses of water. Transport of water to the surrounding wetlands mostly occurs due to the contribution of snowmelt during freshet [79, 116], and the water is laterally transported from the permafrost plateaus through the zone of high saturated hydraulic conductivity above the permafrost [116]. Permafrost plateaus impound water in bogs and redirect flow to the fens, as the permafrost sits at a higher elevation than the surrounding terrain [47, 106].

Connon et al. (2014) [30] created a conceptual model whereby the generated runoff from permafrost plateaus can flow into channel fen (primary runoff), discharge into the channel fen through a series of connected or cascading bogs (secondary runoff) or flow into isolated bogs where the water will be stored [30]. Bogs and fens are two major types of wetlands existing in the NWT; In this research, their classification is based on their hydrological properties rather than their ecological functions (Figure 2.1). To delineate the runoff area of fens and bogs, the permafrost plateau area can be discretized into primary runoff and secondary runoff areas (Figure 2.1). The primary runoff area, which is the area where water is drained directly into channel fens, is depicted in dark gray in Figure 2.1. In contrast, the secondary runoff area, which contributes water to isolated bogs, is distinguished by a relatively lighter gray shade in the same figure (Figure 2.1).

Fens are formed as wide channels comprising the drainage network of basins, and bogs are presented as patches distributed in a discontinuous permafrost region [106]. Channel fens and bogs have contrasting hydrological functions; channel fens are water conveyors, and bogs are not typically able to convey water. The primary sources of water for bogs are rainfall and snowmelt, while fens obtain water both vertically and laterally from groundwater discharge [133].

Based on a thorough investigation of hydrometric data, Quinton et al. (2003) [106] concluded that there is a positive correlation between the basin's annual runoff and the fen coverage. In contrast, the negative correlation between bog and fen spatial coverage was reported as negative, which indicates that bogs play a major role in storing water. In some instances, bogs or a series of connected bogs can transfer water to channel fen (secondary runoff) and the basin outlet which occurs during periods of high moisture supply (i.e. in response to snow melting or large summer rain) [30].

2.3 Thaw-induced Changes to Land Cover

Numerous studies have reported a recent increase in the rate of lateral permafrost thaw, and climate warming is affecting the lateral exchange of water and energy between permafrost

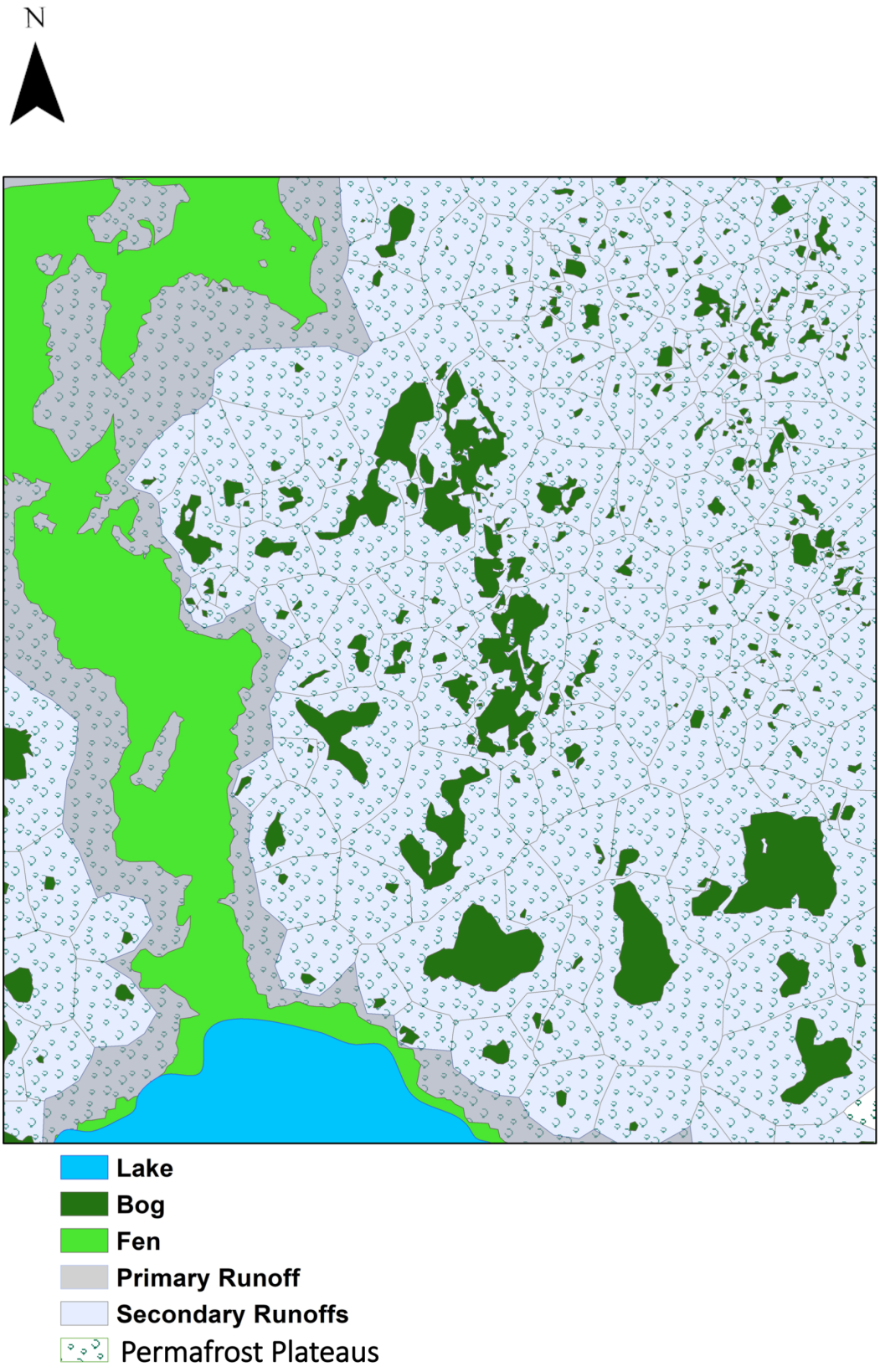

Figure 2.1: Classified map of the SCRS in 1947 representing fen, bog cascades, and their estimated contributing area.

plateaus, fens, and bogs [12, 27, 64, 67, 105].

The interdependence of thaw-induced land cover evolution and climate change, specifically temperature change, is now altering the distribution of permafrost plateaus, fens, and bogs in discontinuous permafrost regions of Northern Canada. Investigations into permafrost thaw reveal numerous impacts upon the environment and hydrology of the NWT, including an increase in baseflow [46], alteration of lake drainage [96], and drastic changes in the land cover. Changes in the energy balance trigger permafrost degradation in the NWT, thawing of peat-rich zones, and transformation of land cover.

Quinton et al. (2011) [105] identified a reduction in the area of regions covered by permafrost plateaus and an increase in the distribution of wetlands as a result of permafrost thaw in the SCRS (Figure 2.2). Figure 2.2 depicts the main land cover transitions over a 30-year period in the SCRS. The transitions were predominantly observed in areas closer to the thawing edge of permafrost plateaus; the gray color indicates an increase in the fen area or a transition from permafrost plateaus to fen. The blue color represents the transition of permafrost plateaus to bog due to permafrost thaw, while the red color depicts bogs that became hydraulically connected to and then transitioned to fen during the 30-year time step (called the "bog capture" phenomenon [30]).

Elimination of permafrost plateaus from between channel fen and a series of isolated bogs ("bog capture") increases the runoff contributing area, especially primary runoff contributing areas [30, 130]. The changes in the extent of the secondary runoff area were found to be controlled by the storage capacity of the bogs.

The evolution of permafrost plateaus, fens, and bogs caused by lateral permafrost thaw changes the local hydrological cycles. Connon et al. (2014) [30] concluded that transformation from plateaus to wetlands (flat bogs) caused by permafrost thaw has a direct effect on the generation of runoff and contributing area because of the increasing hydrological connectivity through the surface and subsurface pathways. Quinton et al. (2011) [105] analyzed the linkage between land-cover changes and river flow in the wetland-dominated discontinuous permafrost of the SCRS. A combination of remote sensing and field studies was utilized to understand the effects of horizontal heat flow on the land cover and basin runoff when the permafrost plateaus thaw. The result of the analysis discovered a 38% permafrost plateaus decline over 60 years. These remotely sensed observations were supported by field studies showing changes in surface saturation, loss of tree canopy, increase in the transfer of thermal energy to the ground, and more permafrost degradation. These changes also cause more drainage from the isolated bogs, allow hydrological connections among bogs, and form more channel fens. An analysis of the spatial distribution of vegetation at the SCRS, changes in their structural characteristics, and alterations in the

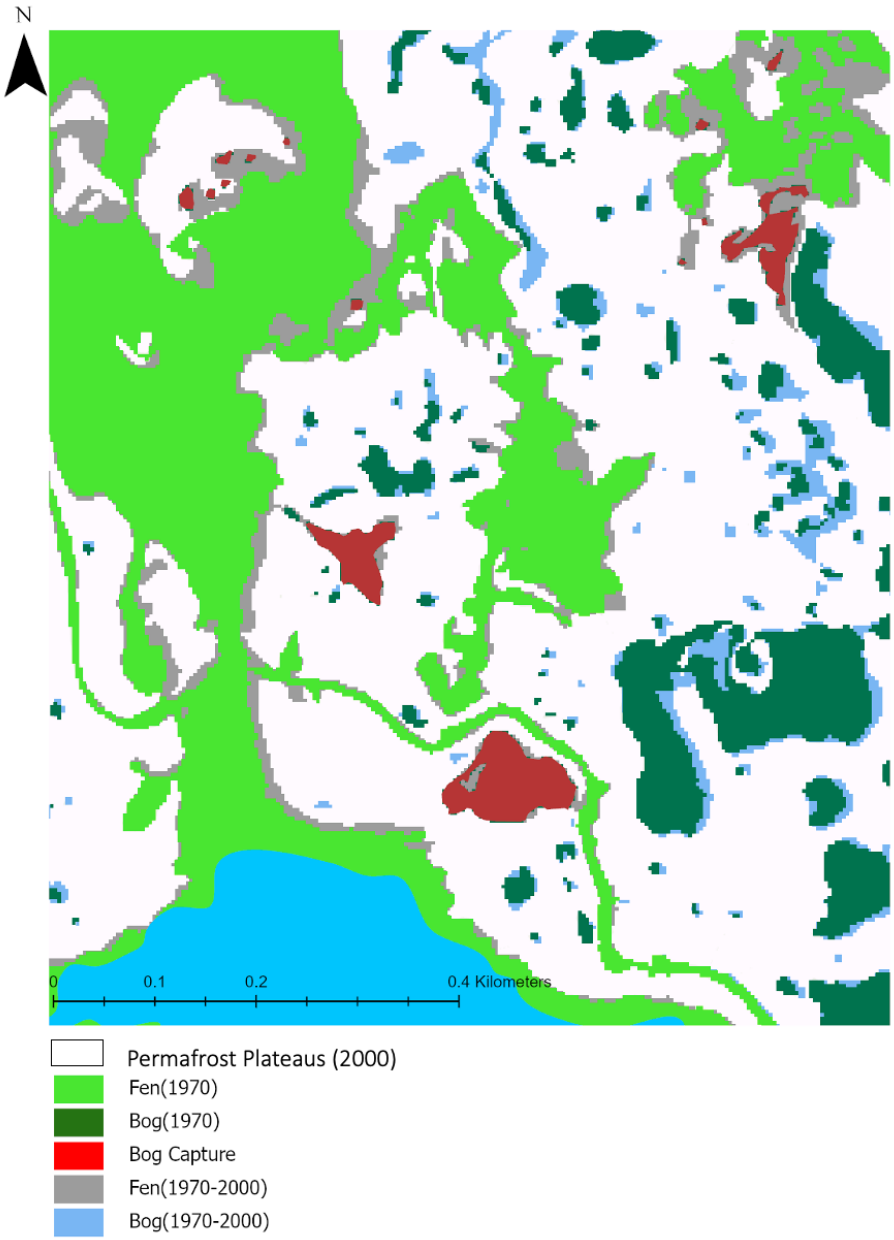

Figure 2.2: A 30-year (1970-2000) evolution of the SCRS illustrating the transition of dominant land covers.

permafrost-covered area was conducted by Chasmer et al. (2010) [23]. The study demonstrated that most of the reduction in permafrost area occurred at the edge of permafrost plateaus due to vegetation loss yield by the lateral thawing, the increase in meltwater runoff, and the soil saturation at plateau edges. The chain reaction between the dissipation of permafrost and ecological change has been scrutinized, especially for the Scotty Creek watershed. As permafrost plateaus are higher than the wetlands around them and the permafrost core is ice-rich [106], the thawing core of the permafrost results in subsidence of the ground surface. The increase in wetland areas as a consequence of thawing leads to an increase in the energy inputs at their surface, this can be one of the main drivers of lateral thawing through subsurface heat transfer via groundwater flow [130]. Because of the importance of land cover transition, it is desirable to be able to predict the evolution of land cover to investigate the effects of permafrost thaw on the hydrological characteristics of a permafrost environment. Moreover, analyzing the impact of land cover evolution on the extent of secondary and primary contributing areas over time is necessary to understand how each type of runoff area contributes to a basin water balance.

2.4 Land Cover: Classification and Change Analysis

We are sometimes able to predict future changes to land covers by using the pattern and intensity of change captured by satellite imagery. Here, we intend to use classified imagery to estimate the distribution of wetlands and permafrost-covered areas, detect land cover transitions over time, track the rate of land cover evolution, capture the spatio-temporal pattern of change, and reveal the hydrological effects of land cover evolution on the discontinuous permafrost land covers in the NWT. Tracing the evolution of the dominant land covers in discontinuous permafrost zones requires:

- An accurate means of classification of dominant land covers.
- Models for simulating long-term and short-term land cover evolution both spatially and temporally.
- Methods for delineating the runoff area of the wetlands for hydrological modeling purposes.

To develop and train an accurate land cover change model, we need classified maps. Both pixel-based and object-based classification methods have been used for classifying

dominant land covers of the southern NWT's discontinuous permafrost zones to determine the scale and magnitude of change during the last 70 years [23, 20, 26, 103, 42, 85, 84, 82, 57, 69]. Mapping permafrost plateaus via remotely sensed data on a large scale requires a combination of statistical and numerical methods [108, 130]. The complicated process of gathering remotely sensed data, and the availability and frequency of the data are the main obstacles to using most of the developed statistical and numerical methods. For instance, Hachem et al. (2009) [45] utilized the MODIS's land surface temperature (LST) product for mapping permafrost presence/absence. The regional map of permafrost was created by estimating the mean annual surface temperature and freezing and thawing indices. A sinusoidal model for representing seasonal thermal variation for each pixel is fitted over the daily LST. The validation of the method was done by finding the correlation between the calculated mean annual surface temperature and freezing and thawing indices derived from the reference stations and the sinusoidal curve. The results illuminated that there is a low correlation between indices derived from both methods, the low correlation caused by the number of cloudy days, ignoring heterogeneity, and the low spatial resolution of MODIS imageries. Recently, the spectral, spatial, and temporal qualities of remote sensing products have been improved by the use of machine learning and deep learning-based algorithms in the fields of object detection, scene classification, image segmentation, change detection, geospatial land cover prediction, and land use and land cover classification [136, 140, 53, 107, 5]. The performance of deep learning and machine learning algorithms in land cover modeling and classification have been analyzed in several studies [135, 76]. Numerous research studies have been done to enhance the Canadian wetland mapping products using machine learning and deep learning algorithms [21, 26, 85, 7, 6, 72, 71, 70, 33]. A maximum likelihood classification model was one of the first methods developed for classifying wetlands, uplands, and permafrost plateaus in the Scotty Creek watershed [106] using Landsat and IKONOS remote sensing data. In another study, Stadnyk et al. (2005) demonstrated inaccuracies in the classification of bogs and fens in the Scotty Creek watershed using Landsat data which proves that the complexity of the wetland landscapes demands high-resolution imagery and the deep architecture of deep learning algorithms [6, 70, 115]. Chasmer et al. (2014) [24] presented a decision-tree (DT) classification methodology which combines airborne LiDAR and high-resolution spectral data sets to classify the landscape into permafrost plateaus, bogs, fens, uplands, and water. The decision-tree classifier is used to determine the highest probability of prediction of a given land cover type. The selected hierarchical models for predicting the land cover of the training sets were tested due to elevation derivatives, vegetation characteristics, and spectral classification of land cover types. For evaluating the accuracy of this method, the classification inaccuracies were compared against field measurements. Moreover, Chasmer et al. (2014) [24] drew a comparison between this method and supervised land cover

classification from the spectral WorldView2 by using sensitivity analysis. The results of modeling and validating in this study illustrated the accuracy of the hierarchical classification was between 88% and 97% of the validation sub-area, and topographical derivatives were more accurate in identifying variations in land cover types. In contrast to the findings of Quinton et al. (2003) [106], the percentage of bogs identified by the decision tree [24] model were higher than fens in the Scotty Creek watershed; these findings demonstrate the influence of edge uncertainties, especially for bogs due to their fragmented structures, as well as the possibility of pixel value range confusion between bogs and fens when employing lower resolution remote sensing data. The main concern of the model developed by Chasmer et al. (2014) [24] is that the model has never been evaluated by assessing and testing the model on other taiga wetlands areas in discontinuous permafrost zones. Most of the permafrost landscape classification methods are restricted by a lack of computing power or a suitable working environment, particularly during the data preparation step and during the application to big data sets.

In the context of hydrological modeling of discontinuous permafrost zones, an automatic classification solution would be helpful for long-term and large-scale analyses of land cover change. Bhuiyan et al. (2020) [16] developed an automatic mapping workflow for delineating ice-wedge polygons distributed in arctic tundra complexes on the north slope of Alaska. This study incorporated deep learning algorithms to facilitate and improve the process of data preparation and classification to detect ice-wedge polygons from sub-meter resolution commercial satellite imagery[16]. In the discontinuous permafrost wetland systems found in the taiga plains, no study has yet established an automated and scalable method for precisely recognizing wetlands and outlining the run-off area of isolated and connected wetlands.

To expand our investigations on the hydrological effects of land cover evolution both temporally and spatially, we need land cover change models. The outputs of classification models, which are land cover maps, have been used as input for land cover change models to provide long-term predictions of land cover changes in various environments. These models are used to describe and predict the past, present, and future classification of land use and land cover in different systems, and have been applied to simulate changes due to agricultural, forestry, and urbanization. A diversity of modeling methods have been used to analyze the land cover change, for example, statistical and empirical models [37, 62, 118], dynamic models such as Cellular Automata [89], agent-based models [125], machine learning and deep learning models [95, 87], and hybrid models [11, 89, 88, 54]. The land cover change models simulate evolution by extracting spatial and temporal correlations and important features from the available data and the driving factors of change (such as climate or economics). The traditional methods, such as cellular automata and statistical

models, have two major drawbacks: they cannot simultaneously capture both spatial and temporal changes, and their simulations are entirely governed by earlier states. These challenges can be addressed by the deep architectures of deep learning and machine learning algorithms and advanced computer vision techniques. A diversity of machine learning and deep learning methods have been used to predict and simulate land cover change [37, 62, 118, 89, 11, 88, 87, 73]. Abdullah et al. (2019) [2] utilized eXtreme Gradient Boosting (XGBoost) and Random Forest (RF) to capture the spatio-temporal patterns of land use and land cover across coastal areas over a 28-year period from Landsat imagery. This study showed that the XGBoost is a successful method in feature selection for solving the issues of land cover heterogeneity and spectral complexities of the image data. It should be noted that Abdullah et al. (2019) [2] never tested the accuracy and performance of the model in terms of long-term land cover change prediction. Pijanowski et al. (2002) [95] developed a land transformation model by applying an artificial neural network and GIS to model land-use change in Michigan's Grand Traverse Bay watershed. They analyzed the effects of feature presence (roads, highways, residential streets, rivers, inland lakes, and agricultural density) on urbanization. The model had better predictions at larger scales when using a moving scalable window metric. Kanevski and Pozdnoukhov (2008) showed that machine learning algorithms can be sufficiently used for exploratory spatial data analysis, recognition and modeling of spatio-temporal patterns, and decision-oriented mapping [55].

Future assessments of land use and land cover change play a significant role in urban planning, policy-making, and environmental studies. An artificial neural network and cellular automata model was used by Javed Mallick et al. (2021) [73] to predict the change in land cover in the Saudi Arabian city of Abha for the year 2028. The trained model forecasted an increase in the built-up area, indicating the necessity for long-term sustainable management measures. A similar methodology was used to predict future land use and land cover changes to help environmental engineers and policy makers lessen the possible effects of the urban heat island phenomena in a developing megacity [54]. Kafy et al. (2021) [54] incorporated a combination of support vector machine algorithm, cellular automata, and the artificial neural network algorithm to retrieve and simulate the pattern of land cover change in one of Bangladesh's fastest-growing regions. The validation results demonstrated excellent accuracy. The model projected a 10% increase in urban built-up areas by 2029, and the research findings revealed a significant relationship between changes in urban areas and the rising LST, suggesting the need for long-term plans that emphasize the significance of urban plantation and the preservation of natural resources [54]. Four statistical techniques—Markov chain, logistic regression, generalized additive models, and survival analysis—were tested for their efficacy in land use and land cover

change modeling by Sun and Robinson (2018) [118]. In terms of overall accuracy, the generalized linear model performed better than the other three models, whereas logistic regression and survival analysis performed better when modeling changes for certain land-use types. The study by Sun and Robinson (2018) [118] demonstrated that the selection of model by land use change type is an important method for land use and land cover change studies, and a hybrid model composed of the best modeling methods for each land-use change may be more reliable than those where an individual statistical method is applied [118].

We provide a thorough overview of recent deep learning and machine learning applications in Chapter 4 and Chapter 5 for categorizing wetlands and permafrost plateaus, simulating spatio-temporal land cover change in discontinuous permafrost zones, and improving the quality and accuracy of remote sensing outputs. These studies demonstrate a significant benefit of using machine learning and deep learning algorithms for long-term simulations of land use and land cover change, which helps policymakers and urban planners take the effects of climate change into account in upcoming projects. However, these methods have not yet been applied to predict the evolution of the discontinuous permafrost lowlands impacted by climate warming. Despite the excellent performance of deep learning, machine learning, and advanced computer vision techniques, there are still unexplored aspects in the use of these methods for land cover classification and land cover change simulation of discontinuous permafrost wetland systems in the taiga plains.

2.5 Land Cover: Hydrological Analysis

The evolution of land cover impacts watershed storage, streamflow, and the watershed-scale hydrological response of the discontinuous permafrost regions of the NWT [105]. Quantifying the impact of land cover changes on watershed features like flood potential, soil water availability, or groundwater recharge may potentially be achieved by combining hydrological models and land cover change models.

There is some precedence for coupling hydrological models and land cover change models; a coupling method was presented by McColl and Aggett (2007) [77] to enhance the formulation of land-use policies at the watershed scale. In this study, a land-use forecasting model called "What If?" was combined with a rainfall-runoff model (HEC-HMS) with a GIS platform. While taking into account both low and high population growth scenarios, the "What If?" model assessed the spatial distributions of low-density residential land uses for the years 2015, 2025, and 2050. The "What If?" model's output was then used as an input in the HEC-HMS hydrologic model calibrated for a specific storm time within central

Washington State. By quantitatively comparing the results of the anticipated stormwater runoff volumes generated for each pattern of land-use distribution, it was possible to establish which land-use policy is more hydrologically advantageous for land-use managers and policymakers.

The hydrological effects of thaw-induced fen–bog–plateau complex evolution have been examined in many studies [30, 31, 25, 48, 116]. Kurylyk et al. (2016) [63] analyzed the influence of vertical and lateral heat transfer on permafrost thaw by stimulating the development of thaw, and the evolution of groundwater flow in single permafrost plateau-wetland complex. The results of the simulations were compared to observed data. Simulated soil temperatures in the surface energy balance model were used as the upper boundary conditions to a three-dimensional model of subsurface water flow and coupled energy transport using the SUTRA-ICE model [101]. The results of simulations indicated that the landscape transition of a permafrost plateau-wetland complex caused by permafrost thaw increases energy absorption. Nevertheless, such computationally intensive 3-D modelling cannot be scaled up to the level of a watershed. Further research is needed to better understand the mechanisms of water transfer and storage between fens, bogs, and basin outlets at larger scales in order to improve the performance of hydrological models and examine the hydrological effects of changes in contributing runoff areas of fens and bog (primary and secondary), bog cascades, and forested covered area. The interaction between the Canadian NWT's discharge properties and the conversion of forests to wetlands (fens and bogs distribution) should be taken into account by the numerical models [116]. Stone et al. (2019) [116] used the cold regions hydrological modeling [98] platform and field water balance observations to model the hydrological behavior of a single channel fen sub-basin in the headwaters of Scotty Creek, to show the effects of permafrost thaw-induced land cover change on wetland discharge. The model performed well when compared to measured water balance components, and the results showed that the total annual discharge from the channel fen diminishes and the surface storage capacity is affected by a decrease in permafrost distribution [116]. One problem with this study is that despite the possibility of utilizing land cover change models to estimate the transitions of forested area, the effect of permafrost plateaus conversion to wetlands is investigated by changing the proportion of wetland to permafrost plateau area in the modeled sub-basin. Particularly, there has been little work done regarding explicitly simulating the long-term effect of land cover evolution on permafrost thaw patterns and hydrological properties. Painter et al. (2013) [93] concluded that modeling the evolution of discontinuous permafrost and the reaction of the environment is a big challenge which is caused by the complexity of the controls affecting permafrost thaw, the spatial and temporal resolution, and the nonlinear nature of the freeze/thaw [1, 93]. It should be noted that additional background information rel-

evant to the topic of each chapter will be provided at the beginning of each Chapter. This information will provide context and further detail on the specific topic being discussed and will serve to enhance the understanding of the content presented.

In this study, we seek to understand how changes in land cover—from permafrost plateaus to fen, permafrost plateaus to bog, and bog to fen (a phenomenon known as "bog capture")—affect the hydrological responses of the Scotty Creek Basin and similar environment. These changes could significantly affect the connection between fens and bogs, the stored water in the basin, and consequently the runoff responses at the basin scale.

Chapter 3

Hydrological Classification of Isolated Wetlands in Discontinuous Permafrost Regions using only RGB Imagery

3.1 Introduction

Northern regions are rapidly evolving as an outcome of climate warming. Permafrost thaw is one of the driving factors of land cover change in discontinuous permafrost zones of Northern Canada and elsewhere; the thawing edges of peat plateaus lead to a gradual transition from forested lands to wetlands [30]. Delineation of the extent and spatial distribution of wetlands and peat plateaus at different snapshots is needed to investigate the magnitude and impact of this permafrost thaw and the resultant land cover change.

Satellite imagery enables us to mine information about the pattern and degree of change and use that data to forecast future changes. We can use classified imagery to estimate the distribution of wetlands and forest-covered regions, detect land cover transitions across time, delineate runoff areas, and investigate the effects of land cover transitions on the hydrological characteristics of discontinuous permafrost wetland systems such as those found in the NWT, Canada.

Pixel-based and object-based classification has been applied to remotely sensed imagery of discontinuous permafrost regions of the southern NWT; these approaches have been critical in estimating the extent and magnitude of change over the past 70 years [23, 20, 26, 103, 42, 85, 84, 82, 57, 69].

Although existing pixel-based classification models have helped determine the pattern and spatial extent of changes, the models encounter some challenges [24, 106]. One of the main concerns regarding the application of pixel-based classification methods is that the method usually needs training data that includes all of the land cover characteristics to boost the classification accuracy [26]. For example, classes with similar spectral information can be wrongly allocated to pixels with characteristics not present in the training data [26]. Another issue with wetland identification is the spatial heterogeneity of wetlands, which leads to unclear and blending boundaries between these highly fragmented landscapes and the neighboring land covers [26, 99]. The blending boundary issue can be a challenge for hydrologists interested in classifying the wetlands into two hydrologically important land covers—fens and bogs—and determining their local contributing runoff areas.

In this study, we consider three primary land classes: forested land, open water, and wetlands. Wetlands can be further subdivided into bogs (which are geometrically isolated from the surface water network) and fens (which connect open water features) . Bogs and fens are recognized for their distinct hydrological functions, serving as storage and conveyance features, respectively. Forest can be subdivided into forested peat plateaus, strips of land interspersed between wetlands which is perched atop permafrost and at a slightly higher elevation, and larger forested upland regions. Notably, we use a hydrological

(rather than ecological) definition of bogs and fens, with bogs as storage features and fens as conveyance features [4, 103, 59, 106]. Bogs and fens share similar spectral information, making it difficult to distinguish using pixel-based methods [26]. However, when hydrologically defined, bogs are geometrically isolated whereas fens are part of a connected network connected to lakes and streams. These geometric differences between bogs and fens can be leveraged using machine-learning-based classification tools. Compared to traditional pixel-based classification, which uses only the spectral information within individual pixels, the geometric categorization of fens and bogs has the advantage of minimizing classification errors in these two land covers by using (multi-pixel) information about the geometry of these features.

Depending on the employed classification methods and the necessary input data, generating classified maps may have an unavoidable cost; the process of preparing the data for image classification (such as image restoration, geometric (or ortho-) rectification, radiometric corrections, resampling, and other similar operations) can be complicated and time-consuming. These data preparation challenges are also an additional shortcoming of the previously developed pixel-based methods for wetland identification. These previously developed methods require a considerable amount of computer memory, remote sensing expertise, and access to specific data sets.

To address some of these wetland classification challenges, the main objective of this study is to develop and test a feature classification approach that simplifies and accelerates the data preparation and land cover classification procedures for discontinuous permafrost wetland systems within the Taiga Plains Ecozone. The method is intended to classify earlier airborne photos and sites using only RGB imagery (i.e., without access to multi-spectral data), RGB image classification is largely avoided in the literature due to limited information provided by 3 spectral bands in the classification of lands for discontinuous permafrost zones (relative to more spectral bands with multi-spectral imagery).

New developments in computing based on shape-based features avoid these limitations. Considering the limitations, this paper aims to:

1. Develop and test an automatic classification approach for classifying remotely sensed imagery features into wetlands, forests, and water, focusing on discontinuous permafrost wetland systems in Northern Canada.

2. Develop and test a method to categorize the classified wetlands as either hydrologically isolated (bogs) or connected wetlands (fens) based on geometric characteristics.

3. Delineate and estimate the primary and secondary runoff area of the categorized wetlands for hydrological analysis.

Fortunately, deep learning methods have demonstrated their capability to address several similar contemporary challenges in remote sensing and computer vision classification tasks, including image classification, object recognition, and semantic segmentation [124, 143, 28, 83, 131]. Deep learning approaches use a multi-layer neural network architecture or numerous hierarchical layers to learn the spatial characteristics of the existing components in an image [107].

Convolutional Neural Network (CNN)s are one of the most effective and popular deep learning methods in environmental and geographical research for feature identification, classification, and hazard prediction. As such, CNN methods have been applied to building detection, land type classification, Spatio-temporal simulation, cloud removal, and flood risk prediction [136, 56, 76, 43]. In contrast to traditional pixel-based techniques that demand training data comprising all the characteristics of the existing labels, CNN's multi-layer interconnected architecture enables them to identify important features from data in each layer to classify images.

A combination of deep learning methods and advanced computer vision techniques comprise the TWINN solution, which consists of three steps. First, we implement a CNN model with ResNet34 [49] architecture for semantic segmentation of dominant land covers in discontinuous permafrost zones using World View 2 (WV2) RGB imagery. The CNN model implemented in this study is capable of segmenting RGB imagery into three distinct classes: water, wetlands, and forests. Here, features such as ponds and lakes are identified as water [24].

Then, the classified wetlands generated by the CNN are categorized into isolated wetlands (bogs) and connected wetlands (fens) based on their geometric characteristics by employing a four-layer Multi Layer Perceptron (MLP) model. Finally, we use the watershed algorithm from the OpenCV library in Python using the watershed and Euclidean distance functions, effectively estimating the contributing runoff area to each categorized wetland as its "nearest neighbor" region, a useful first-order approximation in very flat landscapes such as Scotty Creek Basin (61.44°N, 121.25°W), in the Northwest Territories of Canada. Hydrological analysis requires delineating the contributing runoff area of classified wetlands [106, 24], i.e., the portion of forested land cover which drains to the fens (primary runoff area) and that which drains to bogs (secondary runoff area). This information can be used for hydrological simulation under current conditions or used in conjunction with a land cover evolution model (e.g., [4]) to examine changing hydrological responses due to climate change.

To assess the performance of the developed models, we run the final solution on eight Areas of Interests (AoI)s located in similar discontinuous permafrost wetlands within the

NWT and British Columbia, Canada. We also investigate the effects of batch size, data augmentation, and image size (tiling) on the performance of the TWINN solution.

3.2 Related Works

CNNs are deep learning algorithms mainly employed for image processing. The spectral, spatial, and temporal qualities of remote sensing products have been improved by the use of CNN-based algorithms and computer vision techniques in the fields of object detection, scene classification, image segmentation, and land use and land cover classification [137, 72, 136, 140, 53, 107, 5]. The architecture of the CNN, geographical location, spatial extent, and image resolution can all influence the accuracy of the CNN-based models for land cover classification [50]. Here, we briefly review recent applications of CNN-based techniques in remote sensing and Canadian wetland mapping studies.

A typical application of CNNs is object detection. Applications in remote sensing include identifying clouds in images, which can facilitate cloud removal as a pre-processing step and improve solar forecasts [75, 112]. CNNs have also been used to identify buildings, roads, vegetation types, or urbanized areas [75, 112]. Bhuiyan et al. (2020)[16] developed an automatic mapping workflow for delineating ice-wedge polygons distributed in arctic tundra complexes in the North slope of Alaska. They incorporate a CNN-based instance segmentation technique to detect ice-wedge polygons from sub-meter resolution commercial satellite imagery [16].

It has been demonstrated that CNN-based techniques often outperform traditional pixel-based methodologies in land cover classification [135, 76]. Merchant (2020)[80] compared the performance of a Random Forest (RF) model to an object-based CNN technique for detecting open water over the Peace Athabasca Delta; based on the reported results, the CNN technique outperformed the RF model in terms of accuracy.

Numerous investigations and studies have been conducted to examine machine learning and deep learning methods to derive wetland mapping products [21, 26, 85, 8, 6, 72, 71, 33]. Montgomery et al. (2019)[85] developed a decision-based methodology using data fusion of multiple remote sensing data sources to classify boreal wetlands. The performance of the proposed method was assessed by comparing the results with field measurements and applying the methodology to other boreal environments in the Peace-Athabasca Delta. The results demonstrate both the decision-based method and data fusion are not restricted to a particular ecosystem or a particular geographic location and can be used to classify different types of boreal wetlands; the availability, frequency, and skill required to analyze the data set are the main challenges of employing this wetland classification approach.

The Canadian Wetland Inventory is the result of a machine learning-based wetland classification approach and the first Canada-wide remote sensing method for wetland classification over large areas [6]. The Canadian Wetland Inventory was developed by training a RF algorithm on many field samples and Landsat-8 imagery within the Google Earth Engine platform. The Canadian Wetland Inventory showed an overall accuracy of 71% for categorizing wetlands. [72] generated a 10-m resolution Canadian Wetland Inventory by training a RF classifier using multi-year summer composites of Sentinel-1 and Sentinel-2 data in Google Earth Engine. The 10-m resolution Canadian Wetland Inventory showed an overall accuracy of 80%, outperforming the Canadian Wetland Inventory produced by [6].

Further research is required to increase the Canadian Wetland Inventory's accuracy for classifying wetland areas due to potential field data inaccuracies and the complexity of the wetland landscapes, which demands high-resolution imagery [6, 72]. Using high spatial resolution remotely sensed data for wetland classification may result in errors due to the blending boundaries issues between the edges of wetlands and other land covers [26]. Additionally, there has been no attempt to evaluate alternatives to RF [6, 72].

Regarding the blending boundary issues, multiple studies have compared pixel-based classification and object-based classification (which spatially cluster pixels) methods to find the best approach for wetland delineation [26, 15]. [15] applied pixel- and object-based (parametric and non-parametric) algorithms on the Lake Baikal, Russia, drainage basin using four Quickbird multi-spectral bands plus various spatial and spectral metrics. The researchers reported that there is no statistically significant difference in the overall accuracy of the classifiers. The pixel-based method is preferred for classifying wetland-dominated landscapes since the object-based method requires substantial resources.

Chasmer et al. (2014)[24] presented a decision-tree classification approach for identifying the heterogeneous land cover types in a northern watershed located in the zone of discontinuous permafrost using airborne LiDAR and high-resolution spectral data sets. The method outperformed the past classification approaches in the same area with an overall accuracy of 91%. This study showed that topographical derivatives were more successful at explaining the variations in land covers compared to spectral and vegetation structure characteristics. However, the study also reported validation accuracy between 38% and 74%, suggesting that alternate techniques may be needed to improve classification performance.

Determining the unknown boundary of heterogeneous land covers like wetlands is often a difficult task due to their gradual transition into another class [33], which benefits from the deep architecture of CNN-based models. The layer-based architecture of CNN models

makes them capable of capturing more features and natural complexities of land cover classes such as wetlands. Pouliot et al. (2019)[99] and DeLancy et al. (2019)[33] tested the performance of CNN-based models for the classification of wetlands over a similar region in Alberta using different sets of training data. DeLancy et al. (2019)[33] study's validation and testing results revealed that the accuracy of the CNN-based model is 5% higher than the eXtreme Gradient Boosting (XGBoost) model in wetland classification.

The CNN-based model tested by Pouliot et al. (2019)[99] reported an overall accuracy of 69% for classifying bog, fen, marsh, swamp, and water classes using Landsat data. Rezaee et al. (2018)[107] evaluated the performance of a pre-trained CNN-based model in the classification of the complex wetland by comparing the outputs of the CNN model with a RF model, the overall accuracy of the trained models showed that CNN performs better (95% accuracy) than RF with a 16% improvement. ArcticNet is another deep neural network-based solution for the semantic segmentation of six important land covers distributed in permafrost regions [52]; the ArcticNet solution achieved an overall high accuracy of 94% on the testing data. Still, the solution was not applied to other similar areas to analyze the transferability of the ArcticNet.

Most of the developed methods for Taiga Plains wetland classification struggle with the wetlands' fuzzy boundaries which leads to leads to classification uncertainties within transition zones; the results of comparing deep learning methods to non-neural network methods reveal that the deep architecture of the CNN-based algorithm is more accurate at delineating wetland boundaries and categorizing the wetlands. Although these CNN-based solutions were successful in terms of classifying the wetland complexes, there are still unresolved issues and gaps in the application of deep learning techniques for the classification of discontinuous permafrost wetland systems in the Taiga Plains of the NWT. These issues include determining whether CNN-based models are efficient at classifying the wetlands in discontinuous permafrost zones and whether using RGB images can help users with the data preparation process. Most of the developed methods are focused on more sophisticated wetland types (marsh vs. bog vs. heterotrophic bog, etc.) rather than the much simpler hydrologic definition. Additionally, these methods require hyperspectral information and LIDAR as input data, which makes the data preparation procedure more difficult.

The advantages of employing RGB images are that they are cheaper, can be acquired from aircraft in air photo programs, and that high spatial resolution data sets, which are usually expensive, can be easily extracted through Google Maps/Google Earth/ESRI, etc. without costs. It is also important to note that tiling, batch size, and data augmentation techniques are crucial parameters for the development of CNN-based models. However, none of these parameters have been well investigated and have yet to be evaluated how

they affect the performance of CNN-based models developed for categorizing wetlands. Before training the model, the input data are tiled to a smaller size due to the large size of the images[68]; Lee et al. (2022)[68] proved that the size of tiling images noticeably affects the accuracy of the trained CNN models for non-small cell lung cancer detection. The TWINN approach outlined here is intended to address a number of these limitations and data gaps. Within this study, we not only apply the method to 8 different landscapes, but we explore the effectiveness of batch size, data augmentation, and sample size (tiling) on the accuracy of the TWINN solution.

3.3 Study Area and Data Set

This study builds upon the extensive image classification work done by Chasmer et al. (2014, 2020) [23, 24] at the SCRS, located 50 km south of Fort Simpson in the Northwest Territories, Canada (Figure 3.1.a). This region is characterized by extensive wetlands, with permafrost-underlain peat plateaus interspersed with fens, collapse-scar bogs, and lakes (Figure 3.1.c) [23, 24]. Fens are seen as wide channels comprising the drainage network of basins, and bogs appear as patches distributed between forested plateaus sitting atop permafrost mounds. Bogs and channel fens are crucial to the hydrological process of the SCRS due to their different hydrological functions [106, 104]. Channel fens are one of the primary drainage systems of this region, which convey water to the basin outlet, and bogs are not typically able to convey water [63, 106], but may hydraulically connect during larger snowmelt and rainfall events [30].

To assemble the training and testing data set for the TWINN solution, we initially used the WV2 imagery of the SCRS acquired in the summer of 2010 (Figure 3.1.b). Although the image includes a high-resolution panchromatic band and eight multi-spectral bands, the TWINN solution is solely trained on the RGB bands of the WV2 imagery with a spatial resolution of 1.6 m by 1.6 m to determine whether RGB images are sufficient for classifying land cover. Using only RGB images simplifies the data preparation step, does not require specialized knowledge to analyze and prepare the input data, and is useful when multi-spectral data are unavailable. The training input data are derived from a classified map developed by Chasmer et al. (2014) [24] on the same image WV2 image, with bogs and fens grouped as one class (wetland) (Figure 3.1.c); then, the main image and classified map were re-sampled to 1m resolution.

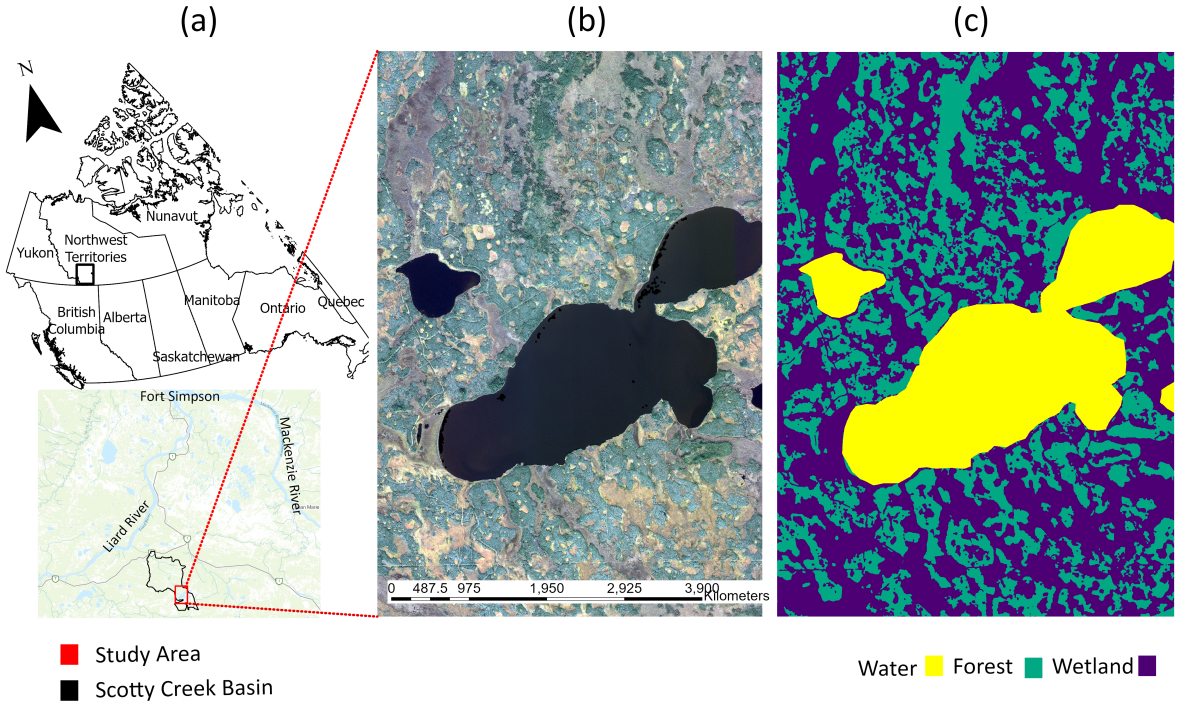

Figure 3.1: The data set used for training TWINN solution: (**a**) the geographic location of the SCRS in the Northwest Territories, Canada. (**b**) the WV2 imagery of SCRS (**c**) the labeled map of the study area representing three classes of forest, wetlands, and water. Bogs and fens are not discriminated between in this image.

3.4 Methodology

The TWINN solution proposed here consists of three independent steps:

1. Multi-label/multi-class classification using a CNN-Based semantic segmentation method to delineate the RGB image into forest (forested regions), wetland features, and open water.

2. Wetland identification as either bogs or fens based upon the area, perimeter, and roundness ratio of the wetland polygons using a MLP method.

3. Further delineation of the permafrost plateau regions into primary runoff areas (draining to fens) and secondary runoff areas (draining to bogs) using a nearest-neighbor approach.

These steps are depicted in Figure 3.2.

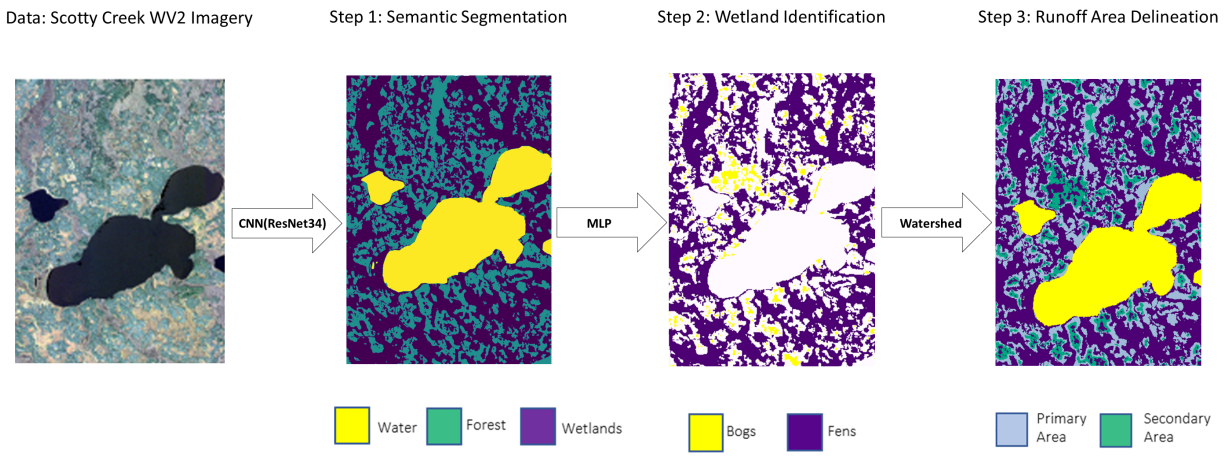

Figure 3.2: The flowchart of developing TWINN solution for classification of wetlands using RGB image.

3.4.1 Step 1: CNN-Based Semantic Segmentation

Semantic Segmentation is a category of image segmentation that clusters an image's pixels to determine category labels on a pixel-by-pixel basis [97, 56]. Here, we used a transfer learning UNet architecture with pre-trained ResNet34 encoder [109, 49]. In transfer learning, the parameters of pre-trained neural network architecture are updated while using new data.

The process sequence in UNet may be visualized as two paths resembling a U shape (Figure 3.3), a contracting path and an expansive one. The contracting path represents an

encoder of a typical CNN network that collects information from the image by successive down-sampling or reduction of the grid size [109]. The encoder of UNet (the contracting path) is composed of the following:

1. Convolutions: implement filters by applying weights with the input data set for recognizing features in pixels and producing feature maps from images.

2. Rectified linear unit activation function: uses a max() function to replace any negative values of feature maps with 0.

3. 2x2 max pooling operation: compresses the features by calculating the maximum value of each subsection of an image received from convolution [5].

The expansive path on the right of the U shape functions as the decoder of the model and successively increases the grid size to generate an image of the same or greater size and resolution as the original input using up-sampling[109].

In the expansive path of the CNN model, the final layers comprise a global average pooling layer and a fully connected layer, which are added subsequent to the last convolutional layer. After passing the input image through the convolutional layers, the global average pooling layer reduces the spatial dimensions of the feature maps to a single value per feature map representing the average value of each feature map. This produces a vector of feature values that are then passed through the fully connected layer. The fully connected layer converts the feature values into probabilities by applying the softmax activation function to the vector. The resulting probabilities represent the likelihood of the input image belonging to each class in the dataset. The class with the highest probability is selected as the predicted output. In other words, the softmax activation function in the fully connected layer produces the final class probabilities for the input image.

The application of deep networks in image segmentation problems might shrink the gradient of the loss function to zero, slow the training pace, and decrease the model's accuracy. To solve the vanishing gradient problem during the training of the image segmentation model, we used a residual network with 34 layers called ResNet-34 (Figure 3.2). ResNet was trained on the ImageNet data set, which includes millions of labeled high-resolution images. The architecture of ResNet-34 is made up of residual blocks with skip connections which address the degradation problem [49, 137]. A residual block uses skip-connection to add the outputs from a layer to the next layer deeper in the block.

The ResNet segmentation model has multiple hyperparameters which can influence classification skills. As part of the training process, we evaluated the use of two different

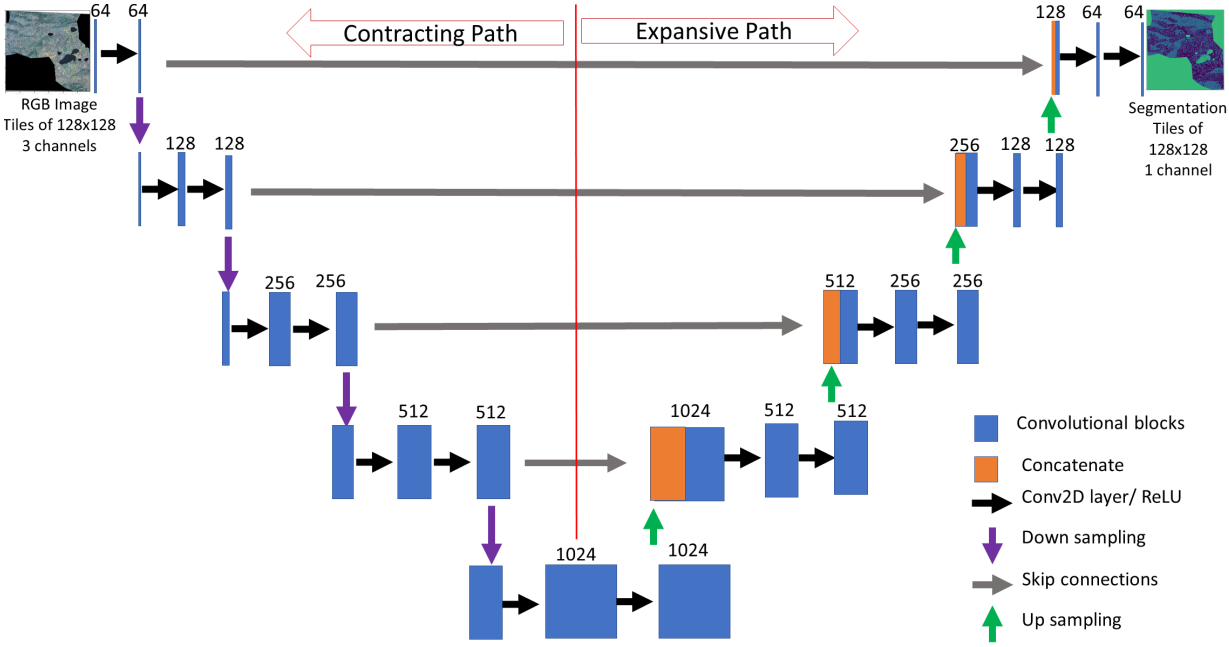

Figure 3.3: The architecture of ResNet34 used for semantic segmentation of the RGB image to a classified image consisting of permafrost plateau/wetland/lake.

batch sizes: 16 and 32. Batch size refers to the number of samples from the available training data set processed before updating the model's weights and parameters. Training such deep architectures from scratch is time consuming and expensive for computer vision projects, so we used a transfer learning technique from the fast.ai deep learning library to implement the semantic segmentation model; fast.ai simplifies the process of training model by providing neural network API [51].

In this study, the image was split into 2860 tiles of 128x 128 pixels. 80% randomly selected tiles were used for training of the CNN, 15% for validation, and 5% for independent testing.

Additionally, a data augmentation method was utilized to boost the quantity and diversity of the input data and evaluate its impact on the model's performance. This approach has been successfully employed in computer vision for training classification models by generating synthetic images from the original data through various transformations such as flipping, cropping, rotation, and contrast and brightness adjustments. In the case of

land cover classification, data augmentation can enable the model to learn to detect features under distinct environmental circumstances, such as different weather conditions and times of day, enhancing its ability to generalize to unseen data and avoiding overfitting.

The input to the network is normalized RGB images with the size of 128 pixels x 128 pixels x 3 RGB color bands, and the output is a segmentation map represented as 128 $\times$ 128 matrices; the model first predicts pixel-wise probabilities for each class, and the class that has the highest probability is portrayed on the classified map as the final result. The model is trained with 1000 epochs (the number of times the CNN model iterates over the entire training set of data) using the Adam optimization algorithm [58]. Adam combines Root Mean Squared Propagation and stochastic gradient descent with momentum to scale the learning rate by squared gradients (like Root Mean Squared Propagation) and take advantage of the momentum by using the moving average of the gradient (like stochastic gradient descent with momentum).

To assess the classification's performance, we employ cross-entropy loss. For multiclass classification, the cross-entropy loss is calculated for each predicted and observed label and summed over all pixels in an image:

$$L = -\sum_{n=1}^{128\times128}\sum_{i=1}^{3} g_{in}\log p_{in} \tag{3.1}$$

where i represents each class (wetlands, water, and forest), n is the set of pixels in an image (the predicted and observed labels are images of 128x128x1), p_{in} is the predicted probability of pixel n belonging to label i, and g_{in} is equal to one if the label in pixel n is the same category as the observation, zero otherwise.

The test data set (%5 of input data) is used to evaluate the model; we used four metrics commonly used for segmentation tasks to compare the performance of all the trained models, including cross-entropy loss in the training and validation steps, accuracy, and Intersection over Union (IoU). IoU ranges from 0 to 1, and, for each label, it calculates the number of overlapping pixels between the observed labels and the predicted labels divided by the total number of pixels existing in both observed and predicted labels:

$$IoU_i = \frac{|A_i \bigcap B_i|}{|A_i \bigcup B_i|} \tag{3.2}$$

where A_i is the set of pixels predicted by CNN for label i and B_i is the set of pixels observed to be in label i. Lastly, the accuracy of models in classifying each land cover class will be described using a confusion matrix, which reports the percentage of misclassification for each class during validation.

3.4.2 Step 2: MLP Wetland Categorization

The semantic segmentation model trained in the previous step labels the pixels as one of three classes: wetlands, water, and forest. Discriminating between fens and bogs in an RGB image is historically a challenging part of wetland classification in the Taiga Plains because fens and bogs share similar characteristics at the thawing edges of the forest which can lead to many misclassifications. Here, however, we are aided by the hydrological distinction between the two feature types: fens are wide and long channels located along the drainage network of basins, and bogs are isolated patches surrounded by peat plateau [106, 104, 26]. The geometric differences between fens and bogs helped us to solve the wetland identification problem by using area, perimeter, and roundness ratio instead of pixel-based classification.

The TWINN solution categorizes the wetlands into fens and bogs based on these geometric metrics using a MLP model. MLP is an artificial neural network including three types of layers with non-linearly activating nodes, typically referred to as the input layer, hidden layers, and output layer [140].

In a neural network, each layer is connected to the previous and next layers, and adding more hidden layers increases the complexity of the task. Here, the input layer of the MLP model is a vector of data that includes the model's features (geometrical features of bogs and fens) and distributes input data values to the following layers for further processing. The hidden layer consists of neurons that perform computations on the input data and send the results to the next layer. The final hidden layer passes the output to the output layer, which applies a sigmoid activation function to generate the final binary classification prediction. The sigmoid function maps the output to a value between 0 and 1, where values closer to 0 indicate a prediction for the negative class (fen), and values closer to 1 indicate a prediction for the positive class (bog). The output layer is the model's classes or output in vector format. During training, the weights are adjusted by using the Adam optimization method to reduce the error in the prediction of the model, which helps in improving the accuracy of the model's predictions.

The MLP model used in this study comprises four fully-connected layers with a 0.5 dropout implemented on the fully-connected layer, as depicted in Figure 3.4. The dropout technique with a rate of 0.5 is implemented on the final fully-connected layer (Figure 3.4). The dropout layer randomly omits a fraction of input data or nodes during training, and this serves as a regularization method that aids in addressing the overfitting issue in artificial neural networks. By randomly dropping some of the input data, the model is forced to learn more robust and generalizable features, improving its performance on unseen data. The implementation of dropout on the fully-connected layer of the MLP

model contributes to a more effective and accurate classification model for the given task.

Here, the input layer is a vector of three values representing perimeter, roundness ratio, and area of each wetland polygon. To generate the input data set for the MLP model, the wetlands in the initial data set are extracted from the labeled image and polygonized in ArcGIS Pro (2.9.0) (Figure 3.1.b). Then, area, perimeter, and roundness ratio are calculated for each polygon and added to the attribute table. Finally, the vector file of the polygons is converted to a raster, and each pixel in the raster contains labels and the calculated geometric features. The data set is split into three sets 70% train, 20% test, and 10% validation.

The accuracy of the MLP model in categorizing isolated and connected wetlands will be analyzed by the confusion matrix using the validation data, which calculates the percentage of misclassified fens and bogs. It should be noted that the trained model may be biased toward the majority class predictions (in this case, fen) due to the unequal distribution of bogs and fens in the study area. To address this issue, an upsampling class balancing technique is used, which generates synthetic data from the bog and adds them to the original data set [13].

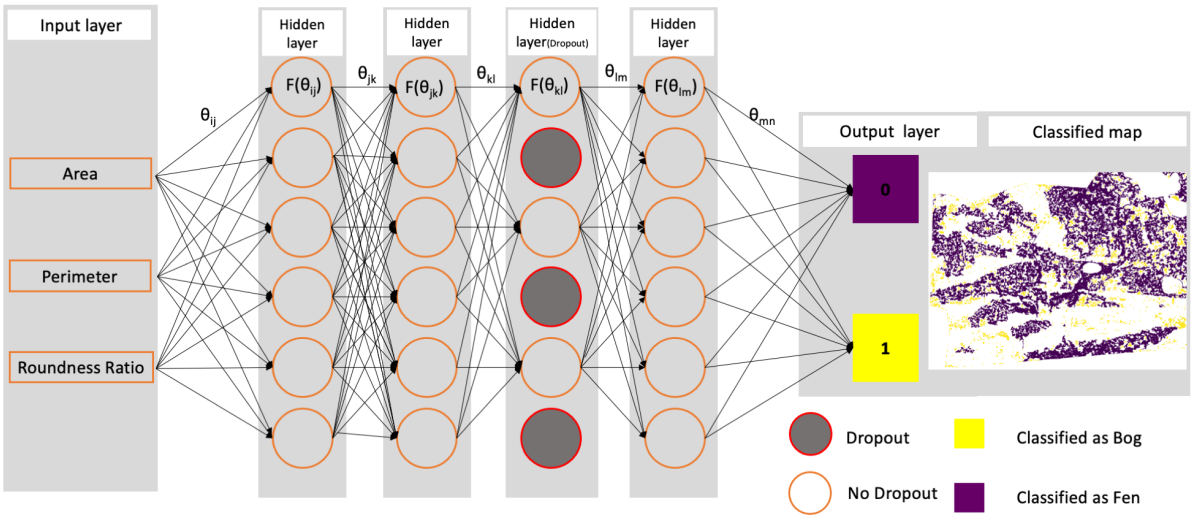

Figure 3.4: The architecture of MLP model used for categorizing wetlands.

3.4.3 Step 3: Delineate Runoff Area

Identifying the runoff area of isolated (secondary) and connected (primary) wetlands is necessary to comprehend the consequences of land cover changes on discontinuous permafrost zones of the NWT. Discretizing the primary and secondary contributing areas helps to understand how isolated bogs connect over time and how the conversion from isolated bogs to connected bogs alters the hydrological function of the watershed. The classified maps of bogs and fens generated by TWINN solution can be incorporated to define primary and secondary contributing areas and landscape units to investigate the effects of land cover change on the hydrological response of any discontinuous permafrost zones. The contributing area of bogs and fens will be delineated by leveraging the Watershed function from the OpenCV library. This method has been previously applied to image segmentation, particularly for extracting touching or overlapping components in RGB images.

This method uses a map of wetlands and non-wetlands to delineate contributing areas. The first step of watershed delineation is generating the Euclidean distance map of the wetland features (Figure 3.5.b). This distance map plays the role of a synthetic topographic surface (Figure 3.5.b), because the actual topographic surface is very flat and difficult to characterize without high resolution Lidar data. It shows the distance from each wetland pixel to the nearest non-wetland pixels, with the farthest pixels being peaks and the nearest pixels being valleys. The minima of the Euclidean distance field is used to find the markers (in red Figure 3.5.c) which are used as pour points in the watershed algorithm. The watershed algorithm then can estimate the local contributing area to each wetland, which is equivalent to a nearest neighbor region for each wetland polygon.

3.4.4 Evaluating Transferability of the TWINN Solution

To measure the generalization of the TWINN solution to similar regions in the Taiga Plains (Figure 3.6), we applied the method to WV2 imagery of 8 areas of interests (AoIs) [102] which represent peatland complexes. The selected AoIs are located in the extensive-discontinuous and sporadic-discontinuous zones of the NWT and northeastern British Columbia.

Snapshots were separated from the RGB WV2 imagery of each AoI and manually classified and digitized in ArcGIS Pro (2.9.0). These 800x800 pixel snapshots of the AoIs are divided into tiles of 128x128 (the same size as the training data), 256x256(larger than the training data), and 64x64(smaller than the training data) in order to evaluate the method's sensitivity to the input size.

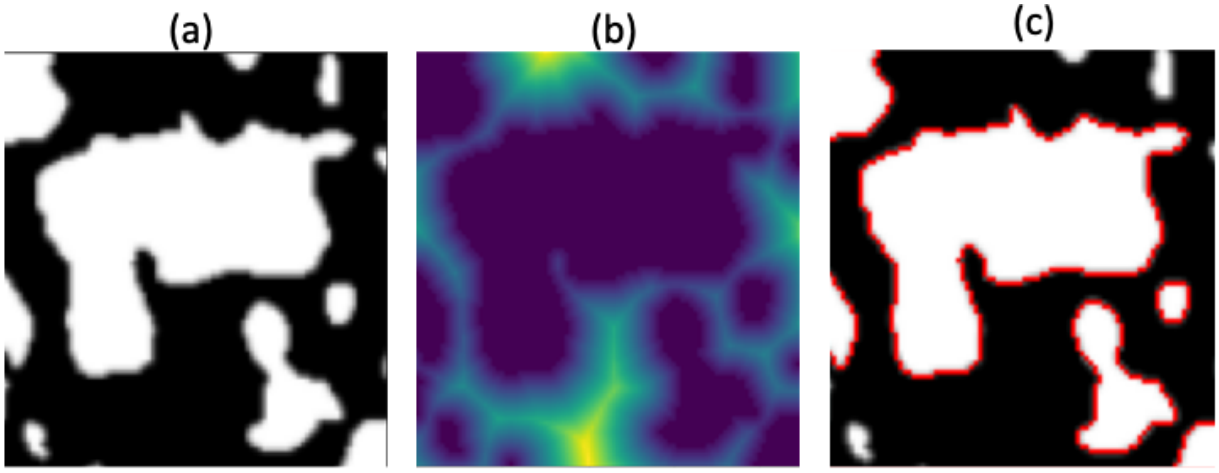

Figure 3.5: The process of image segmentation using Watershed function from OpenCV library : (**a**) binary image. (**b**) delineated nearest neighbor polygons.(**c**) the delineated markers.

3.5 Results

In this section, we report the results of applying the TWINN solution to a range of input images. First, we present the accuracy of trained semantic segmentation and MLP models evaluated by the test data set. Next, we apply the TWINN solution to other case studies to quantify the performance of the TWINN solution for the general classification of wetlands in the Taiga Plains.

3.5.1 Semantic Segmentation: Performance on the Test data set

We initially trained four models (Model1-Model4) on 80% of the classified images to investigate the importance of data augmentation and batch size on the accuracy of classification of wetlands from RGB images (Figure 3.7). Figure 3.7 visually compares a subset of the outputs of each model to the target test data set. The visual representation of these models is in most cases a visually accurate reconstruction of its target image (Figure 3.7). The reported performance metrics in Table 3.1 confirm that the model trained on augmented data set and with batch size 16 outperforms other trained models in terms of both the classification accuracy and processing time (Tab.3.1). Another metric used to assess the high accuracy of model2 is IoU; the calculated IoU for Model2 is higher than all the trained

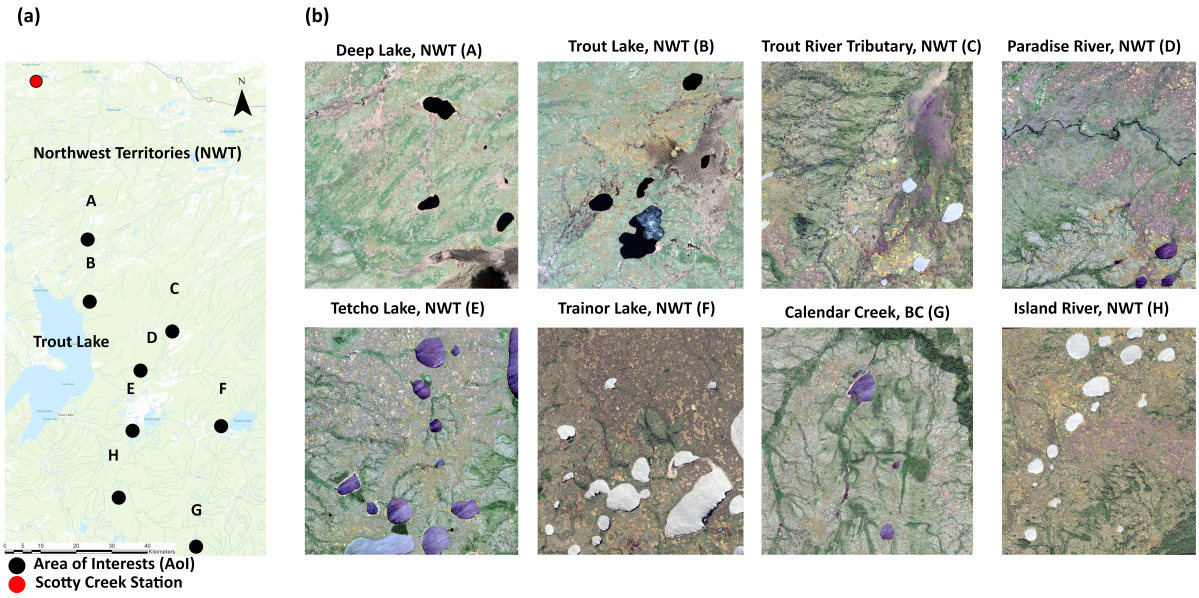

Figure 3.6: Geographical setting of the selected areas of interests for analyzing the performance of final TWINN Solution which represents discontinuous permafrost zones distributed in NWT: (**a**) Location of all the selected areas of interests. (**b**) WV2 imagery from each area of interest [102].

models, which is close to 0.9 (a value of one implies perfect classification, with zero being the worst performance) (Tab.3.1).

Figure 3.8 shows the confusion matrix of the best trained model, and the diagonal values of the matrix indicate that over 95% of pixels are classified correctly, with 100% accuracy for wetland pixels.

3.5.2 Semantic Segmentation: Performance on other Case Studies

The best semantic segmentation model (Model2) is here evaluated in more detail. We separated a 800x800 image from the RGB bands of each AoI's WV2 imagery and then manually classified each image in ArcGIS. This manual imagery (in the rightmost column of Figure 3.9 was used to test the wetland/forest classification skill of Model2. Moreover,

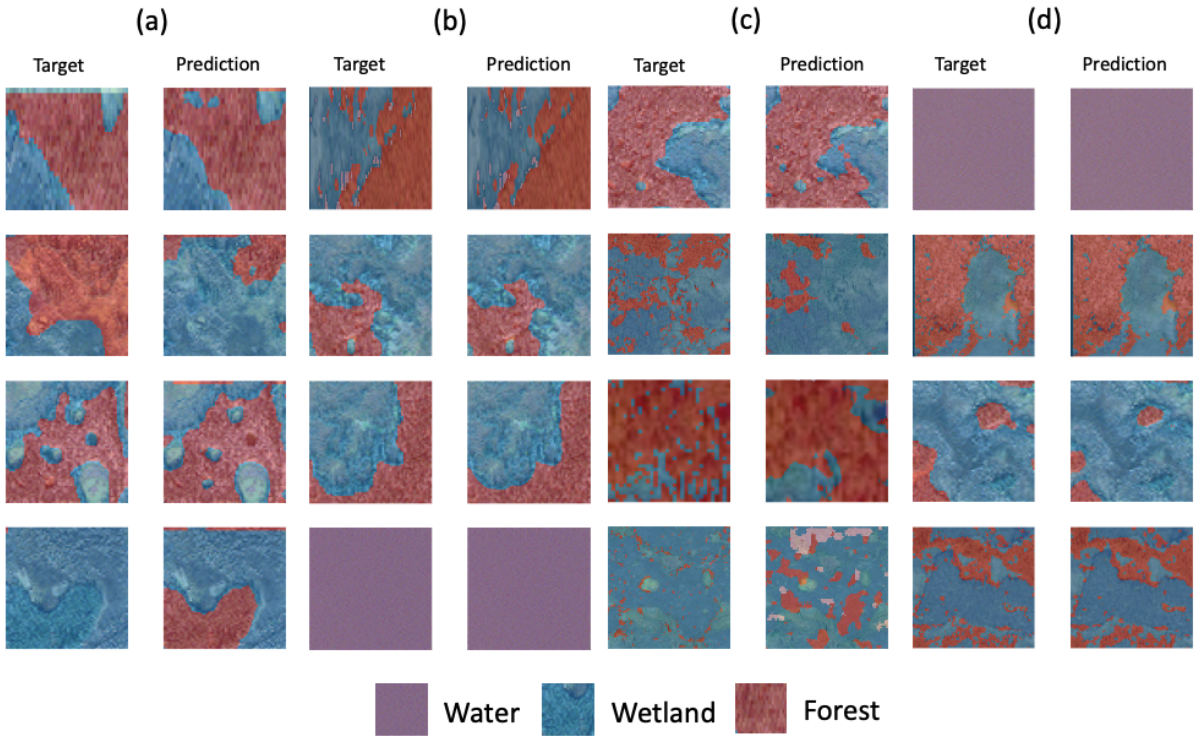

Figure 3.7: The predicted labels by each model to the target labels of the same image in the test data set : (**a**) Model1, with batch size of 16 and no data augmentation. (**b**) Model2, with batch size of 16 and data augmentation. (**c**) Model3, with batch size of 32 and no data augmentation. (**d**) Model4, with batch size of 32 and data augmentation.

the effects of image size on the accuracy of the model are determined by running the model on three different image tiles: 128x128 (same as the input size for the training semantic segmentation model), 256x256 (higher than the input data set), and 64x64 (lower than the input data set) (Figure 3.9). Note that the resolution was maintained at the resolution of the original data set; only the input image size was varied. The 800x800 snapshots are split into tiles of three different sizes; then, the model is applied to each tile to segment

Table 3.1: Accuracy metrics of all the semantic segmentation models trained on the input data set and evaluated by the test data set. Model1: batch size16 and no data augmentation, Model2: batch size 16 and data augmentation, Model3: batch size 32 and no data augmentation, Model4: batch size 32 and data augmentation.

Features	Model1	Model2	Model3	Model4
Batch Size	16	16	32	32
Data Augmentation	X	✓	X	✓
Average Accuracy	91.2	97.8	89.4	94.3
IoU	0.65	0.89	0.59	0.77
Validation Loss	0.24	0.06	0.27	0.14

the RGB image, and all the images are merged to compare the final output of the model to the manually labeled images (Figure 3.9). The rows in Figure 3.9 illustrate the model output for different image sizes, and each column includes the images for separate AoI (A-H). Comparing the central three columns of the Figure 3.9 indicates that the model's performance model is noticeably affected by the size of the image since there are many misclassifications of the model when the 800x800 image is split into tiles of 256x256, which is higher than the size of tiles in input data set.

Figure 3.10 provides quantitative details of these classification results for only the 64x64 and 128x128 image sizes in the form of a confusion matrix. The rows of the figure report the estimated true and false positive for each AoI when the 800x800 snapshot is divided into tiles of 64x64 (Figure 3.10.a) and 128x128 (Figure 3.10.b) (same size as an input data set). The columns of both figures correspond to the predicted label of each class (True label-predicted labels). Each cell displays the percentage of a specific true label existing in each 800x800 snapshot is predicted as the true label (true) or predicted as other classes (false); for instance, the value of a cell on column 6 and row 3 of Figure 3.10. a confirms that 0.06 of the water in the 800x800 snapshot of AoI (C) is incorrectly labeled as wetlands. Figure 3.10 showcases that the model's overall performance is influenced by the size of the image, comparing the first three columns of Figure 3.10.a to the first three columns of Figure 3.10.b indicates that the accuracy of the model applied on 128x128 tiles is higher than the set of 64x64. The last row of Figure 3.10 summarizes the average true positives (first three columns) and false positives of all the AoIs; It is clear that the most common misclassification is the classification of wetlands as forests, with an average misclassification rate of 19% for all the 128x128 images. The major source of these misclassifications could

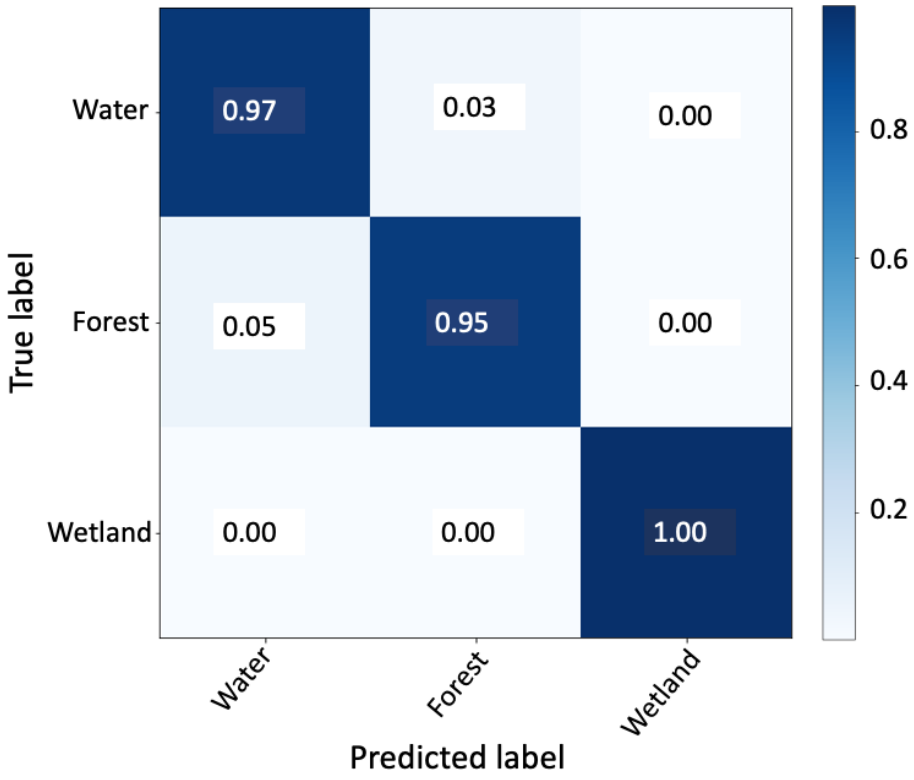

Figure 3.8: Confusion matrix of Model2 evaluated by test data set.

be the fuzzy boundary between wetland and forest that is in transition, this can be seen naturally between the margins of wetlands and peatlands; another limitation is that the target labels may contain inaccuracies. According to our results, the semantic segmentation method is superior to previous methods for segmenting land covers in permafrost zones because the method achieved the greatest reported accuracy when applied to other areas.

Figure 3.11 includes the original RGB imagery and the classified maps of all 8 AoIs. The classified map of AoI (B) suggests that the performance of the TWINN solution is noticeably affected by cloud covers (highlighted in red), and there are misclassifications (mostly labeled as water) in regions where images are covered by cloud. Forest fires have

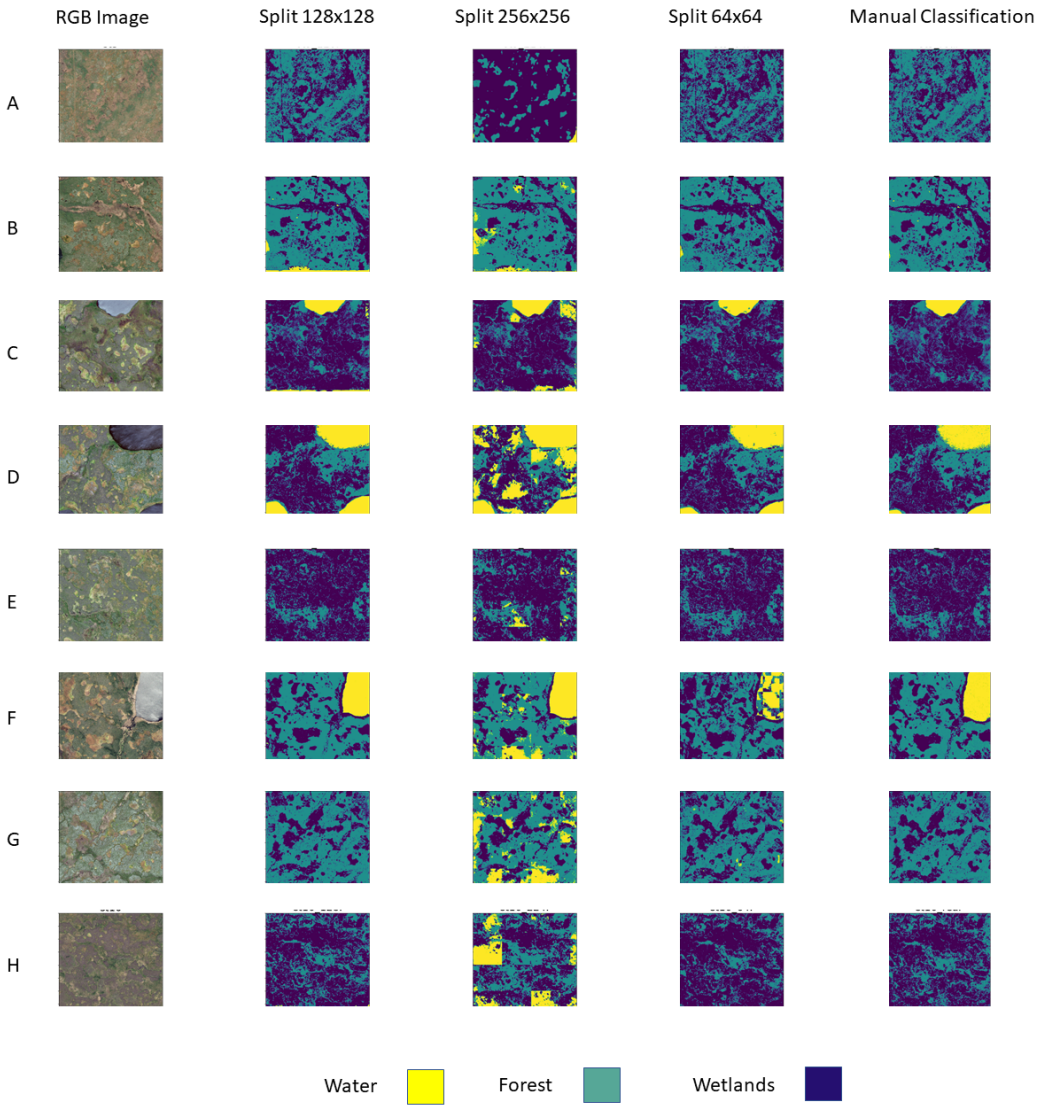

Figure 3.9: Results of semantic segmentation model on 800x800 snapshots from each area of interest; rows represent the image, and classified labels of each area of interest, and columns illustrate the performance of the model when the 800x800 snapshot is divided into different sizes

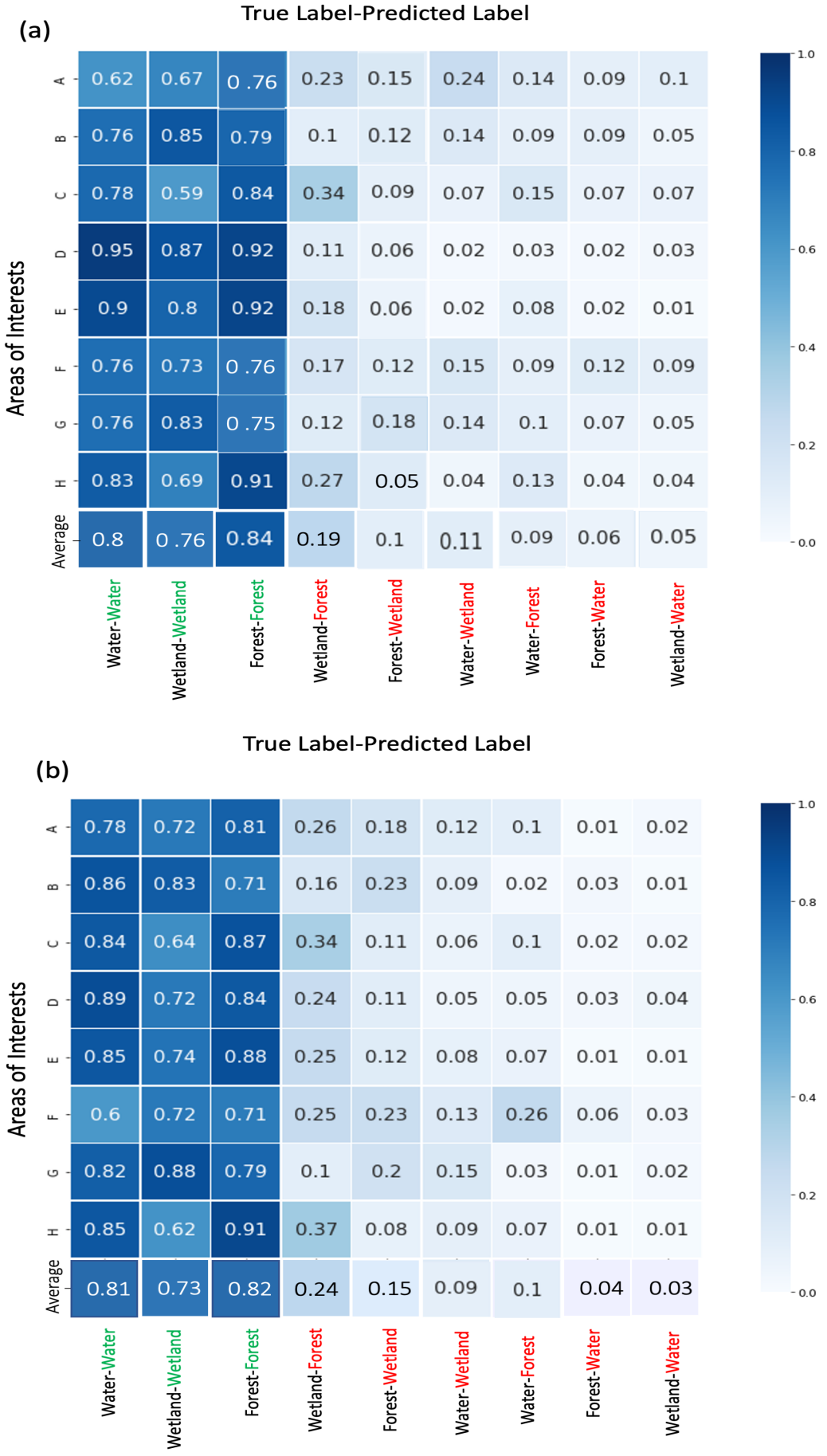

Figure 3.10: Summary of the Confusion Matrices generated for 800x800 snapshots of images (the normalized percentage of predicted classes divided by the total number of the true label) (Figure 3.5): (**a**) the 800x800 snapshot is divided to tiles of 128x128. (**b**) the 800x800 snapshot is divided into tiles of 64x64.

occurred in some of the NWT's discontinuous permafrost zones, and some of the AoIs are directly affected by them. The training procedure of TWINN was assessed for wetlands, waters, and forests except for forest fire. The TWINN solution cannot detect this type of land since the training data set does not include labels for forest fire since forest fire was not yet occurring in our case study at the time of the WV2 acquisition.

3.5.3 MLP Performance

Figure 3.12 presents the accuracy metrics used for the MLP model to evaluate its performance on the test data; the confusion matrix proves the high accuracy of the trained MLP model for categorizing fen and bogs based on their geometry. Figure 3.12 illustrates the spatial distribution of the predicted bogs which compares them to the labeled image to show some of the misclassified bogs generated by the MLP model (Figure 3.12.b).

The performance of the MLP model for categorizing wetlands as fens or bogs is evaluated by applying the model on AoI (B) from the selected AoIs, which shows a decrease in the accuracy of the model for identifying bogs (Figure 3.13) on this independent testing data set.

3.5.4 Watershed: Delineating the Contributing Area

Figure 3.14 illustrates the output of the developed Watershed() function using OpenCV library. The outputs of the TWINN solution are converted to a binary image(Figure 3.14); the value of one is assigned to wetlands, and the value of 0 is assigned to other land covers (Figure 3.14.a). The function incorporates the Distance Transformation function from OpenCV to generate the euclidean distance from the boundaries of wetlands to forest (the topographic maps) which is used as input in the final step (Figure 3.14.b). Figure 3.14.c shows the delineated runoff area of a snapshot of the Scotty creek basin.

3.6 Discussion

This study introduces a novel solution intended to classify readily available, often inexpensive, and multi-platform RGB imagery which simplifies and accelerates the processing steps for the classification of images. TWINN solution enables the classification of open water, fens, bogs, and forests in discontinuous permafrost landscapes, and the further delineation

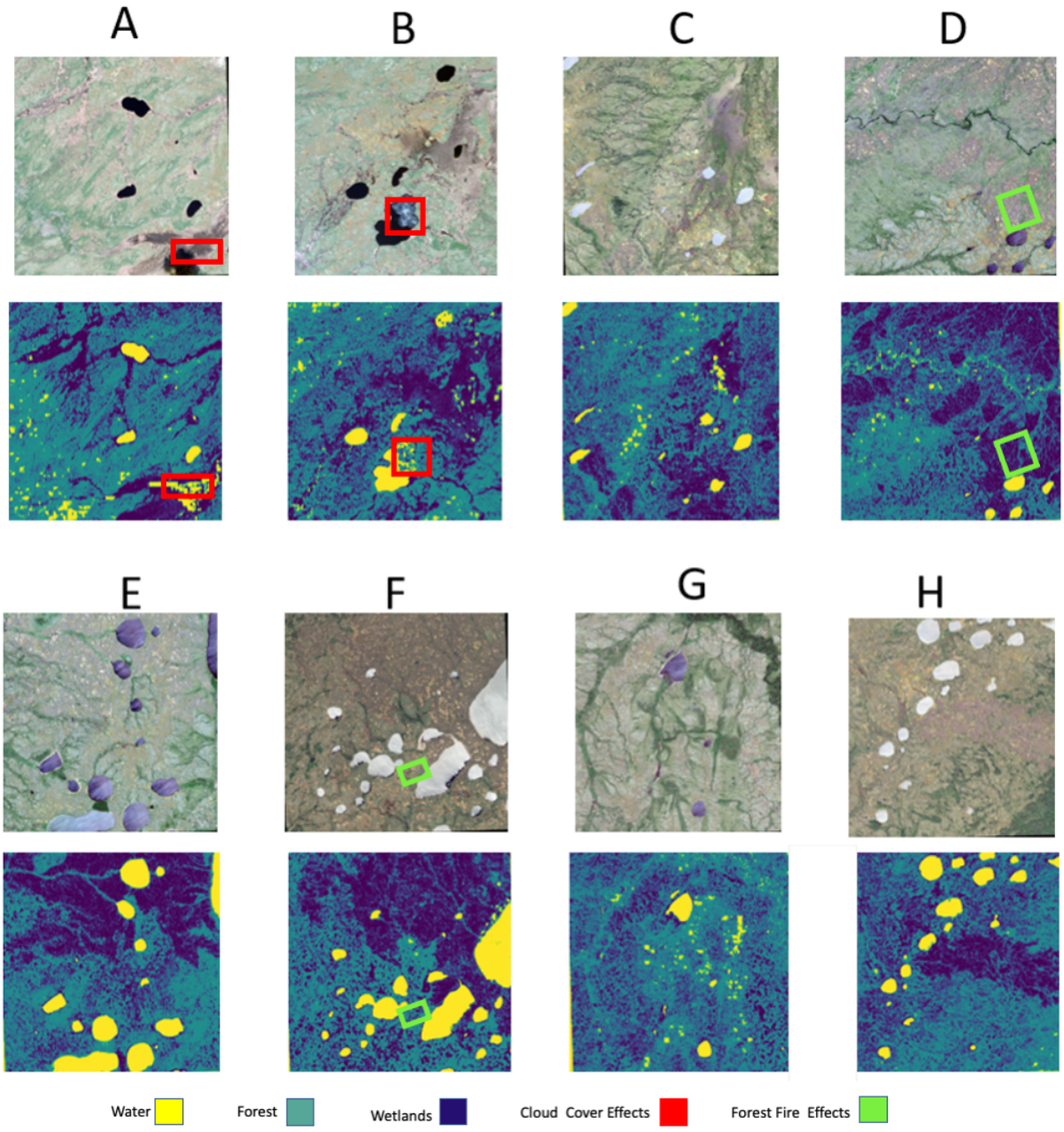

Figure 3.11: The original WV2 RGB images of the selected areas of interest and their segmented map generated by the semantic segmentation model

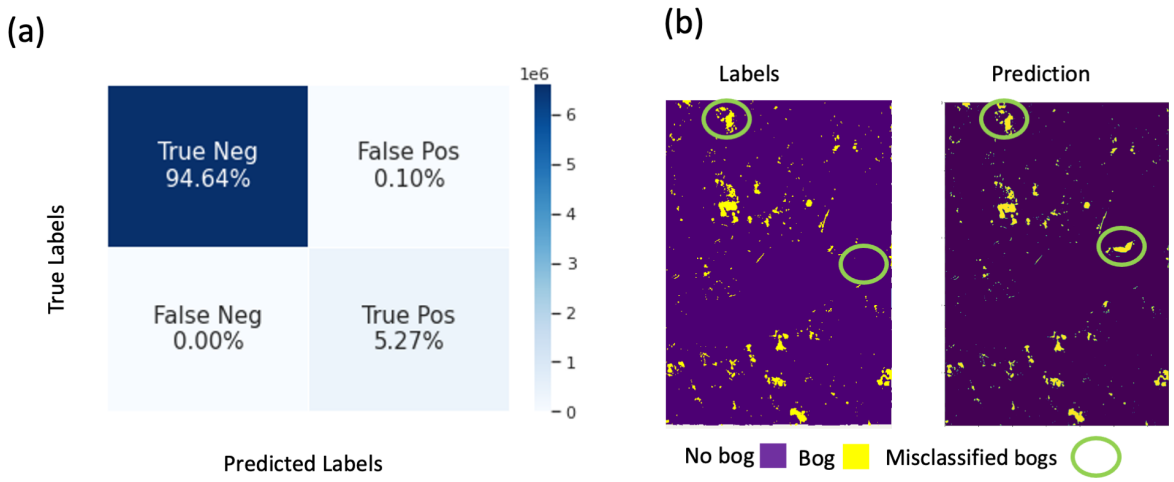

Figure 3.12: The results of the MLP model: (**a**) confusion matrix of MLP model evaluated on the test data set. (**b**) map of categorized bogs.

of runoff contributing areas for these features with minimal data requirements. Figure 3.15 briefly displays the automatic Taiga Plains wetland identification process using the devised TWINN solution. The final output of the model is a raster file delineating water, fen, bogs, and forest and a shape file including a polygon of the existing bogs and fens and the calculated contributing area for each polygon (Figure 3.15).

We found that the trained semantic segmentation model on step 1 was 97% accurate in identifying water, forests, and wetlands, and the trained MLP model was 98% accurate in detecting isolated bogs from other types of wetlands. The results of these evaluations confirm that deep learning methods are highly efficient in classifying RGB images of complex wetland areas. We also examined the effects of batch size and data augmentation on the semantic segmentation model's performance. It was concluded that the data-augmented models gave clearly better results than the models trained without data augmentation, and the data-augmented model with a batch size of 16 showed the best performance.

This best segmentation model was evaluated on 8 study sites in the extensive-discontinuous and sporadic-discontinuous zones of the NWT and northeastern British Columbia to evaluate the model's applicability to other discontinuous permafrost zones distributed in the NWT of Canada, which were outside the training data set.

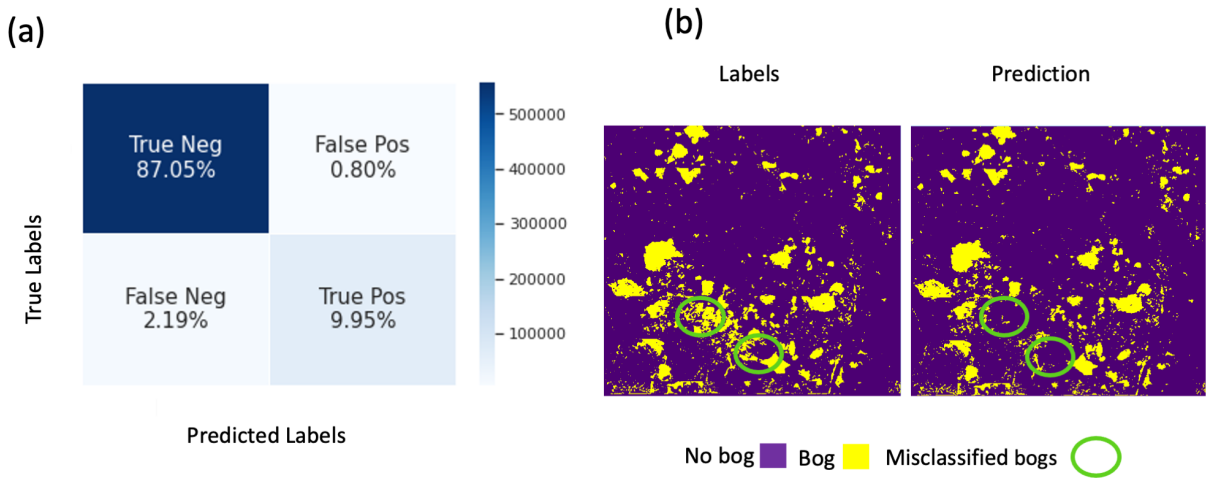

Figure 3.13: The results of MLP model: (**a**) confusion matrix of MLP model evaluated on the independent validation data set of AoI (B). (**b**) map of categorized bogs for AoI (B).

Despite only using RGB imagery, the segmentation model showed a good performance in identifying wetlands, forests, and water of other AoIs. However, the methodology was challenged by the presence of cloud cover, fuzzy or transitional boundaries, forest fire burn scars, and other features not present in the training imagery. Confusion in the classification methodology occurs at the transitional boundaries between wetlands and permafrost plateaus. These are areas that undergo cumulative seasonal and land cover change, and therefore have the ecological and hydrological characteristics of both peatlands and permafrost plateaus [105, 12, 22]; these boundaries are not discrete, rather they are 'fuzzy' boundaries, also noted in wetland hydro-ecology and remote sensing literature [36, 91]. In addition, TWINN suffers from a limitation that can only be applied to high-resolution imagery and has not been tested on data with coarser resolutions.

3.7 Conclusion

Here, we applied a semantic segmentation neural network model, a MLP, and a watershed algorithm to classify Taiga Plains wetlands of discontinuous permafrost zones and delineate their contributing runoff areas. The TWINN solution employed in this study generates

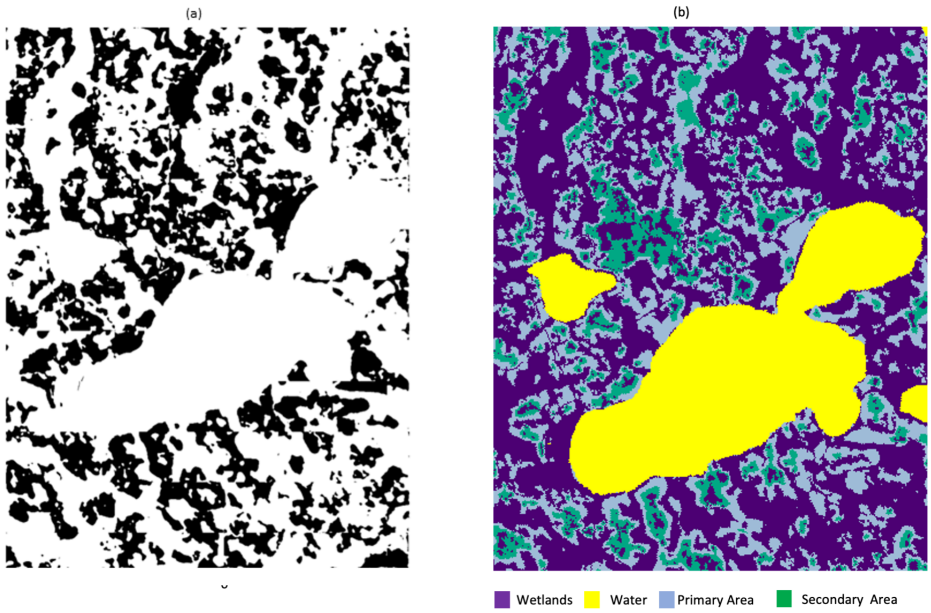

Figure 3.14: The output of Watershed function for delineating the contributing area of categorized bogs and fens: (**a**) binary image of the study area. (**b**) generated runoff area for each fen and bog.

classified maps that discriminate between isolated wetlands (bogs), connected wetlands (fens and connected bogs), and forested areas.

TWINN facilitates the application of CNN-Based techniques for wetland mapping by using only RGB images and can be used to delineate the runoff area of bogs and fens for hydrological purposes. This novel approach enables the incorporation of high spatial resolution images with limited spectral information (e.g., the NASA Arctic-Boreal Vulnerability Experiment or historical RGB aerial photography) within a framework for wetland classification. Accurate classification of land covers using inexpensive RGB imagery also provides an opportunity to use multi-temporal data to quantify wetland change over time, which largely includes photogrammetric/manual methods with single/few temporal images [129] or lower spatial/high temporal imagery [141].

Our results showed these techniques may be useful for the long-term evaluation of the thaw-induced land cover change due to climate change and for evaluating the hydrologic impacts of such change. Quantification of wetland areas and transitional zones (which may be impacted by cumulative climate-mediated and other disturbance factors) and the

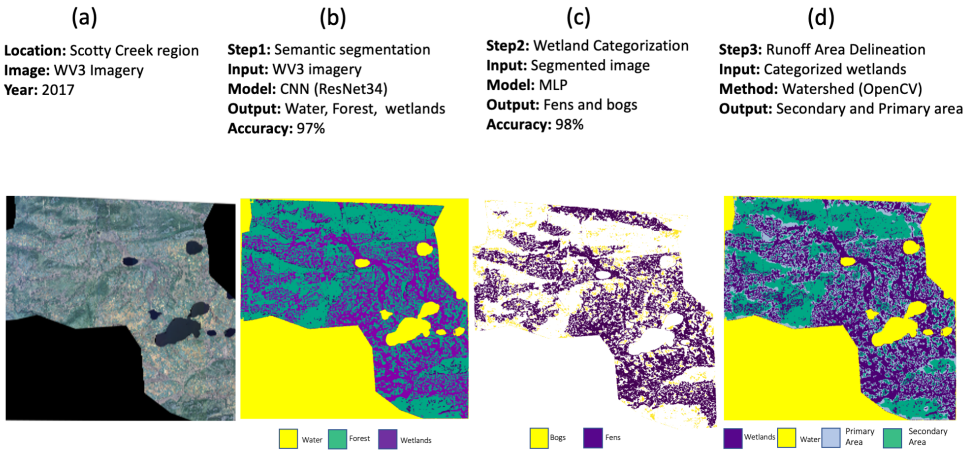

Figure 3.15: The process of hydrological wetland identification using TWINN: (**a**) The input image of TWINN solution (WV3 imagery of SCRS in 2017). (**b**) the first output of TWINN solution is a raster file presenting segmented water, forest, and wetlands. (**c**) the second output of TWINN solution is a raster file and a shape file, including bogs and fens. (**d**) the final output of TWINN solution is a raster file and a shape file, including wetlands primary and secondary runoff area.

potential to apply this method to other similar high-resolution imagery in the past/future is critically important, especially in northern environments that are undergoing rapid change. Such methods may also be used to inform local communities of changes and hazards using data sets that may require different platforms or sources [44].

This study presented a novel and useful approach for discretizing the runoff area of wetlands in lowland discontinuous permafrost zones, which has the potential to facilitate hydrological and ecological assessments in areas where digital elevation models do not provide sufficient information for runoff area delineation. However, it should be noted that the method assumes that the flow divides between the local contributing area of wetlands are equidistant to these adjacent wetlands. In reality, these flow divides are functions of complex local topography and, in some cases, subsurface permafrost topography. Such a simplification is necessary for regions where detailed topographic information is unavailable, and is likely to provide reasonable regional estimates of primary/secondary area cover, but will typically not be locally valid.

In general, the TWINN solution showed promising results for wetland mapping and hydrological assessments in northern environments, but the solution still has limitations that need to be addressed to improve its accuracy and applicability. The sensitivity of the TWINN solution to cloud cover, forest fire, and other land types not present in the training data increases the number of misclassifications in the final outputs of the model. Future research should focus on incorporating methods that can address these limitations, such as boosting the input data of the model from other data sources or refining the segmentation algorithm.

Additionally, the challenge of accurately classifying transitional boundaries between wetlands and permafrost plateaus is another concern that can lead to the inaccurate discretization of runoff areas. Exploring new approaches that can better handle these types of boundaries, such as designing new algorithms that can better capture the complexity of these transitions, may help to improve the accuracy of the TWINN solution.

Future research can be used examine the utility of this method applied to variable spatial resolution data to assess transferability and classification accuracy across scales. For instance, one could incorporate the CNN-Based approach for the classification of wetlands, water, and forest utilizing RGB bands of freely available satellite imagery, such as Landsat, Sentinel-2, CubeSats, and aerial photography. To improve the performance of ResNet34, we should consider optimizing hyper-parameters based on the architecture of the model used in this study . Addressing these limitations will be crucial for the development of more accurate and reliable techniques for wetland mapping and hydrological assessment in northern environments.

Chapter 4

Simulating thaw-induced land cover change in discontinuous permafrost landscapes

4.1 Introduction

The gradual thawing of discontinuous permafrost in the Northern Hemisphere has led to dramatic hydrological and ecological changes to wetland-dominated terrains, including an increase in baseflow [46], increases in runoff due to changes in hydraulic connectivity [30], alteration of lake drainage [96], and drastic changes in the land cover as permafrost alters the topography and water storage on the landscape [20]. This evolution has hydrological and ecological impacts, but will also impact the carbon and energy balance at the land surface, likely leading to further warming at both local and regional scales [111, 9]. Because of the important role of this evolving land cover, it is desirable to be able to simulate its long-term trajectory.

Wetland landscapes in the Taiga plains are generally rather heterogeneous, with variable forest and shrub cover, treed and untreed bogs, with minor elevation differences contributing to spatial variation in the water table, vegetation cover, and trophic status. While each of these criteria could be used to determine unique land cover classes, the initial focus of this research is predominantly on the hydrologic impacts of land cover evolution, and therefore we focus solely on the transitions between three hydrologically relevant land cover types (fen, bog, and permafrost plateaus) as done in [23]. Note that these terms do not strictly follow classic ecological definitions of fens and bogs; rather we use the terminology of [103, 31], whereby bogs are typically isolated vegetated water bodies with seasonal hydraulic connections, fens are the primary conveyance feature moving water downstream to the basin outlet, and permafrost plateaus are drier elevated landscape features (sometimes referred to as 'runoff generators' [106]) that drain to bogs and fens, but also impound water in bogs. As the permafrost melts beneath the plateaus, the edges of the plateaus get assimilated into the adjacent bogs or fens [94, 105]. Elimination of permafrost plateaus from between a channel fen or a chain of isolated bogs increases the runoff contributing area [130], leads to the transition of bogs to fen (termed 'bog capture') [30], influences the wetting-drying cycles of the ground, and changes the primary runoff characteristics of the landscape.

Because of the large spatial extent (>100 km^2) of wetland complexes and the complexity of the three-dimensional energy and water balance that determines local thaw and erosion patterns, it is likely infeasible to simulate long-term permafrost plateaus shrinkage using physically-based models. While there are a number of numerical models that support the simulation of local lateral permafrost thaw [63, 10], they have intensive data and computational requirements, which is why most earth systems models only simulate 1-D vertical permafrost freeze/thaw, known to be a secondary mechanism in plateau degradation [35]. However, both hydrological models and regional climate models will benefit from

reasonable long-term estimates of evolving land cover, as land cover influences not only runoff and net evapotranspiration but also net greenhouse gas production. We here focus on generating such estimates using machine learning methods trained on detailed historical observations of land cover at the SCRS in the Northwest Territories, Canada. Similar empirically-informed land cover models (LCMs) have been applied to simulate land use and land cover change [11, 122, 110, 113, 118] impacted by socioeconomic and environmental factors. Such methods have not yet been deployed for the simulation of natural land cover change due to permafrost thaw. It is hoped that such a model may both provide useful projections of long-term climate-induced land cover change but also potentially provide insight into the driving factors behind this change.

The primary goal of this research is to develop and test a TSLCM to simulate continuous land cover evolution induced by permafrost thaw and apply the TSLCM to predict land cover scenarios at SCRS from today to the future. We assess two distinct approaches: ensemble learning and logistic regression techniques, to determine which method is most robust in being able to replicate historical land cover observations without over-fitting over time. We apply a novel 'boosting' strategy based upon the ensemble learning approaches to make the most of our limited historical imagery (1970-2008) over a much longer future time period (2020-2120). The newly introduced means in which we use cumulative variables (time and accumulated land surface temperature) will be shown to be effective as compared to standard approaches which are mainly focused on incorporating spatial variables and the available data set (not boosting the data nor using scalar temporal input variables) [113, 11, 41].

4.2 Material

4.2.1 Case Study

The study area is the SCRS (61.3°N, 121.3°W), 50 km south of Fort Simpson in the Northwest Territories, Canada (Figure 4.1.a). It is located south of the McKenzie River in a wetland-dominated discontinuous permafrost zone. The landscape of the study region is composed of permafrost plateaus, fens, and patches of flat collapse scar bogs [23] (henceforth, bogs). The primary drainage system of the SCRS includes channel fens, open stream channels, and intervening lakes (Figure 4.1.b). The site has been the focus of continuous research into cold regions hydrology and ecology for more than 20 years [103], and benefits from the availability of classified land cover imagery over a period of 38 years from 1970 to 2008 [23, 105].

4.2.2 Data Acquisition and Processing

The TSLCM is designed to estimate land cover evolution from an initial land cover state over a specified time interval. It is both trained and validated against observed final land cover states over the same time interval. The key data requirement is classified imagery of a site (discriminating between the key land cover types of bog, fen, and permafrost plateaus). Four classified maps of SCRS were acquired for the years 1970 (1.1 m resolution), 1977 (0.53 m resolution), 2000 (4 m resolution), and 2008 (0.18 m resolution) using historical aerial photography, satellite imagery, and digital imagery to classify the main three land cover types for each year [23, 105]. The classified data was derived by spatial analysis of the remote sensing imagery of a 1 km^2 area of Scotty Creek [23]. All data were re-sampled to a spatial resolution of 3 m for consistency (Figure 4.1.d). [23] noted there are potential errors in edge delineation and feature detection using historical imagery and these errors lead to some misclassifications, which will influence our analysis. In Figure 4.1.c, the bulk evolution of land cover can be discerned, with permafrost plateaus generally thawing, laterally shrinking, and being converted to bog and fen.

The initial raster land cover maps are needed both to characterize the initial classification and to generate spatial metrics that are correlated with permafrost thaw for use as input variables to the machine learning model. These metrics are similarly calculated at a resolution of 3m. Because thaw occurs from the edge of each plateau inward, over a given time period areas near the interface between a plateau and bog/fen cover are more likely to transition between land cover classes than areas far from this interface. Thus, we chose the Euclidean distance of each land cover to other land interfaces as three of the spatially distributed input variables. This distance was calculated using the Euclidean distance tool in ArcMap(10.7) (Figure 4.2). Complicating the use of this simple metric alone is the occurrence of 'bog capture' [30]. Bog capture refers to the instantaneous hydraulic connection of an entire bog to the fen network once the impounding plateau between a bog and fen is lost, which often results in drainage of the bog or equilibrium of the water level between the two. With consideration of bog capture, locations within the same bog both near and far from a thin impounding plateau feature have near equal susceptibility to land cover change over a given time step. This is here handled by calculating (again, in ArcMap) a cost distance for each bog's and permafrost plateau's pixel to fen interfaces where the 'travel cost' is 1.0 within permafrost plateaus and 0.0 within bogs (Figure 4.2.d). This cost distance may be physically interpreted as the smallest width of the plateau that needs to thaw before a bog pixel is converted to fen.

Another known critical control on plateau thaw is the availability of melt energy. While the distribution of energy available for thaw can be quite complicated at the local scale and

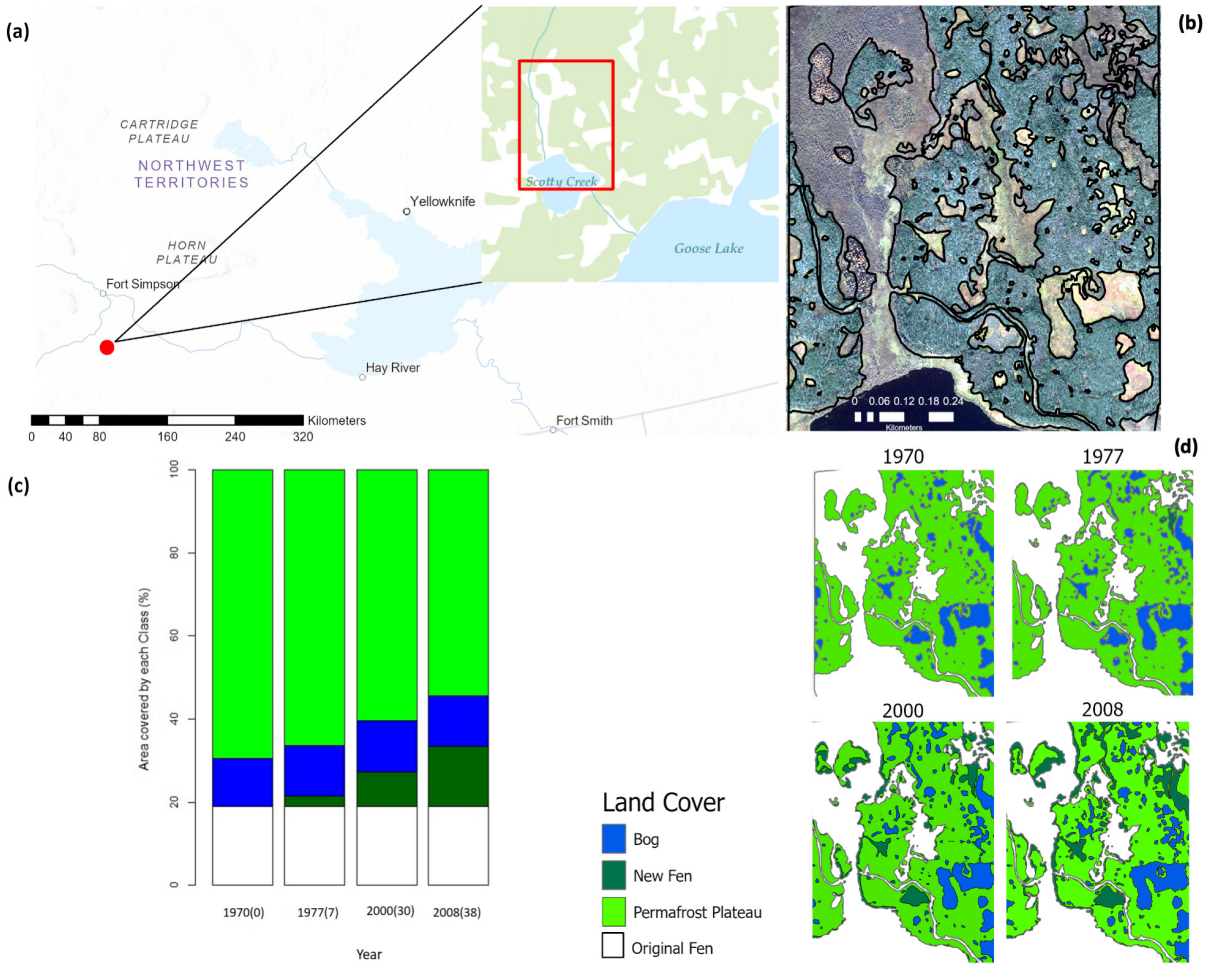

Figure 4.1: Location of the SCRS and the land cover maps; (a) Location of the SCRS in the NWT, (b) Imagery collected in 2010 and outline of the three dominant land covers, (c) Area covered by each land cover during each time step in initial data, (d) Classified map of the SCRS (1970, 1977,2000, 2008) ([23]).

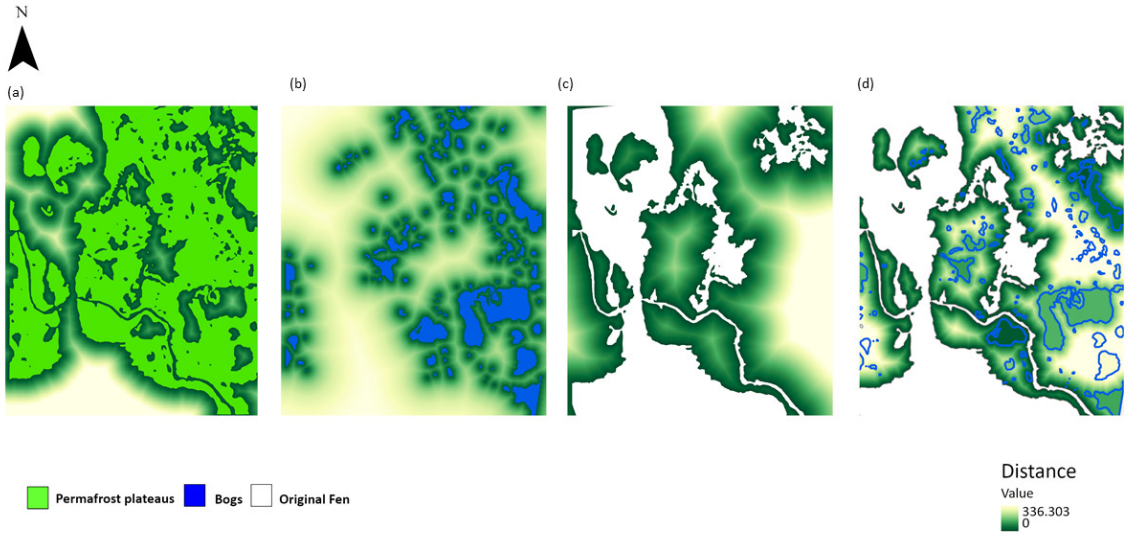

Figure 4.2: Geometric independent variables used for training the TSLCM: (a) Euclidean distance to permafrost plateaus, (b) Euclidean distance to bog, (c)Euclidean distance to fen, (d) Cost distance to fen.

is a function of air temperatures, water flow, incoming radiation, and advection [133, 34], we here solely consider the available data set of land surface temperature (LST) from the all the available series of Landsat Surface Reflectance, collection1 product. First, we filtered images with a threshold of less than 30% cloud cover; then, a cloud mask function based on the Quality Assessment (QA) band and an emissivity method algorithm are implemented in the Google Earth Engine to retrieve LST [66]. The LST values in this work are based on the Landsat Collection 1 Tier 1 data and all the available Landsat bands were resampled to a 30 m spatial resolution using the bicubic method in Google Earth Engine. The final results were verified by comparing the LST values against the temperature data measured using HOBO Shallow thermistors located at the edge of the fen (61.3083°N, -121.3083°W) collected by Elise Devoie. It should be noted that most of the derived images from Landsat are concentrated in the summer season since images with a high level of cloud cover are removed from the image collection. The summertime LST anomaly is estimated for each year, where anomaly refers to the difference between the mean domain LST and the local pixel LST. This indicates where locally warmer and cooler locations are while removing the impacts of inter-annual fluctuations in temperature. The calculated summertime LST anomaly does not show a noticeable inter-annual change, so we used the average value of all the available LST anomalies from 1970 to 2021.

The daily accumulated air temperature (i.e., the temperature time series integrated over time) is calculated by using historical climate data collected at nearby Fort Simpson (61.45°N, 121.14 °W) by Environment and Climate Change Canada. Note that time step and air accumulated temperature (which are spatially uniform) is the only time-dependent variables selected for use as input to the machine learning models.

It is recognized that other remotely sensed landscape properties such as soil moisture, Normalized Difference Water Index, Normalized Difference Vegetation Index, and elevation could potentially be used to inform the machine learning model developed here and may be considered in future studies. Here, we attempt to develop the model given the chosen inputs without examining the potential gains in performance by adding additional data sets.

Generating a data set for training the TSLCM requires a stack of raster data layers for each time increment. The vector of time increments corresponds to the set of pairwise time differences between observed imagery. In this case, the set of 4 observed images (1970,1977,2000, and 2008) yields 6 time increments (7, 8, 23, 30, 31, and 38 years), plus one zero-year duration training increment. Each stack includes a) a land cover change map and the initial land cover classification map, b) a set of geometric metrics and spatial attributes at the start of the time increment, and c) time-integrated information. Each pixel of the change map represents one of the nine possible combinations of starting and

ending land cover classification, which is denoted by a combination of the abbreviations for each land cover type. For instance, $P \rightarrow P$ indicates that the pixel was classified as plateau at both the start and end of the time increment, while $P \rightarrow B$ indicates that the pixel was classified as plateau at the start of the time increment and bog at the end. Similarly, $B \rightarrow F$ indicates that the pixel was classified as bog at the start of the time increment and fen at the end. The abbreviations P, B, and F represent plateau, bog, and fen, respectively. The geometric characteristics include Euclidean distance to the nearest fen, Euclidean distance to the nearest bog, Euclidean distance to the nearest permafrost plateaus, and cost distance to the nearest fen. All of these characteristics were calculated only for the starting year of the time increment, acting as 'initial conditions' for a forecast. Lastly, the time increment (in years) and mean air accumulated temperature over the time increment were included as spatially uniform variables. All stacks were transformed into a single data frame, where each row represents a pixel and each column of the data frame represents a variable.

The SCRS is covered by permafrost plateaus, fens, and bogs and the classified imagery of this region does not contain a uniform distribution of the three main classes. Using class-imbalanced data is a common challenge in machine learning modeling potentially leading to poor results and inclining the trained model toward the majority class [135, 52]. We used the upsampling class balancing technique to deal with unequal proportions of land cover in the observational data set. The upsampling technique synthetically creates data from the minority class (here, bog) and adds them to the original data set [13].

4.3 Modelling

Figure 4.3 illustrates an overview of the TSLCM implementation. The TSLCM methodology consists of two stages: (1) application of an ensemble learning (EL) or a Log-Linear Regression classification technique in order to generate synthetic data consistent with historical observations of land cover change (the 'boosting' stage), intended to overcome the data limitation problem; (2) fitting a machine learning-based classification model on the boosted data set to estimate land cover change over a fixed time step given any initial condition (the 'simulation' stage). At both stages, we will here identify a preferred (or 'best') option for which classification algorithm (ensemble learning or regression) should be used.

To avoid over-fitting in both stages, we shuffled the data set and randomly allocated 80% of the original data set as a training set to fit the model and the remaining 20% was used for evaluating the final model. All the implemented classification algorithms used on

the training data set are evaluated by a triply repeated k-fold cross-validation using the 'caret' package in R [61, 60]. The repeated cross-validation method divides the training data into k =10 folds and repeats the process of evaluation three times; after identifying the best model in hyper-parameter tuning, the performance of the final model will be analyzed on the test data set.

ensemble learning and logistic regression have been applied for land use and land cover change predictions [89, 18, 118]; the performance of these techniques is sensitive to the type of input variables (continuous, discrete, and categorical), and size of the input data. Moreover, each technique owns specific limitations. For example, despite the fast and efficient performance of EL methods in solving classification problems, one of the major limitations of using these techniques is that tree-based methods don't always perform well in forecasting a trend over time. There is no clear indication in the literature as to which technique is most likely to produce the best results for spatio-temporal modeling of land cover evolution happening in discontinuous permafrost regions. To address this knowledge gap, we compared the predictive performance of two ensemble learning techniques and logistic regression in modeling land cover change for permafrost-covered regions.

4.3.1 Ensemble Learning (EL) Models

Machine learning approaches have been widely used for both classification and regression problems in landscape modelling [132, 81, 53, 100]. In this study, we examine the performance of ensemble learning models such as bagging (Random Forest (RF)) and boosting (eXtreme Gradient Boosting (XGBoost)) techniques for spatio-temporal modeling of climate-driven land cover change using the 'caret' and 'xgboost' package [61, 60]. ensemble learning techniques are based upon ensembles of decision trees; each decision tree represents a flowchart of nodes (splits of the data set informed by if-else conditions) and leaves (the final output classification). ensemble learning models select the majority class predicted by all the trees as the final output for classification problems and take an average of all the predictions for regression problems.

RF is an ensemble machine learning model composed of a collection of parallel decision trees that are sampled by the bagging technique [17]. The bagging technique creates an ensemble of trees from random subsamples of the training data; each tree represents a separate ensemble member. The output of the model is estimated by averaging the predictions of all the trees. An alternative ensemble learning method, XGBoost, implements a boosting technique, which builds the ensemble member models sequentially. Each model corrects the mistake from the previous model to enhance the estimator performance in each step, then integrates the predictions sequentially.

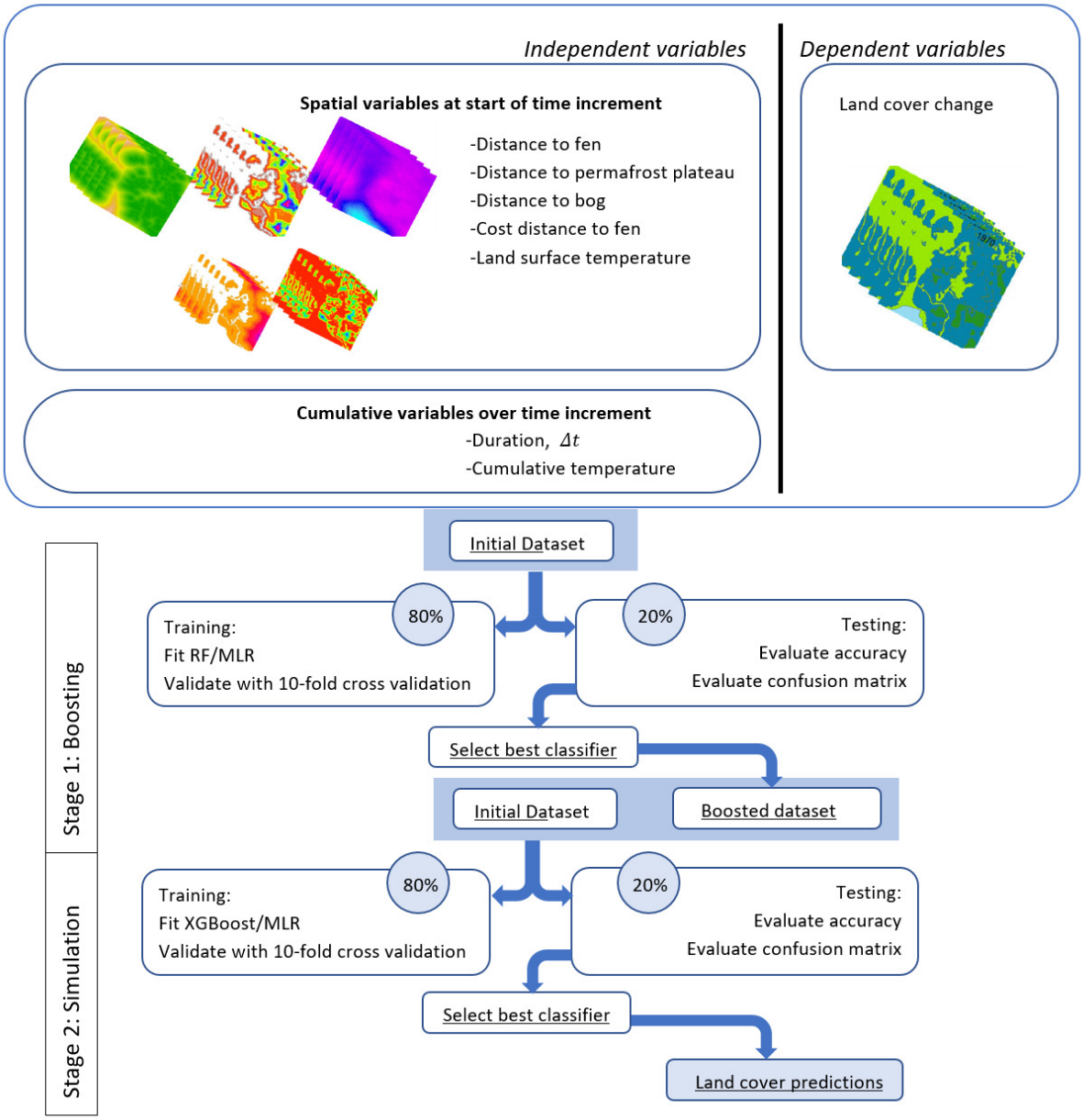

Figure 4.3: Process schematic of implementing TSLCM. The methodology includes two stages: 1) train the synthetic data model, 2) train the TSLCM.

In this study, RF and XGBoost hyper-parameters were tuned using the grid search function in the 'caret' package [61, 60] to improve their k-fold validation performance. The training process in RF model included tuning `ntree` (number of trees) and `mtry` (number of variables). For the random XGBoost model, the tuning algorithm adjusted both `max-depth` (the maximum depth of the trees) and `eta` (the learning parameter which controls the boosting process).

4.3.2 Multinomial Log-Linear Regression(MLR)

MLR is a technique for estimating the probability of occurrence for categorical data when the dependent variable of model includes multiple categories. The technique is similar to a logistic regression model but it predicts the likelihood of occurrence for each category. Here, the dependent variable (land cover change) $\mathrm{Y_i} \in \{n = 1, \ldots, \mathrm{N}\}$ include N categories, the probability that $i-th$ output can be written as [138]:

$$\pi_n^i = \Pr\{Y_i = n\}$$

In our case, π_n^i is the probability that pixel i will belong to the land cover category n at the end of the timestep. The calculated probabilities (π_n^i) depend on a vector of independent variables X_i (here, the spatio-temporal driving factors of land cover change). MLR fits $N-1$ logit equations in terms of the π_n^i which can be written as follows [90] :

$$\pi_n^i = \frac{\exp\left(\mathrm{X_i}\beta_\mathrm{n}\right)}{\sum_{\mathrm{S}=1}^{\mathrm{N}} \exp\left(\mathrm{X_i}\beta_\mathrm{S}\right)}$$

where β_n is a vector of regression coefficients for $n = 1, 2, ..., N-1$. MLR incorporated lasso regression regularization work to minimize the β_n of the less contributive independent variables toward exactly zero.

4.3.3 Synthetic Data Model for Time Series Prediction

Spatio-temporal forecasting of land cover category can be challenging when the input data is multivariate, and the limited training data is not enough to analyze the relationship between the time-dependent variables and the categorical outputs. To overcome the potential data limitation problems in extrapolating beyond the historical data, the initial data set was boosted by adding synthetic classified maps to the input data. First, we applied a RF and a MLR model on the initial data set to train a model for generating

synthetic data that represents the change of land cover in the SCRS for the time increments existing in the initial training set. The land cover maps for the added time horizons were created by combining the predicted land cover change maps (generated by the model with highest accuracy) and the real data (Figure 4.4). For example, the land cover change map for the 90 years time interval (1970-2060) is created by three consecutive time steps from 1970-2000 (from the actual data), 2000-2030 (predicted by the best model using 2000 as initial conditions), and 2030-2060 (predicted by the best model using the 2000-2030 result as initial conditions). To estimate the cumulative temperature for future years, we fitted an Auto-regressive Integrated Moving Average model on the historical climate data collected at nearby Fort Simpson (1970-2021) using the forecast package in R. The LST anomaly for future years was derived by averaging the available Landsat data over the last 15 years (2006-2021), and was assumed to be constant into the future. Without this boosting strategy, the prediction method would be unable to extrapolate beyond the largest time increment of 38 years. This approach enables support for continuous predictions in time, rather than only at fixed time steps.

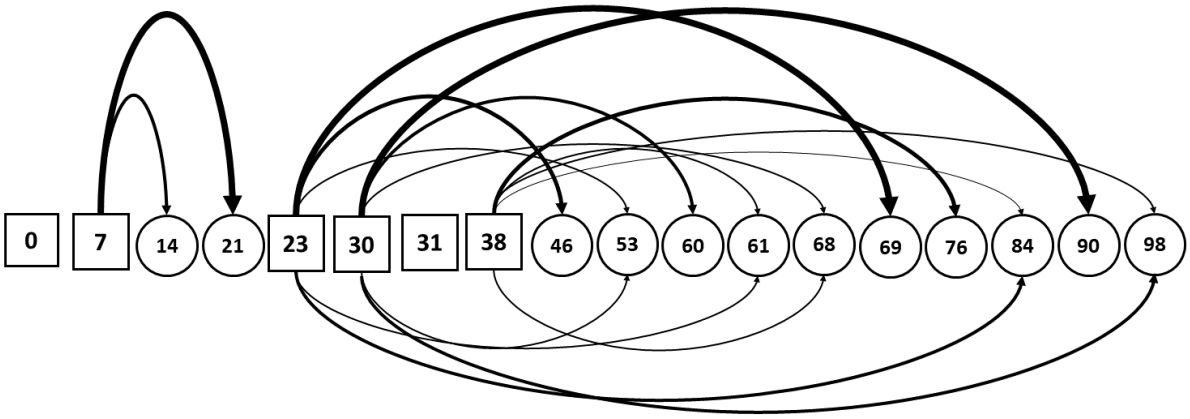

Figure 4.4: Boosting strategy for extrapolating long-term synthetic training data set from a limited historical data set. Boxed numbers indicate available years (since 1970) of observations. Circled numbers indicate synthetic data sets generated via repeated application of single-time increment land cover change, with increments identified from increments between original data sets.

After generating the synthetic data for the longer time horizons, a MLR, RF and an

XGBoost model were trained on the boosted data set to estimate land cover change over time. The XGBoost model is added to this step to compare the performance of bagging and boosting (XGBoost) techniques for predicting time series prediction of categorical data when the initial data set is boosted. This step is also sufficient to assess the relative performance of ensemble learning and MLR methods for simulating the land cover change.

4.3.4 TSLCM Summarized

The TSLCM handles a multi-class classification problem by considering the trend and location of change for each land cover through continuous time steps in two steps. The benefit of using a two-step approach with boosting is that long-term predictions (i.e., over the course of 100 years) respect the incremental change occurring over multiple smaller time increments and it improves the performance of the model for time interpolation or extrapolation. Without this boosting step, the relative importance of time and accumulated energy inputs (the key variants for encapsulating the impacts of climate change) would be diminished, and the model would only reliably estimate potential change over smaller time increments and just consider the role of spatial dependent variables.

The TSLCM is designed to predict the change when exceeding the known period in the input data set. In this study, we adopted the TSLCM to obtain land cover change over in SCRS until the year 2120.

4.4 Results

In this section, we assess the performance of all the implemented methods evaluated by three times repeated 10-fold cross-validation. We first quantitatively examine the performance of the synthetic data models in being able to simulate historical observed land cover trends over discrete time steps from 7 to 38 years. We then apply the TSLCM approach to extrapolate long-term land cover trends to 2120 and qualitatively evaluate the reasonableness of the predictions. To evaluate the historical performance of the classification models, we used classification accuracy, a metric that calculates the ratio of a number of correct predictions to the total number of predictions.

4.4.1 Synthetic Data Models

Figure 4.5 presents the confusion matrix of stage 1 for both the RF and MLR models trained on the historical input data for all intervals, as determined via three times repeated 10-fold cross-validation. The MLR method (Figure 4.5.a) achieved an accuracy of 87.5% and the RF model (Figure 4.5.b) achieved an accuracy of 95.16% for simulating land cover change, where accuracy is defined as the percentage of non-training pixels accurately assigned the correct land cover at the end of the time step. The confusion matrix of both methods illustrates that change in permafrost plateaus is predicted with higher accuracy than the change in other classes; the MLR model incorrectly classified 41.2% of fen pixels and 18.1% of bog pixels as permafrost plateaus (Figure 4.5.a).

To provide more extensive analysis of the performance of each model in separate time steps, the percentage of correctly predicted outcomes of the RF and MLR model for each time increment existing in the test data set is calculated (Tab.4.1). Based on the estimated percentage of correctly predicted fen, bog, and permafrost plateaus by RF model for each time increment, the trained RF model shows consistent performance in both short and long time steps especially for predicting permafrost plateaus and bogs (Tab.4.4.1), whereas the accuracy of MLR model improves rapidly from 5% to 60.1% in predicting fen cover over time (Tab.4.4.1).

(a) MLR

Time step (yrs)	Fen(%)	Bog(%)	PP(%)*
7	5	85.4	96.9
23	11.3	82.3	96.1
30	38.6	80.9	93.2
38	60.1	70.7	89.1

(b) RF

Time step (yrs)	Fen(%)	Bog(%)	PP(%)
7	87.9	96.3	98.9
23	93.8	96.5	98.8
30	94.8	96.4	98.7
38	95.6	96.7	98.3

*Permafrost Plateaus

Table 4.1: Accuracy of MLR and RF in separate time steps existing in input data set; (a) Predicted land cover by the MLR model for each time step, (b) Predicted land cover by the RF model for each time step. Each value represents the percentage of accurately predicted land cover classes.

Example results depicting the RF-predicted change in 2000 from an initial land cover condition in 1970 are presented in Figure 4.6. From these results, it is clear that the MLR model is not adequately capturing the observed patterns of historical land cover change in our observational data set, but the RF model results for this time increment are visually

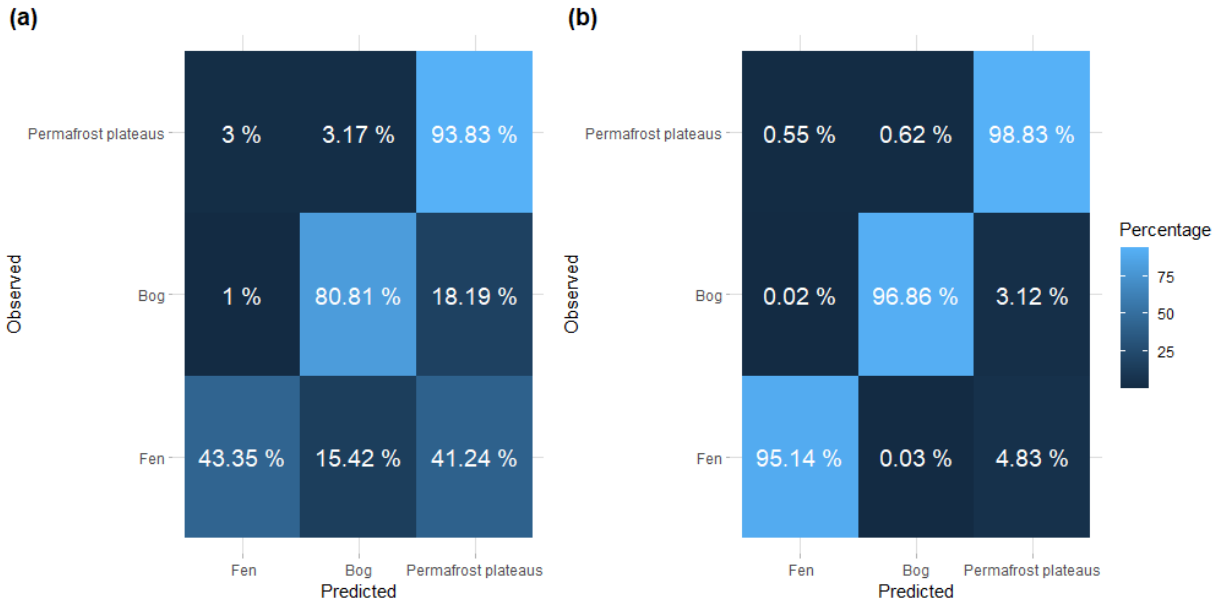

Figure 4.5: Statistical results of MLR and RF models trained on the initial data set for developing a synthetic data model; (a) Confusion matrix of the MLR model trained and tested on the initial input data, (b) Confusion matrix of RF model trained and tested on the initial input data.

similar to the observed land cover, with bog expansion and new fen established in the same regions across the map.

The spatial pattern of all three classes in each map shows that both methods adequately captured the observed relationship between distance to fen-plateau interfaces and land cover change (Figure 4.6). Permafrost plateaus closer to thawing edges of fen are more susceptible to transforming to fen, even though no explicit constraints were included in either the RF or MLR model to enforce this. However, it is clear that the predicted by the RF model is much more consistent with the observed land cover maps for the time horizons existing in the initial data set.

A key concern is that, despite the strong performance under historical conditions, the RF model may not perform well in predicting land cover change when the time increment is larger than those used in training. From Figure 4.7 we can see that, without amendment, the base RF model is unable to effectively be applied over longer time steps: the predicted landscape at 75 years is (unrealistically) nearly identical to that predicted at 150 years.

To assist the performance of the model for extrapolating past the historical observation period, we added more synthetic time increments to the initial data set by combining the predicted land cover change from RF model and the real data (the boosting step of Figure

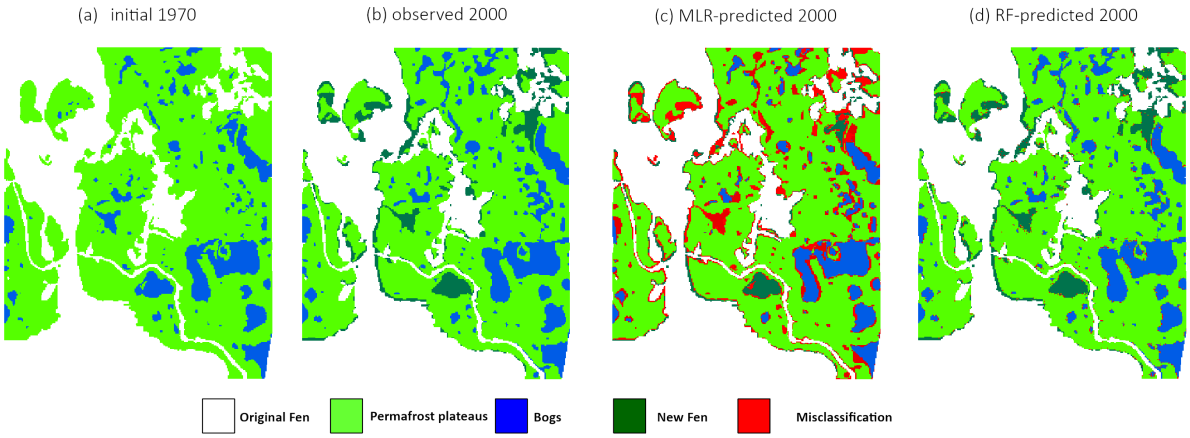

Figure 4.6: Land cover maps generated by models trained on the initial data set compared to the real data using a 30 year time step; (a) initial land cover map (1970), (b) observed 2020 land cover (c) Predicted land cover predicted by the MLR model for a 30-year time step, (d) Predicted land cover predicted by the RF model for a 30-year time step.

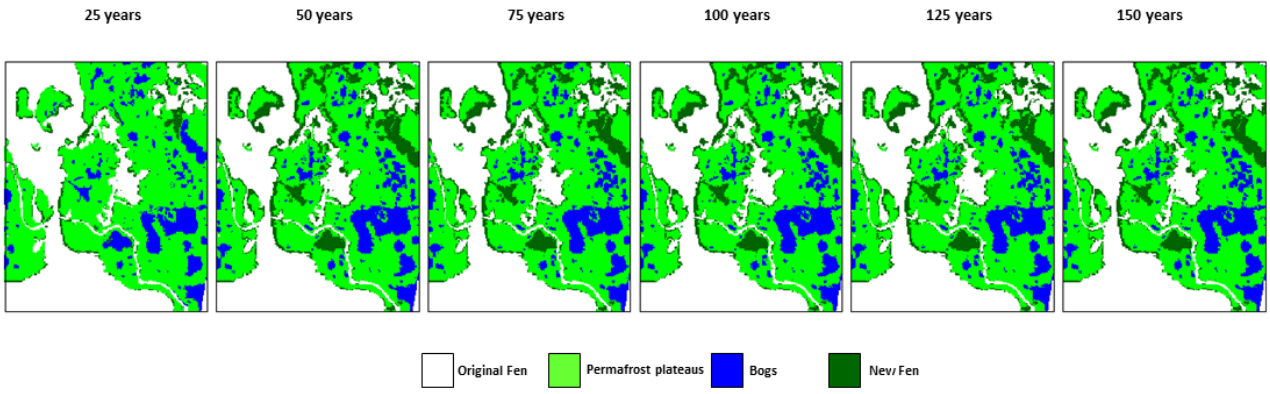

Figure 4.7: The predicted land cover change for 25, 50, 75, 100,125, and 150 time steps using the RF model without data boosting.

4.3). Figure 4.8 illustrates how the data for each new time step is created by repeated application of the single-increment simulated by RF model using initial conditions from observations or a previous simulation. This approach enables us to use a sparse data set of only N =4 images (1970, 1977, 2000, 2008) with $M = N(N-1)/2$ =6 increments to generate a host of (in this case 18) synthetic land cover images.

4.4.2 Final Model

After generating the synthetic data set used in extrapolation with the successful RF model (as demonstrated in Figure 4.8), a MLR, RF, and XGBoost method were evaluated for extrapolating land cover change to future conditions.

The confusion matrix for the three trained models as evaluated using test data set are given in Figure 4.9, illustrating the classification accuracy of each method on the three classes in this study. The overall accuracy of the MLR method on the historical test set of boosted data is 81.09% which is 7% less than the accuracy of MLR model trained on the initial data, but still inferior to the original RF model (Figure 4.9.a). The accuracy of both ensemble learning models were higher than the MLR: the XGBoost model achieved a high overall accuracy of 98.16% by running on the test set of boosted data (6% higher than the RF model) (Figure 4.9.c).

The output of each model was further evaluated for four specific time increments (Tab.4.2). Both MLR and RF exhibit an improved classification accuracy while predicting the change in fen over time (Tabs.4.4.2 , 4.4.2). The results indicate that XGBoost method is appreciably more successful in predicting the transition of each class at all examined time increments.

(a) MLR

time step(year)	Fen(%)	Bog(%)	PP(%)*
7	2.1	78.3	96.5
30	9.8	77.3	95.4
60	47.2	72.4	91.9
90	59.1	70.19	92.8

(b) RF

time step(year)	Fen(%)	Bog(%)	PP(%)
7	78.4	92.5	96.9
30	81.5	91.2	95.5
60	87.1	89.7	92.3
90	95.7	84.8	94.7

(c) XGBoost

time step(year)	Fen(%)	Bog(%)	PP(%)
7	95.1	98.8	98.2
30	97.9	98	97.6
60	96.8	97.5	97.2
90	99.1	96	97.9

*Permafrost Plateaus

Table 4.2: Accuracy of MLR, RF, and XGBoost for separate time increments existing in boosted data set. Each value represents the percentage of true positives for each land cover in a separate time step.

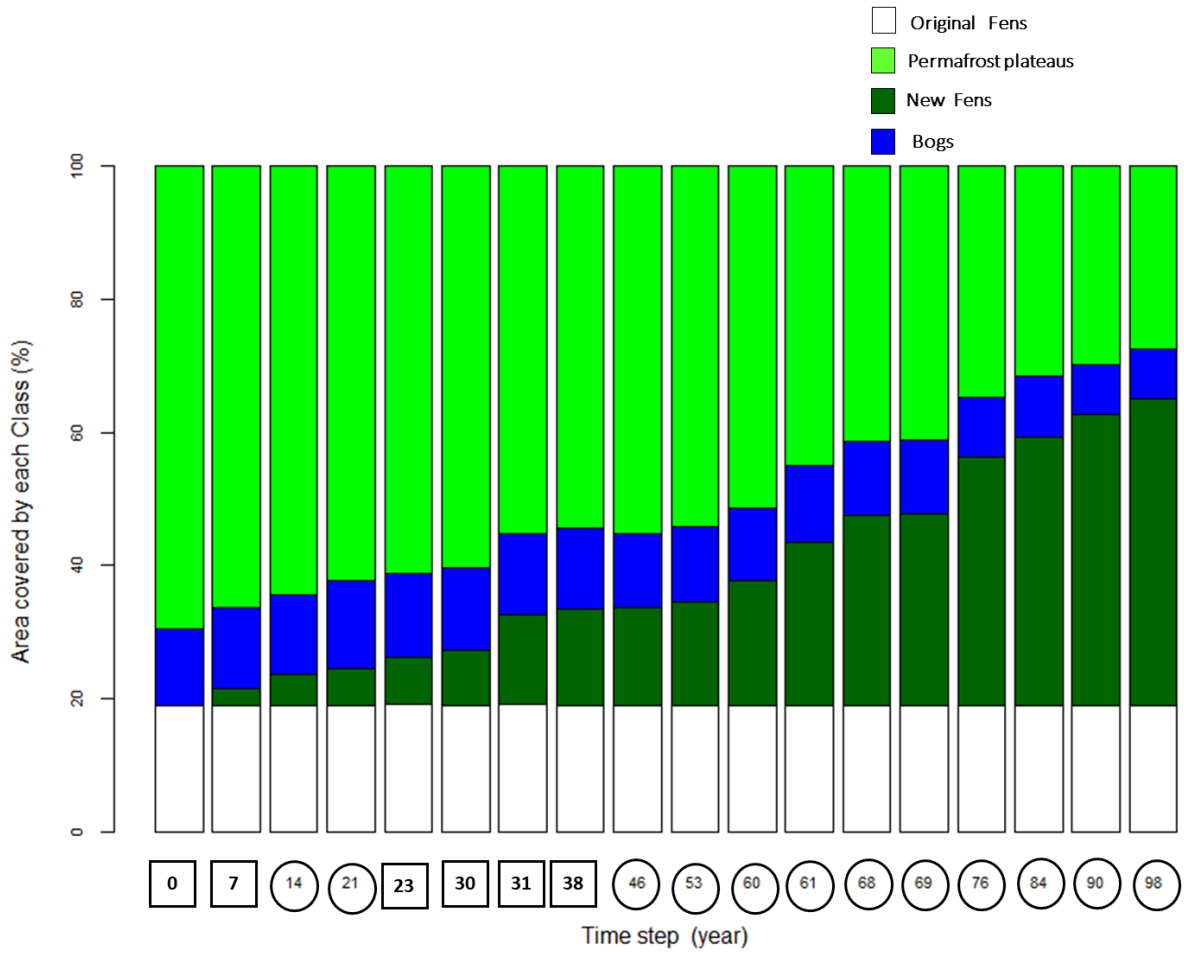

Figure 4.8: Visual depiction of boosting approach for extrapolating long-term synthetic training data set from a limited historical data set. Boxed numbers indicate available years (since 1970) of observations. Circled numbers indicate synthetic data sets generated by RF via repeated application of single-time increment land cover change, with increments identified from increments between original data sets.

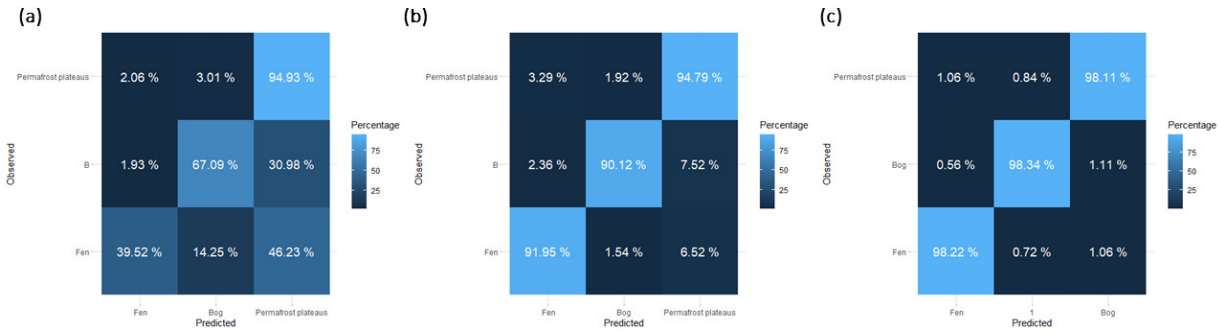

Figure 4.9: Ten-fold cross-validation results of the three machine learning models trained on the entire 18-sample boosted data set from 1977-2068, expressed as confusion matrices. (a) MLR model (b) RF model, (c) XGBoost model.

The pattern and degree of predicted land cover change by the XGBoost model is consistent with the observation data set (depicted in Figure 4.10). Statistically, the XGBoost and RF model outperformed the MLR in the terms of being able to replicate historical land cover.

Note that the final XGBoost model outperforms the original RF model in its ability to successfully replicate historical observations (98.16% accuracy vs. 92% accuracy for the RF model), which begs the question 'why do we even need the original RF model?'. However, the RF model (or an equally successful predictive model) is required to generate the boosted data set which is used to help train this XGBoost model.

The relative importance of each independent variable is quantified for the RF model using the 'varImp' function in 'caret' package [61, 60]. This function estimates the increase in the model's prediction error when the variable is shuffled or modified; the variable is considered unimportant when permuting does not affect the model's error [17]. The results showed that distance to fen, distance to bog, and cost distance were the three most significant variables contributing to the output of the RF model.

4.4.3 Accuracy and Consistency Assessment

To further understand the strengths and weaknesses of these predictive models, three additional tests were run:

1. Visual assessment of predictions out to 150 years (Figure 4.11), assessing the physical plausibility of future scenarios.

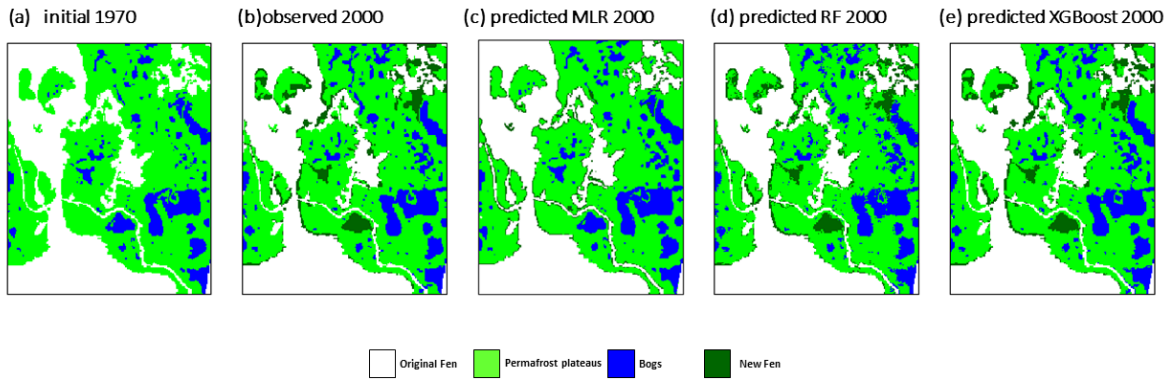

Figure 4.10: Observed and predicted land cover maps generated by models trained on the boosted data set compared to the observed data (year 2000 using 1970 initial conditions). (a) Initial land cover map (1970), (b) Observed year 2000 land cover, (c) MLR-predicted year 2000 land cover change (d) RF-predicted year 2000 land cover, (e) XGBoost-predicted year 2000 land cover.

2. Generation of a consistency map for each model to measure the model's ability to avoid non-physical oscillation between land cover types (Figure 4.12).

3. A comparison of the outputs of each model for four combinations of time steps which add up to 30 years (Tab.4.3), to assess the consistency of predictions with different time increments.

Figure 4.11 depicts the predicted land cover change from MLR, RF, and XGBoost methods for a 25, 50, 75, 100, 125, and 150-year time step, using the 1970 classified map as an initial condition. All three methods method clearly respect time as a controlling factor in land cover change (unlike the results of Figure 4.7 which did not use the boosted synthetic data). Although the accuracy metrics of the XGBoost model were higher than the MLR, the MLR was found to better respect expected physical trends when extrapolated into the future (Figure 4.11). For instance, it is clear that bog capture is not being respected in the major bog in the center of the plateau complex, with the RF and XGBoost models producing patchy new fen coverage. Similarly, these ensemble learning models both predict spotty fens emerging on wide plateau areas. In addition, comparing the simulated time series change by MLR (Figure 4.11.a) to XGBoost (Figure 4.11.c) and RF (Figure 4.11.b), it is clear that the rate of change slows for later years, with the time increment seemingly disregarded by the models. The MLR model more plausibly characterizes long-term changes.

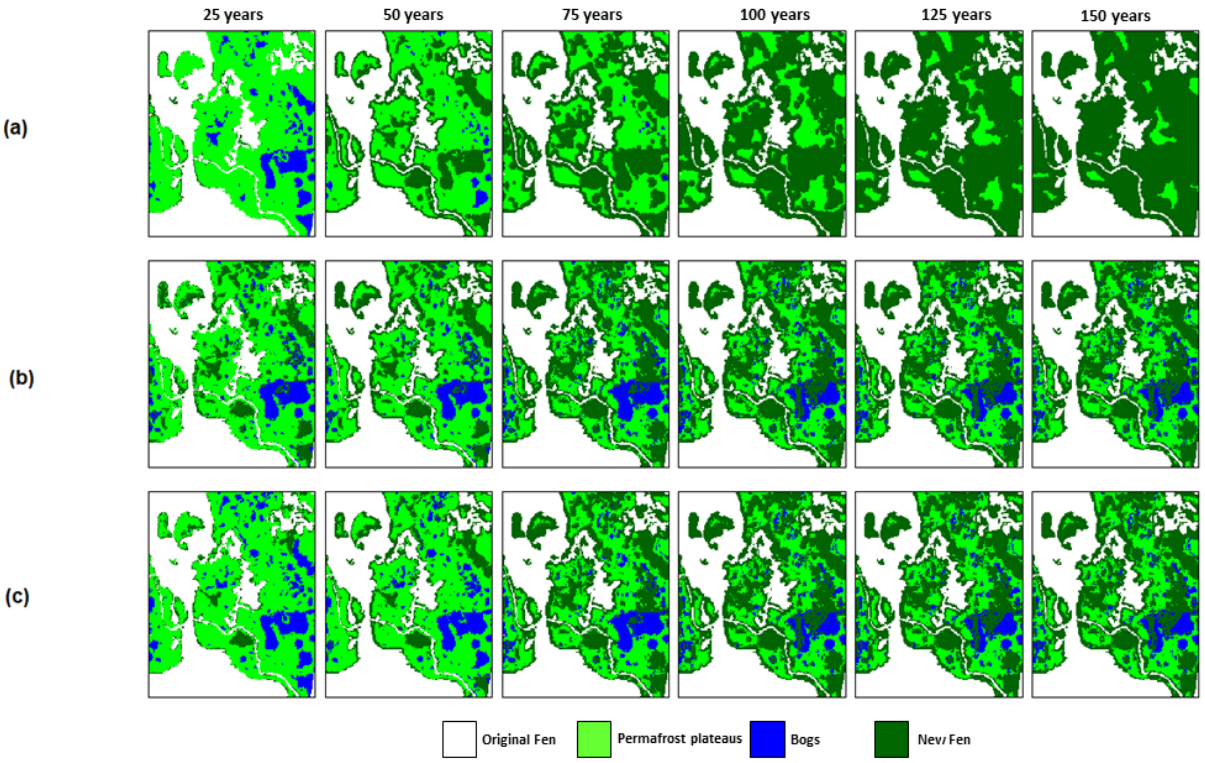

Figure 4.11: The predicted land cover change for a 25, 50, 75, 100, 125, and 150 year time increment; (a) The predicted land cover change by MLR, (b) The predicted land cover change by RF, (c) The predicted land cover change by XGBoost.

It should be noted that it is physically implausible to have certain repeated land cover transitions occur - the natural expectation is that plateaus will convert to fen and bog, and not that (for instance) we see a transition from fen to bog back to fen then to permafrost plateaus. To evaluate the consistency of each model while predicting the type of transitions over time, the models illustrated in Figure 4.12 were processed to generate the consistency maps of Figure 4.12. The values in Figure 4.12 reveal the total number of transitions over 150 years in each cell of the raster map simulated by each model. The expectation is that most of the landscape should experience between zero and two changes. All three models achieved a good performance in this regard: the highest number of transitions in 150 years is 5 which is happening in just 16 cells (the total number of cells in all three maps is around 150,000).

The final test examines the sensitivity of the model to time increment choice, as we have a choice as to how to propagate results forward in time. For instance, a 30-year time increment could be simulated all in one step, or by repeatedly running the model in 5-year increments. Ideally, these two approaches should generate similar predictions. Table 4.3 compares the outputs of each model using four combinations of time steps (whether or not it exists in the boosted data set) which add up to 30 years to observed transitions over a 30

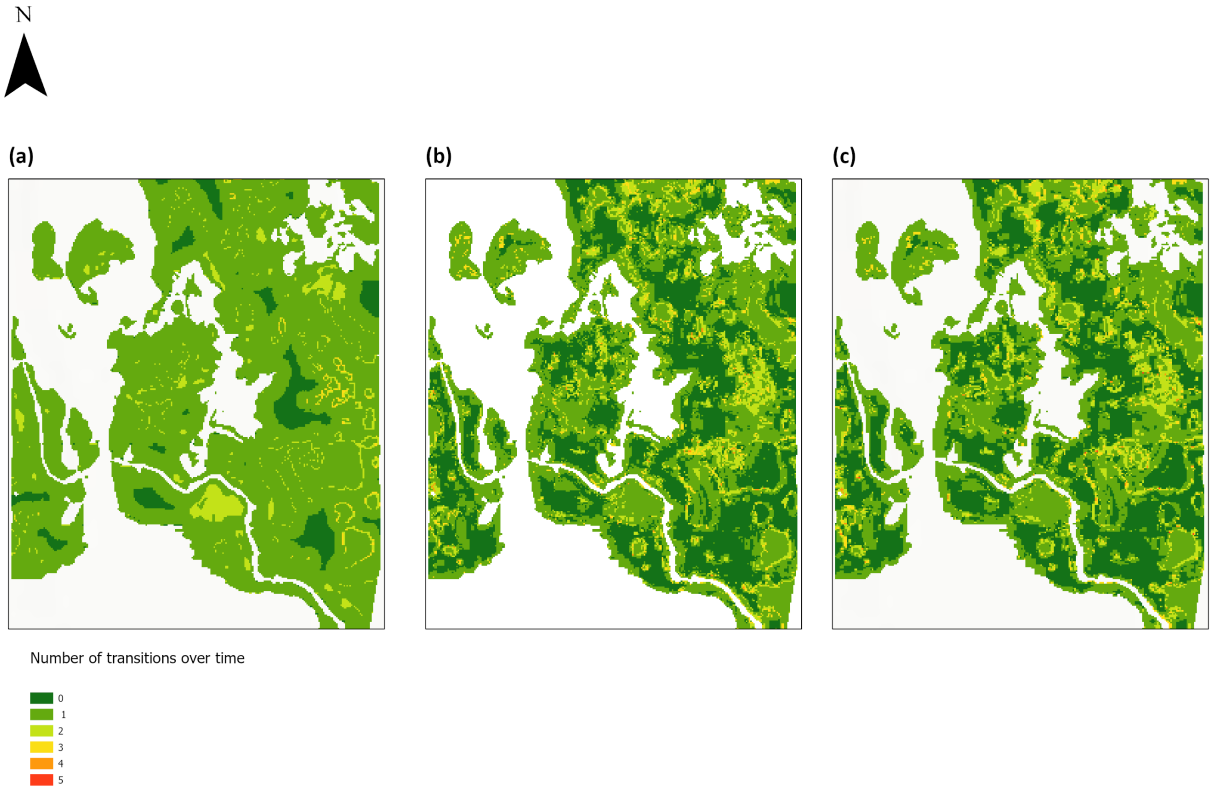

Figure 4.12: The consistency map illustrating the total number of transitions in each cell of the raster maps (representing SCRS) over a 150 years prediction. The consistency map generated by; (a) MLR, (b) RF, (c) XGBoost.

years time step. The RF (Tab.4.4.3) seems to slightly outperform the XGBoost (Tab.4.4.3) and MLR (Tab.4.4.3) model in predicting the change for all the four combinations of time steps.

(a)

combinations	Fen(%)	Bog(%)	PP(%)*
30(observed)	10.2	15.2	74.5
30	8.7	12.1	79.2
7+23	6.4	14.9	79.2
15+15	5.2	14.4	80.4
10+10+10	4.9	15.6	79.5

(b)

combinations	Fen(%)	Bog(%)	PP(%)
30(observed)	10.2	15.2	74.5
30	10.2	15.7	74.1
7+23	9.4	16.4	74.2
15+15	8.6	16.8	74.6
10+10+10	9.5	14.8	75.7

(c)

combinations	Fen(%)	Bog(%)	PP(%)
30(observed)	10.2	15.2	74.5
30	10.4	15.7	73.9
7+23	5.9	15.2	78.9
15+15	8.4	16.8	74.8
10+10+10	7.1	16.9	76

*Permafrost Plateaus

Table 4.3: Comparing the results of each model to 30 years of observed data for different combinations of time ; (a) Predicted land cover by the MLR model, (b) Predicted land cover by the RF model,(c) Predicted land cover by the XGBoost model. Each value represents the percentage of area covered by each class at the end of the 30-year increment.

4.5 Conclusion

A spatio-temporal multivariate land cover change model was developed and trained on continuous and categorical input data sets. The proposed model uses historical spatial data to infer patterns of change, which helps us to simulate future land cover scenarios subject to important environmental driving factors. This model is hoped to be useful in predicting hydrologically-important land cover transitions in discontinuous permafrost regions. Such models may be used, for instance, in the assessment of long-term climate impacts on the hydrology of the Taiga plains in Northern Canada.

This application was not data-rich - a key challenge was building viable predictive models informed by a limited number (here only four) classified historical land cover maps. Because of this limitation, we applied a novel data boosting strategy by first training multiple machine learning models to effectively simulate historical conditions, then stitching together a synthetic future data set from repeated single time-increment applications of the highest accuracy model (here, RF). This boosted data set was then used to train multiple predictive models.

The XGBoost model trained on the boosted data set proved to be the most accurate using basic pixel-by-pixel comparisons (98.16% accuracy vs. 92% accuracy for the RF model vs. 81% accuracy for the MLR model). All models demonstrated an acceptable

level of temporal consistency, as evaluated by counting the number of land cover changes experienced by each pixel in the images. The XGBoost model exhibited the lowest degree of sensitivity to time increment. It is expected that the models would significantly benefit from additional observed classified land cover maps in similar landscapes.

While there were differing long-term predictions provided by individual ML-based models, the predicted time series land cover maps consistently suggested that permafrost plateaus are transforming to fens and increase in the percentage fen cover will accelerate over time. The overall predictions of TSLCM are in accordance with other studies investigating the transition of land cover in the SCRS via field studies [105, 30, 63]. It has been reported that the permafrost plateaus are transforming to fen and bog over time which is also predicted by the TSLCM model. The rate of change is strongly dependent upon time and accumulated air temperature which depicts the critical role of temporal variables in any machine learning simulation strategy.

The TSLCM has been shown to be effective for predicting land cover change in the lowland discontinuous permafrost zones, such as the SCRS. However, it is important to acknowledge the uncertainties associated with the model's predictions and address them in future studies. The TSLCM's outputs are subject to limitations due to uncertainties caused by various factors such as the quality and quantity of the training data, the complexity of the model, hyper-parameter tuning, and the algorithm used for training the model. This study attempted to assess these uncertainties by analyzing the consistency in predicted land cover change over time (consistency map) and comparing different machine learning models' performance. To improve the accuracy of the land cover change models and reduce these uncertainties, future research should consider addressing these various sources of uncertainty explicitly during the process of training the land cover change model.

Another issue may arise when applying the model to other discontinuous permafrost regions. The spatio-temporal variables used to train the land cover change model primarily rely on distance-based variables, given that the main land cover evaluations in the SCRS occur in close proximity to the thawing edge of permafrost plateaus, which may not capture the full complexity of land cover change in other regions. Incorporating more driving factors of land cover change, such as vegetation and water index, in future studies may address these limitations and improve the model's generalization and performance.

Furthermore, the TSLCM has limitations in predicting the potential reversion of wetlands to forested land covers that may not be underlain by permafrost over time (depicted by Carpino et al. (2021) [19]). It also is unable to represent the formation of new wetlands in the interior regions of peat plateaus, which may occur when topographic depressions receive higher input energy than their surroundings. The input data of TSLCM

lacks information about these two transitions since the observed data only covers a period when both forest reversion and wetland formation are rare. To enhance the accuracy of the TSLCM predictions, future studies should consider this transition and the associated spatio-temporal variables that lead to the transitions from wetlands to forested cover regions. This will require additional training data capturing these phenomena.

Moreover, work in Chapter 5 will address the relative impacts of land cover evolution on the hydrology of the Taiga plains via hydrological modeling, using the TSLCM simulated land cover as inputs. This information will be crucial for effective land management and conservation efforts in cold regions.

Chapter 5

Hydrological Responses of Wetland-Dominated Basins to Climate-Induced Land Cover Changes in Discontinuous Permafrost Regions

5.1 Introduction

The transformation of a forest-dominated landscape into one dominated by wetlands and the resulting ecological changes have affected the hydrological responses of the basin [12, 105], including the runoff generation from permafrost plateaus [47], surface and subsurface hydrology [30], lake drainage [96], baseflow [46], and interconnectivity of drainage networks [14].

Due to the hydrological roles of channel fens (as a feature that conveys water), bogs (as a feature that stores water and may generate runoff when a storage threshold is exceeded), and permafrost plateaus (as a feature that generates runoff), these hydrological effects are controlled by the pattern and distribution of land cover. This pattern is changing over time. Connon et al. (2014) [30] and Haynes et al. (2018) [48] demonstrated that the transition from permafrost plateaus to wetlands increases the runoff from the discontinuous permafrost basins. A critical question is to what degree this trend will continue into the future due to changing climate.

The hydrological roles of fens and bogs may be examined by separating the landscape into secondary and primary runoff generating areas [30]. Primary runoff areas are those which drain directly to fens which release water to the basin outlet [47]. Secondary runoff areas drain to bogs, where the water may only be released to the outlet under wet conditions when the bogs hydraulically connect to the fen network. Therefore, fill-and-spill hydrological processes determine the runoff production from bogs.

It has been well established that the dominant land covers in these fen-bog-plateaus complexes play a hydrological role, and that the evolution of these land covers affects the hydrological and ecological properties of these discontinuous permafrost environments. Because of the importance of these long-term changes to land cover, it is still important for numerical hydrological models to be able to simulate these transitions.

Many studies have shown that land use change models and hydrological models can be coupled to provide decision-making tools, especially for assisting land-use decision-making [142, 126, 77]. Most relevant to this work, the study done by Stone et al. (2019) showed the effects of land cover change on wetland discharge in the Scotty Creek basin, NWT, Canada using a sensitivity analysis to assess the impact of permafrost loss on discharge from the sub-basin by reducing the ratio of wetland to plateau in the modeled sub-basin [116]. However, this reduction was not based on a predictive model of land cover change.

In order to accurately forecast the future of a study area, it is not sufficient to define land cover transitions by pre-defined or arbitrary ratios because they do not reflect the real transitions caused by climate warming. The shortcoming of these hydrological studies is

that the hydrological models are not informed about the transitions of the dominant land covers over time based on predicted future driving factors of change.

Furthermore, considering thaw-induced alterations in the runoff area of the wetlands is a persistent challenge for most researchers working on discontinuous permafrost regions of NWT. This analysis requires a method to calculate the primary and secondary runoff area of fens and bogs; it also requires land cover models which can adequately describe the lateral permafrost thaw impacts without explicitly (and expensively) simulating thaw processes.

To the best of our knowledge, no previous study has attempted to simulate the land cover change effects and the interaction between the hydrological role of the dominant land covers in discontinuous permafrost wetland regions by coupling hydrologic models and machine learning techniques.

This study aims to better understand how permafrost thaw-driven land cover transition from forested area to wetland affects the runoff responses of the Scotty Creek basin, both historically and under the future influence of climate change. Coupling hydrological models to the land cover change model developed in Chapter 4 can be used to quantify the contribution of land cover changes to the basin properties such as flood potential, soil water availability, or groundwater recharge. In order to evaluate the long-term impacts of climate warming on hydrology, we coupled:

1. A machine learning model of land cover change (a multinomial time series land cover model, or TSLCM, described in Chapter 4) [4].
2. A runoff area delineation method (the TWINN, described in Chapter 3) [3].
3. A hydrological model (the UWFS method), as implemented in the Raven hydrological modeling framework [120].

The coupled approach is applied to a case study of the Scotty creek basin, trained on the historical data, forced with multiple future climate scenarios, and used to assess the relative influence of lateral permafrost thaw on future runoff changes.

5.2 Case Study

Figure 5.1 depicts the location of the Scotty Creek basin (61.44°N, 121.25°W), in the NWT of Canada. This basin is located 50 kilometers south of Fort Simpson in the zone of

sporadic discontinuous permafrost (Figure 5.1a) and has a water survey Canada (Gauge ID 10ED009) at its outlet [134].

Based on remote sensing products and the generated classified maps of the Scotty Creek basin in different studies, as extrapolated from field studies [23, 106, 14, 114], the 129 km^2 basin is known to be comprised of permafrost plateaus, bogs, channel fens, and small lakes and ponds (Figure 5.1b). The average annual air temperature recorded at Fort Simpson for the whole basin is around -2.8 °C, and receives an average of 388 mm of precipitation each year with around half of it falling as snow (Environment and Climate Change Canada, 2017).

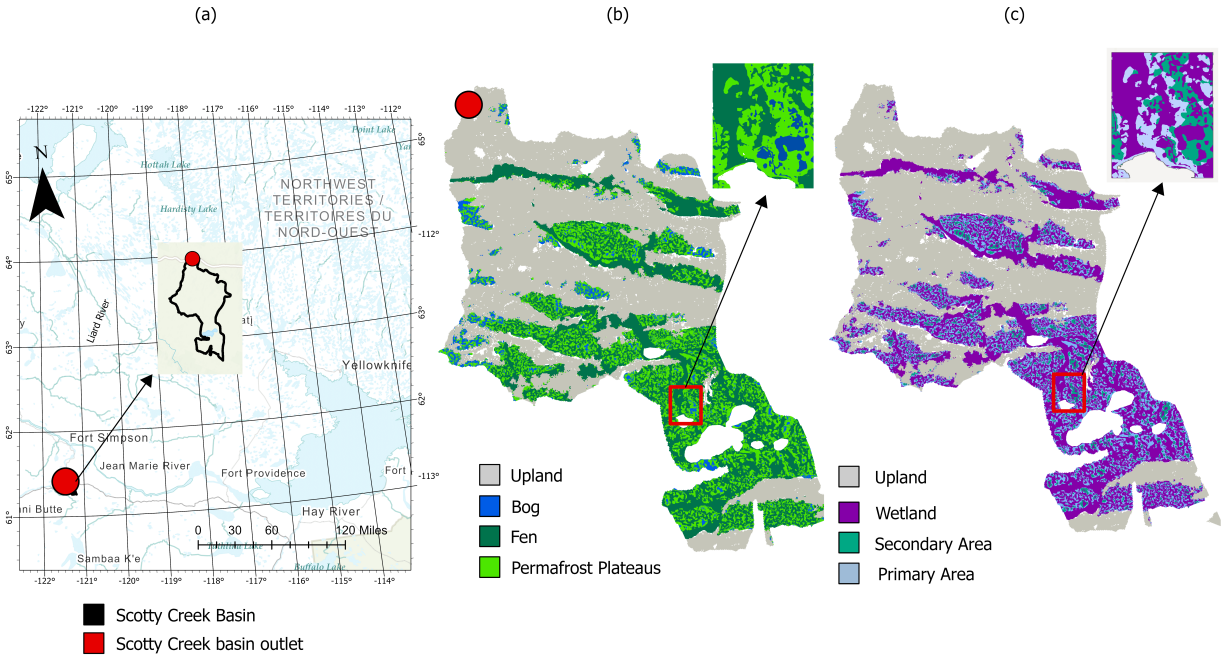

Figure 5.1: Scotty Creek basin: (a) The location of the basin within the Northwest Territories, Canada; (b) Land cover distribution of the basin in 2010; (c) Delineated runoff areas ([3]).

As a result of lateral permafrost thaw, the permafrost plateaus in the Scotty Creek basin have been decreasing in the area over time. According to research by Quinton et al.

(2010) [105, 23], the permafrost plateaus' higher elevation and the surrounding unfrozen wetlands are two primary factors causing specific thermal impacts leading to the loss of permafrost along the plateau perimeter. Duchesne et al. (2008) [38] estimated that 22% of Scotty Creek was covered by plateaus in the year 2000, and they forecasted a decline to 17% by 2055. Beilman and Robinson (2003) demonstrated a reduction of permafrost plateaus coverage by 22% during the previous 50 years in this area [14].

Channel fen and bogs play a significant hydrological function in the Scotty Creek basin [106]; the generated runoff from permafrost plateaus can flow into channel fen (primary runoff), discharge into the channel fen through a series of connected or cascading bogs (secondary runoff) or flow into an isolated bog where the water will be stored (Figure 5.1c) [30] and lost only as evaporation. Bogs are formations surrounded by upraised permafrost plateaus that store water and convey water to the fen only when overflowing (Figure 5.1c). They store water precisely because they are bounded by relatively impermeable permafrost. There are therefore inevitable hydrological consequences when the distribution and pattern of these three land cover changes.

5.3 Methods

This section describes the process of coupling the land cover change model and a hydrologic model for analyzing the effect of thaw-induced land cover change on the hydrologic response of the Scotty Creek basin.

5.3.1 Land Cover Change Model (TSLCM)

The TSLCM, as detailed in Chapter 4, is a tool that can simulate historical land cover transitions, capture temporal changes, and replicate the long-term evolution of land cover. It has been applied in this study to provide input data for hydrological models, allowing us to analyze the effects of climate change over the long term. Despite being developed within a specific training domain (a smaller subset of the Scotty Creek basin), the TSLCM is assumed to be scalable enough to be utilized in various case study locations within NWT's discontinuous permafrost zones.

The process of implementing the TSLCM is explained in Chapter 4, and it involves training a generative model using both Random Forest (RF) and methods. The generative model enhances the performance of the final TSLCM by adding more data to the initial dataset, thereby extrapolating time series changes. After boosting the observational data,

we employed MLR, RF, and eXtreme Gradient Boosting (XGBoost) models to simulate land cover changes. The MLR model was eventually selected as the best machine learning technique for the TSLCM as it can estimate land cover changes over a fixed time step, regardless of the initial condition. The input data of the TSLCM are presented in Table 5.1.

Table 5.1: The input data of the TSLCM

Variable	Source	Generation process	Reason
Estimated summertime land surface temperature	Landsat Image	Emissivity algorithm in the Google Earth Engine [3]	Plateau thaw is controlled by the availability of melt energy
Euclidean distance to land cover interfaces	Classified land cover map	Euclidean distance tool (ArcMap)	Interface between a plateau and bog/fen are more likely to transform to other land cover classes than areas far from this interface
Cost distance to bog	Classified land cover map	Cost distance tool (ArcMap)	Entire bog connects to fen instantaneously once the permafrost plateau between a bog and fen is completely lost (the 'bog-capture' phenomenon)
Accumulated temperature degree	Historical or forecasted climate data	Temperature time series integrated over time	Represents the net energy applied to the landscape over time
Time horizon		Ending year -initial year	Addresses temporal evolution

The TSLCM generates land cover maps that represent the spatial distribution of fen, bogs, and permafrost plateaus over time.

5.3.2 Hydrological Model (Raven)

A hydrological model of the Scotty Creek basin was developed by using the UWFS method in the Raven hydrological modeling framework [32]. Raven supports the development

of semi-distributed hydrological models which can capture the potential impacts of land cover evolution upon basin properties such as flood potential, soil water availability, or groundwater recharge.

In Raven, a basin can be composed of a number of subbasins. The subbasins are assembled from a number of contiguous or non-contiguous hydrologic response units (HRUs). HRUs are identified by unique combinations of land type, vegetation classes, slope, and aspect. In each HRU, for each time step, water is redistributed in response to precipitation and other atmospheric forcings.

The areas of HRUs in Scotty creek's model were determined from a land cover classification and a runoff area delineation map that indicated the extent of the permafrost plateaus, fens, bogs, primary runoff areas, and secondary runoff areas within the basin. The initial model configuration was based on 1995 classified imagery. Five HRUs were created in this model based on the distribution of five hydrologically important land covers in the Scotty Creek basin in 1995: water, upland, fen, secondary, and primary area. The energy and water storage within each HRU in the Scotty Creek basin is defined by storage variables that track the water content of the soil, canopy, and snowpack.

For the UWFS model to run, required forcing inputs included daily precipitation and maximum and minimum temperatures. These meteorolgical forcings are augmented with land cover transition data. The land cover transition over time represents the transition of primary areas to fens, secondary areas to fens, and secondary areas to primary areas at several time increments, with the percent cover of each land cover over time derived from the TSLCM. In primary runoff areas, runoff is shed directly to the fen. The secondary runoff area's abstraction process is defined by the UWFS method that incorporates lateral water movement (rainfall and rainfall excess including snowmelt and runoff) from the secondary contributing area to the bogs.

The UWFS categorizes secondary contributing areas into wetland cascades, which are groupings of wetlands that are serially ordered with one downstream connection to a surface water network [120]. The wetlands are treated as storage units that receive water until a threshold is reached, after which any additional water flows downstream. The total outflow from the most upstream wetland in a cascade can be derived based on the amount of water input minus the storage deficit as [120]:

$$O_1^* = \frac{A_u^1}{A_w^1} \cdot R + P' - D_1 = \beta_1 . R + P' - D_1 \tag{5.1}$$

$$O_1 = \max(O_1^*, 0) \tag{5.2}$$

The potential and actual volumetric outflow of a wetland are represented by the variables O^* [mm] and O [mm], respectively. These variables are normalized by the wetland area to simplify calculations and eliminate the need for wetland area values. The term "potential" is used because Equation 5.1 may produce a negative value, which cannot be considered as outflow. The local contributing area of the first wetland, excluding the wetland area, is represented by A_u^1 [L^2], while A_w^1 [L^2] represents the wetland area. The "local contributing area ratio," denoted by β_1 [-], indicates the relative size of the local contributing area and is defined as $\beta_1 = \frac{A_u^1}{A_w^1}$. The variable R [mm] represents the rainfall excess from the local contributing area, which is the remaining fraction of precipitation or snowmelt after other processes such as evaporation have been applied and can contribute to runoff. During snowmelt events, P' is equal to zero, representing rainfall over the wetland area. The wetland storage deficit is represented by D [mm].

It should be noted that when the local contributing area exceeds the wetland area by a significant amount, the wetlands' role in regulating the outflow becomes minimal, and the deficit term can be disregarded [120]. While the aforementioned equation is applied to a single wetland, the UWFS model treats the outflow probabilistically by considering the probability distributions of the contributing area ratio (β) and the deficit distribution (D), as discussed in [120]. This approach enables the treatment of systems comprising numerous bogs where detailed runoff characteristics of each bog cannot be characterized.

In this study, the hydrological model's performance will be evaluated by using available runoff historical data (1995-2015). For calibration and validation purposes, the simulation period has been separated into two parts: 1995-2010 for calibration and 2010-2015 for validation. Table 5.2 presents the range of selected parameters for the calibration process. The calibration process involves estimating the values of parameters. The Dynamically Dimensioned Search algorithm in OSTRICH was utilized with 2,000 iterations and 10 replicates to identify the most suitable parameters for simulating streamflow accurately [123, 74]. The parameters that led to the best model performance in streamflow simulation were chosen. The model's performance is measured using the Kling-Gupta Efficiency (KGE) metric:

$$KGE = \sqrt{(r-1)^2 + \left(\frac{\mu_{sim}}{\mu_{obs}} - 1\right)^2 + \left(\frac{\sigma_{sim}}{\sigma_{obs}} - 1\right)^2} \tag{5.3}$$

where r is the correlation between simulated and observed streamflow, μ_{sim}/μ_{obs} is the ratio of the mean simulated to mean observed streamflows and $\sigma_{sim}/\sigma_{obs}$ is the ratio of the simulated to observed streamflow variance. Percent Bias (PBIAS) is also another evaluation metric considered to analyze the model's performance, calculated as:

$$PBIAS = \frac{\Sigma_{i=1}^{n} X_i^{obs} - X_i^{sim}}{\Sigma_{i=1}^{n} X_i^{obs}} \tag{5.4}$$

where X_i^{obs} and X_i^{sim} are the observed and simulated streamflow; the acceptable range for PBIAS in simulation is typically less than 10-15% [86].

Table 5.2: UWFS parameters for calibration of the Scotty Creek hydrologic model [119]

Parameter name	Description	Units	Min	Max
RAIN_CORR	Rain bias correction factor	[-]	0.8	1.2
SNOW_CORR	Snow bias correction factor	[-]	0.8	1.2
RAIN_ICEPT_PCT	Relates percentage of throughfall of rain to LAI+SAI	[-]	0.02	0.2
SNOW_ICEPT_PCT	relates percentage of throughfall of snow to LAI+SAI	[-]	0.02	0.2
MELT_FACTOR	Maximum snow melt factor used in degree day models	mm/d/°C	1	3.5
SNOW_SWI	Snow bias correction factor	[-]	0	0.4
RAINSNOW_TEMP	Rain/snow halfway transition temperature	°C	-3	3
PARTITION_COEFF	Runoff fraction	[0..1]	0.5	1
GAMMA_SCALE	Gamma unit hydrograph scale parameters	[1/d]	0.1	20
MAX_PERC_RATE	Percolation rate	[mm/d]	0.01	1000
FIELD_CAPACITY	Field capacity saturation of the soil	[0..1]	0	1
BASEFLOW_COEFF	Linear baseflow storage/routing coefficient	1/d	0.01	1
FOREST_COVERAGE	Fraction of land covered by vegetation canopy	[0..1]	0	1
PET_CORR	Correction of PET	[-]	0.8	1.2
LAKE_PET_CORR	Fraction of PET to apply to open water evaporation	[-]	0.8	1.2
Parameters for secondary area:				
DEP_MAX	Maximum amount of water that stored in depressions	mm	100	450
MAX_DEP_AREA_FRAC	Percent of landscape covered by depressions when full	[0..1]	0.1	0.8
MIN_UWFS_BETA	Minimum concentrating factor	[-]	0	4
UWFS_B	Shape factor of concentrating factor distribution	[-]	0.01	10
Initial Parameters for secondary area:				
DEPRESSION	Initial amount of water that is stored in depressions	mm	50	250
MIN_DEP_DEFICIT	Minimum amount of deficit in each depression	mm	0	50

5.3.3 Coupling

The interaction between land cover evolution in the Scotty Creek basin and the hydrological responses will be analyzed by coupling three models, the TSLCM [4] (Chapter 3), the TWINN solution [3] (Chapter 4, and the Raven-UWFS hydrological model[120]. Figure 5.2 illustrates an overview of the coupling process.

The modeling process includes four steps:

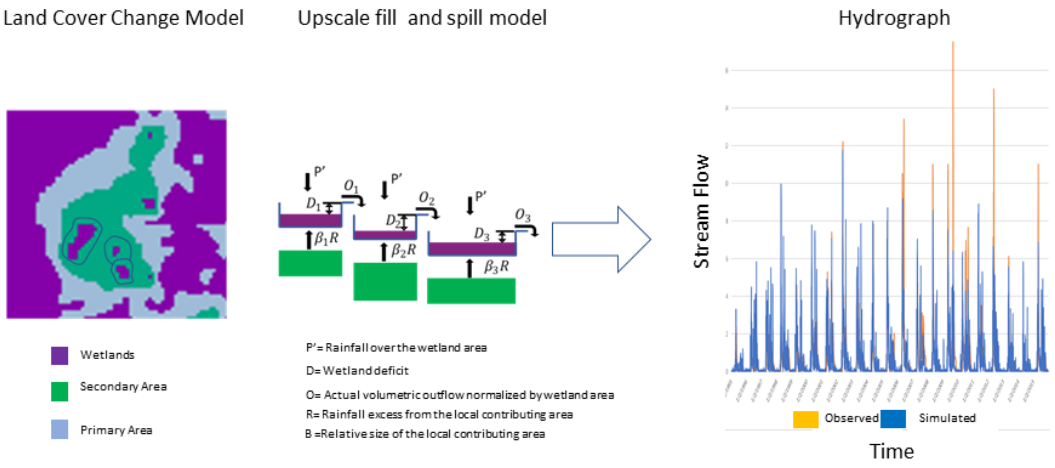

Figure 5.2: Process schematic of the coupling method presented in this Chapter.

1. Generate the classified maps of the Scotty Creek basin at five-year intervals utilizing the TWINN classification solution for historical evaluations. Next, delineate the wetlands' primary and secondary runoff areas present in the classified map.

2. Forecast the future changes in land cover within the Scotty Creek basin from 2010 to 2100 based on three distinct climate scenarios using TSLCM. Employ the TWINN solution to delineate the predicted wetlands' primary and secondary runoff areas for each climate scenario and GCMs.

3. Develop a hydrological model of the Scotty Creek basin in Raven using an UWFS algorithm and the generated historical land cover from step 1 and evaluate the model's performance in the validation period.

4. Analyze the effects of the predicted land cover transition by the TSLCM model on the runoff generation of the basin under three different climate scenarios using three different global climate models, with and without non-stationary land cover.

5.4 Data Preparation

5.4.1 Data Preparation: Historical Data

The TWINN solution was used to generate classified maps of Scotty Creek every five years between 1995 to 2015. The maps were generated using RGB bands of Landsat 5, 7, and 8 Level 2, Collection 2, Tier 1 data. These datasets were processed to remove any pixels with more than 2% cloud cover and then resampled to a spatial resolution of 30 meters using the Google Earth Engine platform.5.3.a).

It should be noted that the TWINN solution was trained and evaluated on high-resolution imagery only within 6 km^2 of the Scotty Creek basin (Chapter 4); In order to verify the accuracy of the historical land cover maps of the Scotty Creek basin generated by TWINN using Landsat imagery, the land cover map of 2010 was compared to the high-resolution classified map derived by Akbarpour et al. (2023) [3] using a World View 2 (WV2) image from the same year.

The Landsat image covering the Scotty Creek basin area in 2010 was obtained from Landsat 7 Level 2, Collection 2, Tier 1. The RGB bands were resampled to a spatial resolution of 1.6 m, using the bicubic method in Google Earth Engine to match the resolution of the WV2 image. According to the comparison results, the TWINN solution classifies about 6% of the permafrost plateaus as fen and 2% as bogs when using Landsat, especially on thawing edges of wetlands where the accuracy of the classifications is already uncertain [3].

By using the runoff delineation method of the TWINN solution presented in Chapter 4 of this thesis, the runoff area of the isolated wetlands (bogs) and connected wetlands (fens) was calculated for each 5 years time increment. The historical data of the land cover change in the Scotty Creek basin was then used to inform the Raven hydrological model to define the changing HRUs definitions over time. We used the historical daily streamflow measured at the Scotty Creek basin outlet (Gauge ID 10ED009) [134]. The daily precipitation data used for the development of the original Scotty Creek model and the temperature data were obtained from the same station at Fort Simpson from 1995 to 2015 (Gauge ID 2202103) [40]. The observation-based annual runoff and precipitation are reported in Figure 5.3.b.

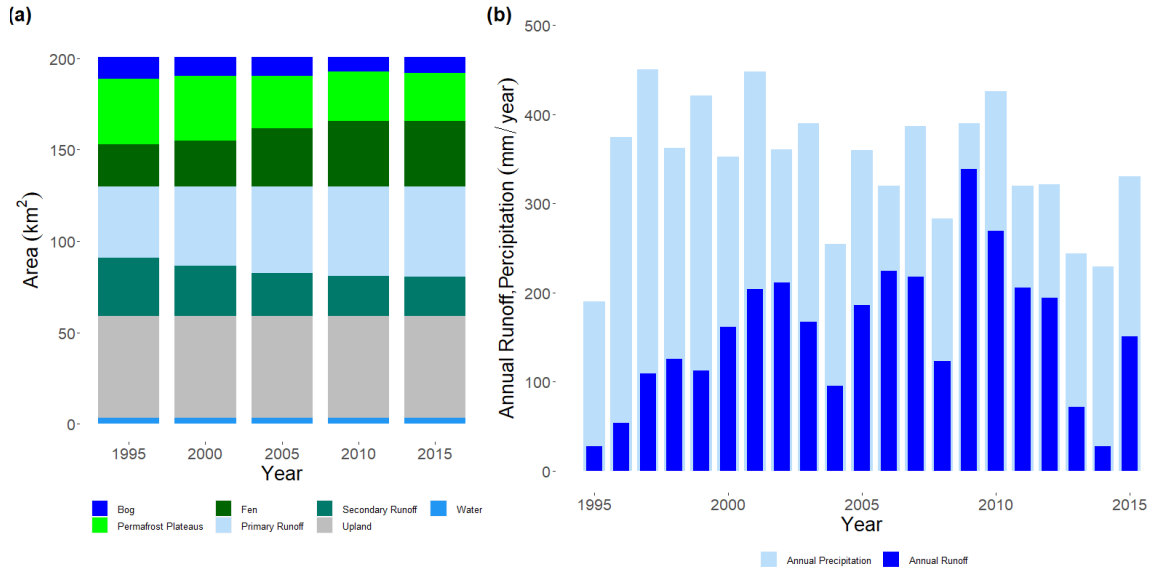

Figure 5.3: Historical land cover, precipitation, and streamflow within the Scotty creek basin from 1995 to 2015: (a) Distribution of dominant land covers in the Scotty Creek basin (1995-2015); (b) Annual historical meteorological data recorded at the Fort Simpson (Gauge ID 2202103) and runoff ratio from water survey Canada (Gauge ID 10ED009) (1995-2015).

5.4.2 Data Preparation: Climate Scenarios

To assess the long-term effects of continued warming due to the transitions of permafrost plateaus to wetlands on generated runoff, climatic inputs, and land cover transition predictions are required. Precipitation and temperature forecasts from 1995 to 2100 were retrieved from three GCMs under the three RCPs [127] from Coupled Model Intercomparison Project 5 (CMIP5) [92, 121](Tab.5.3).

The three selected RCPs (RCP2.6, RCP4.5, and RCP8.5) represent stringent, intermediate, and high Greenhouse Gas (GHG) emissions, respectively. The land use scenarios of the RCPs consider a wide range of future land cover changes. To address climate model uncertainty, three global climate forecasts for each of the RCPs were considered, as shown in Table 5.3. The decision to utilize three global climate models to address this uncertainty is motivated by practical considerations such as computational resources and time constraints. Running a large number of models for each scenario, especially for the TSLCM model, would be impractical due to its significant time and resource demands. While using only three models may not completely capture the range of potential outcomes, it does provide an estimate of the uncertainties associated with the modeled climate projections.

The transformation of dominant hydrologic land covers was predicted by the TSLCM

Table 5.3: Attributes of the selected CMIP5 GCMs [65]

Acronyms	Model	Institution	Resolution (lat/long°)
BCC-CSM1.1	Beijing Climate Center Climate System Model with Moderate Resolution	Beijing Climate Center, China Meteorological Administration	1.1215*1.125
MIROC5	Model for Interdisciplinary Research on Climate 5	Atmosphere and Ocean Research Institute, National Institute for Environmental Studies, and Japan Agency for Marine-Earth Science and Technology	1.4008*1.4063
GFDL-CM3	GFDL Coupled Model version 3	Geophysical Fluid Dynamics Laboratory(GFDL)	2.0*2.5

model over the 2010–2100 period using the forecasted temperature data for the three different scenarios with three GCMs. The classified map of the Scotty Creek basin in 2010 is incorporated to generate input variables for forecasting the land cover change including Euclidean distance to fen (2010), Euclidean distance to bog (2010), Euclidean distance to permafrost plateaus (2010), cost distance to fen (2010) (Figure 5.4). Figure 5.4 also provides a snapshot of the calculated cost distance values for a bog which shows when fen reaches the bog it captures all the bog's pixels due to the 'bog-capture' phenomenon.

Initial land surface temperature in 2010 is retrieved by applying the emissivity method presented in Chapter 3 using Landsat 7 Level 2, Collection 2, Tier 1 (Figure 5.4). The temporal input data includes time increments and accumulated degree days. The TSLCM model (developed in R) requires each input variable to be introduced to the model in a raster format. In the case of the Scotty Creek basin, this results in 51,000,000 pixels per variable. The computation cost of running the TSLCM model can be challenging, particularly when dealing with large study areas and high-resolution input data.

The UWFS was provided with information about land cover changes for every 30-year period starting from 2010, instead of reporting daily or yearly land cover changes. The magnitude of land cover change at this interval is more noticeable and significant than daily changes. Reporting daily land cover changes would result in a large amount of data, a time-consuming and expensive computational process that may not be practical to understand the long-term trends and impacts of land cover change on wetlands.

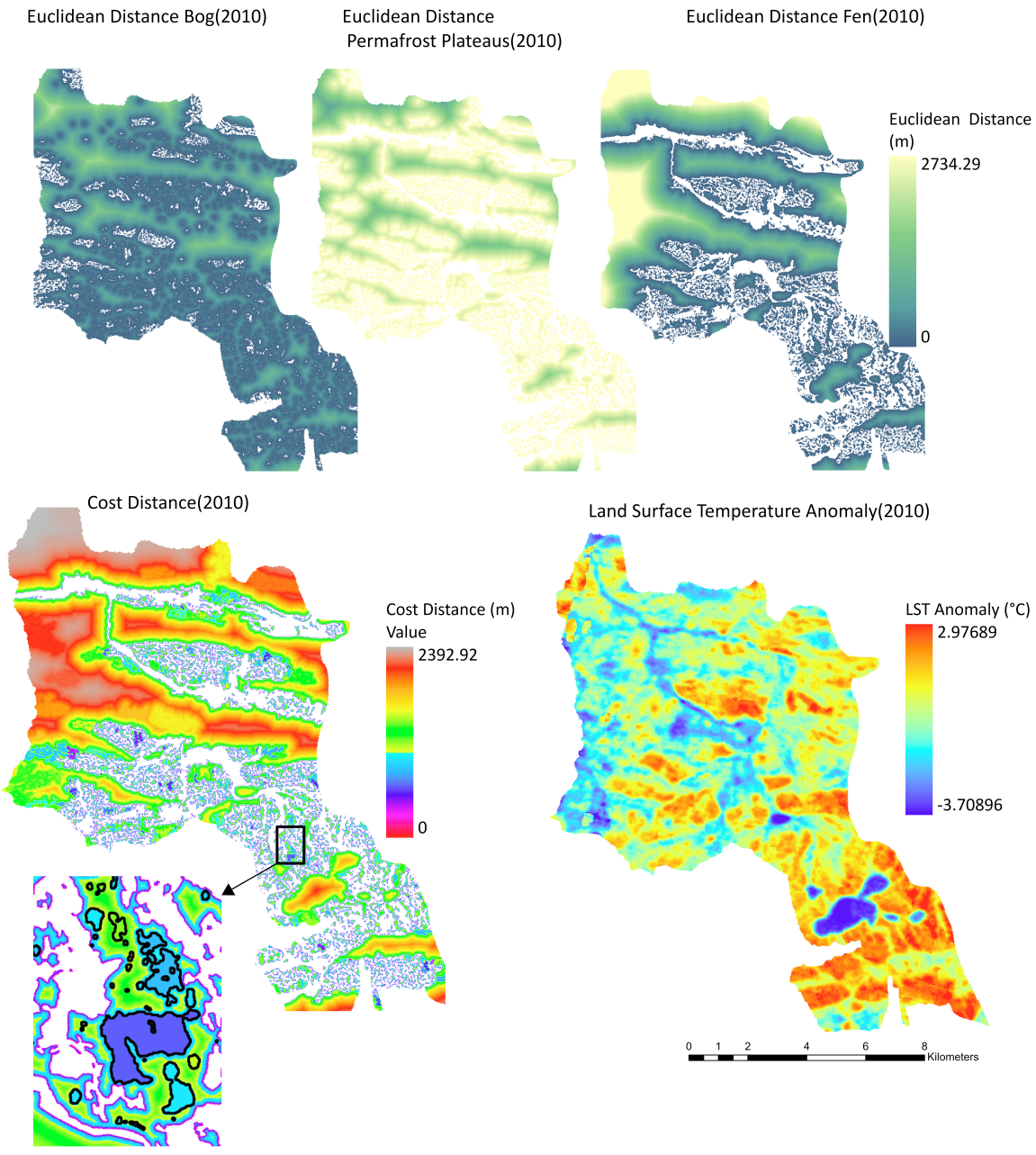

Figure 5.4: The spatial variables used by TSLCM for predicting the land cover change from 2010 to 2100.

Moreover, modeling land cover change for shorter time frames may not accurately capture the larger patterns of change and may be subject to more uncertainty. The generated classified maps for the years 2040, 2070, and 2100, under each climate scenario, were used to identify the primary and secondary contributing areas of the predicted wetlands. Changes in the runoff area can affect the basin storage, hydrological connectivity, and recharge in the Scotty Creek basin at various spatial and temporal scales.

5.5 Results

In this section, we report the results of coupling the TSLCM and Raven hydrological model for simulating the streamflow of the Scotty Creek Basin.

5.5.1 Calibration: Model Performance

The results of the simulated and observed streamflow for a selected snapshot (3.5 years) of the calibration and validation period are presented in Figure 5.5.

These results indicate that the hydrological model is capable of accurately simulating high flows, with a KGE metric of 0.77 and PBIAS of 5.43% for the calibration period (1995-2010), as shown in Figure 5.5a. Despite the generally good performance of the hydrological model shown in Figure 5.5b, the model overestimates the flow during low-flow events and tends to overestimate the peak flows. The simulated streamflow from 2014 to 2015 in Figure 5.5.b illustrates an example of the overestimation of peak during a low-flow event. The validation results reach a similar quality result with a KGE of 0.65 and PBIAS of 1.46%.

5.5.2 Climate Scenarios: Land Cover Change

Figure 5.6 depicts the simulated land cover change from 2010 to 2100 predicted by the TSLCM model for GFDL-CM3 climate model under RCP8.5. Based on the land cover change predicted for other GCMs, it is important to note that these values are also within the range of GFDL-CM3 climate model.

The predicted transient land cover maps generated up to the year 2100 suggest that in general permafrost plateaus are transforming to fens and the increase in the proportion

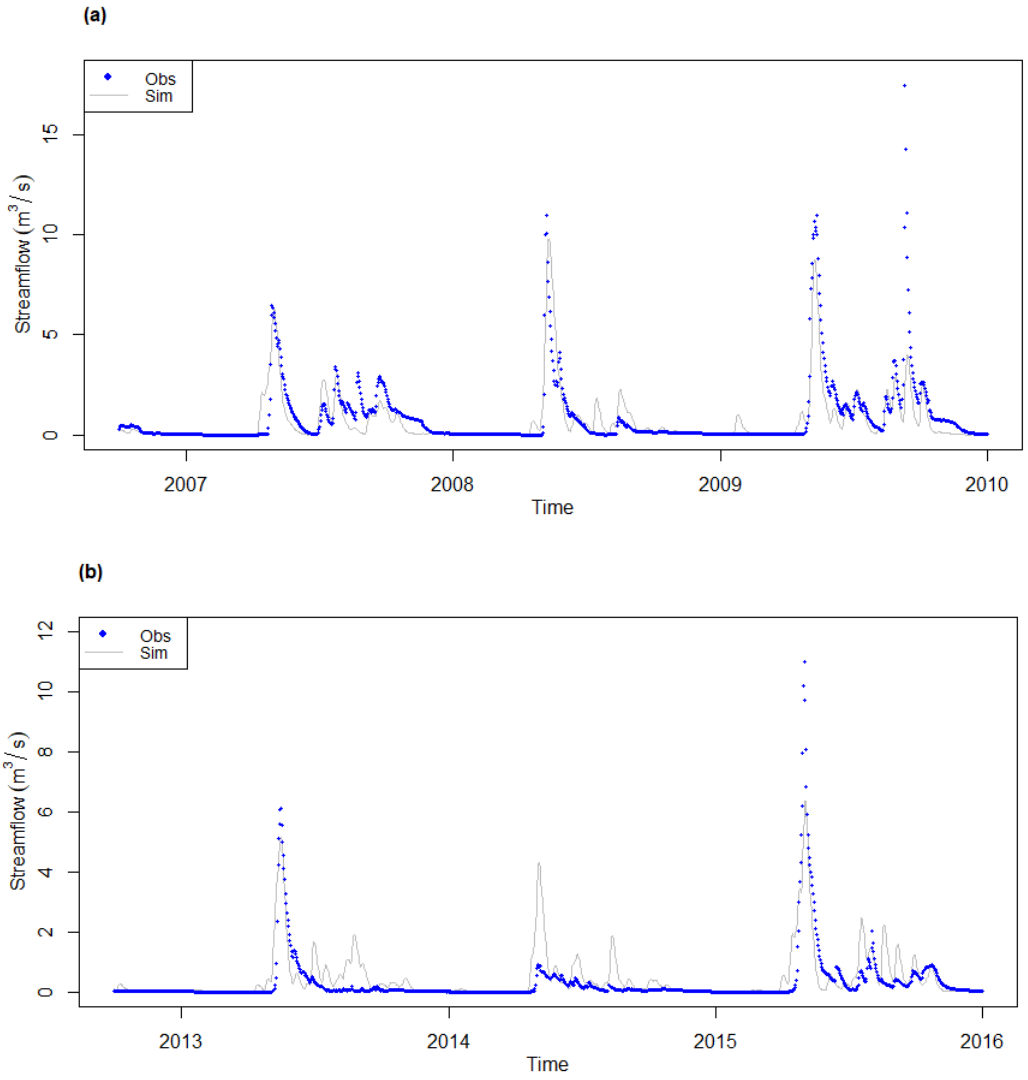

Figure 5.5: Streamflow hydrograph for: (a) A subset of the calibration period from 2006 to 2009 and; (b) Validation period from 2012-2016 [119].

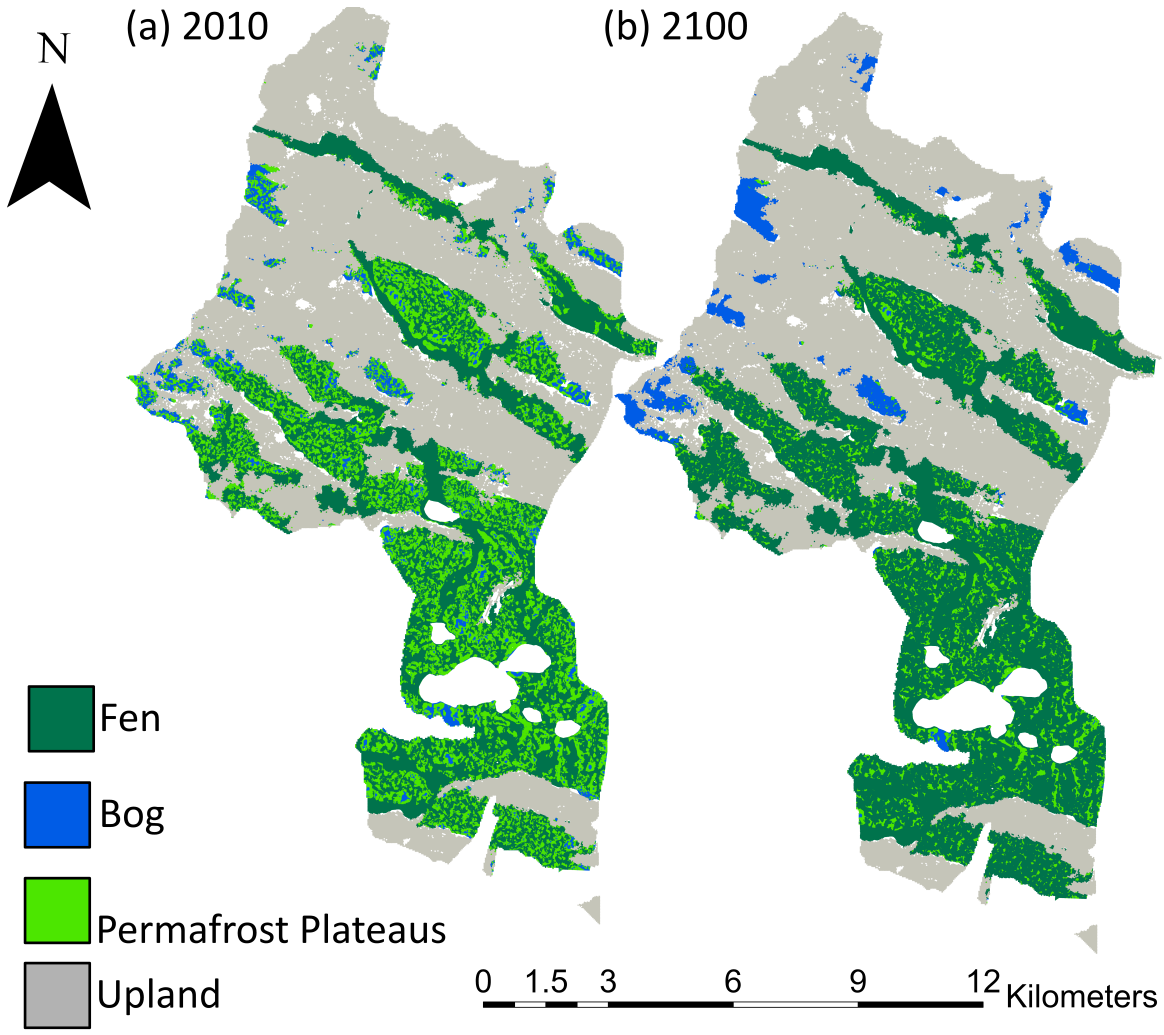

Figure 5.6: Prediction of land cover change over a 100 years interval (2010-2100) simulated for GFDL-CM3 climate model (RCP8.5): (a) Distribution of land cover in 2010; (b) Distribution of land cover simulated by TSLCM for 2100.

of the landscape covered in fen is accelerating (Figure 5.6). This is consistent with other qualitative predictions based upon observations of historical change [23, 114, 14].

Figure 5.7 reports the change in hydrological land cover under each climate scenario over the simulation time for the GFDL-CM3 climate model. The rate of change simulated for RCP8.5 is greater than other selected RCPs. The distribution of primary runoff regions has been increasing across all RCPs, whereas the distribution of secondary runoff areas has been continuously declining; considering these trends, streamflow is expected to rise in the future as a result of this thaw-induced change. The same behavior was observed in the predicted land cover changes for other selected GCMs.

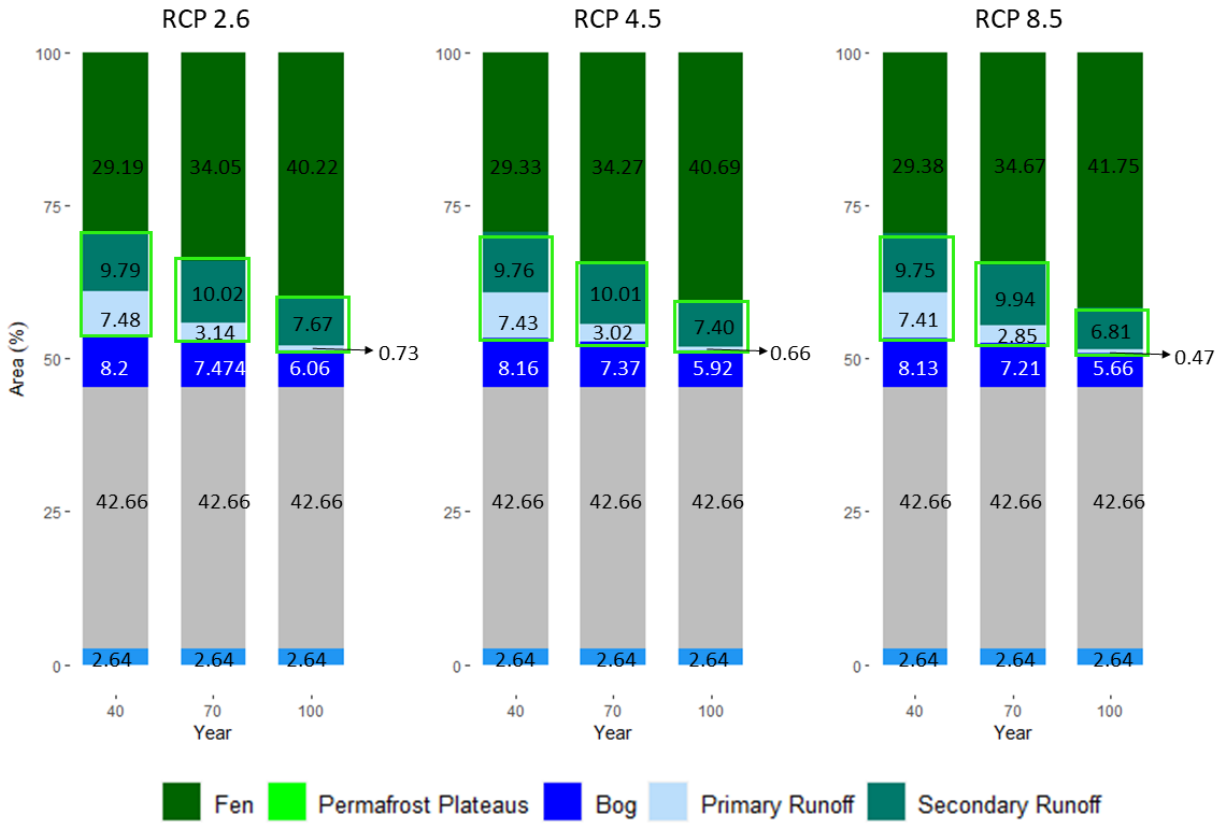

Figure 5.7: Transitions of land covers in three-time increments under three selected RCPs for GFDL-CM3 climate model.

5.5.3 Climate Scenarios: Hydrographs (Before and After)

In order to evaluate the effects of climate change on hydrological responses in the Scotty Creek basin, we compared the simulated streamflow across three climate models (BCC-CSM, GFDL-CM3, and MIROC5) and three scenarios (RCP2.6, 4.5, and 8.5).

Figure 5.8 shows the streamflow values on each day of the year averaged over the period from 1995-2016 (pre-2016), and over the period from 2016-2100 (post-2016). Figure 5.8 illustrates that, in all nine cases, the highest daily streamflow appears earlier in the post-2016 simulations. Additionally, the leftward shift in streamflow observed in the post-2016 simulations suggests that there is a high likelihood of the spring freshet occurring earlier in the future. The higher estimated 90% quantile for post-2016 than pre-2016 in each climate scenario confirms the expected impacts of climate change.

The majority of the basin serves as a primary runoff area during high flow periods (i.e., April and May during the spring freshet), and the fill-and-spill process happening in the secondary runoff area controls the generated runoff magnitude during the moderate flow periods. The importance of climate-induced land cover change, especially, the transition of secondary runoff area to primary runoff during low-flow can be noticed in Figure 5.8 after the spring freshet (i.e., day 150).

5.5.4 Climate Scenarios: Hydrographs (Trends)

The 10-year moving average of annual peak streamflow for three climate scenarios is illustrated in Figure 5.10. Each column reports the trend of the average estimated annual peak of the three selected climate models and observations in each scenario from 1995-2100. The bounds in the figures represent the maximum and minimum of the streamflow simulated by the three selected climate models. This uncertainty indicator helps to improve the understanding of the potential range of outcomes and the level of confidence that can be placed on the model predictions.

A gradual increase is observed in the predicted annual peak streamflow for RCP2.6, and RCP4.5 during the 100 years time increment (Figure 5.10), while there is a sharper rise in predicted streamflow for RCP8.5, especially after 2070. These increases are a result of changes in the climate variables such as temperature and precipitation, which have led to changes in the hydrological response of the basin (Figure 5.9).

The estimated annual volume of streamflow shows a trend that is similar to the trend observed for the estimated annual peak streamflow in the three climate scenarios (Figure

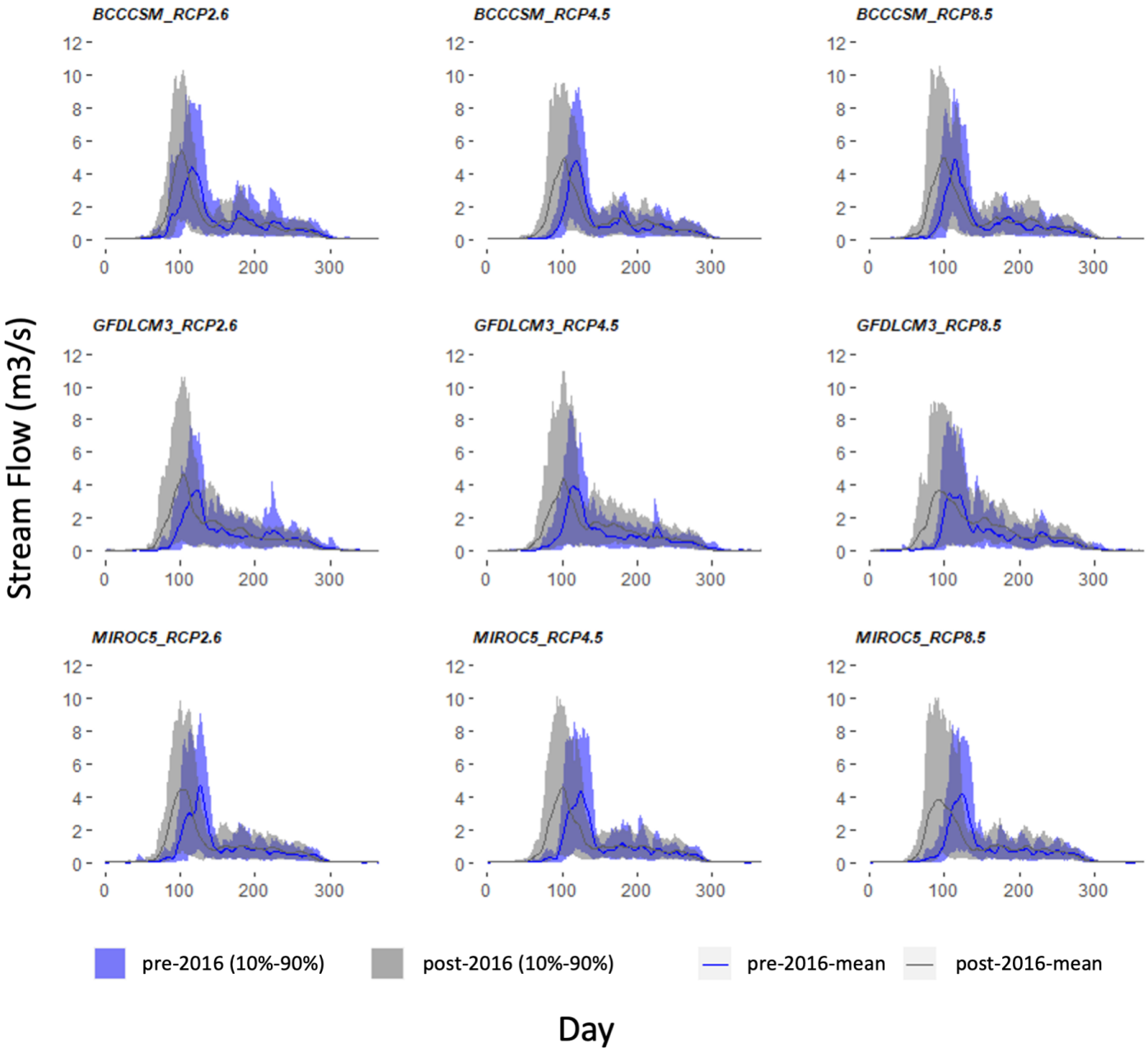

Figure 5.8: The simulated streamflow values in each day of the year averaged over 1995-2016 (pre-2016), and over 2016-2100, (post-2016) [119].

5.11). This suggests that the changes in precipitation and temperature are likely to have a significant impact on the annual volume of streamflow in the basin (Figure 5.9).

Moreover, it is noteworthy that the observed streamflow aligns more closely with the maximum values of the predicted annual peak streamflow and the average values of the annual volume streamflow for the three climate models.

The graph in Figure 5.12 provides valuable insights into the variations in streamflow over the selected time period. Specifically, the 10-year moving average of the maximum, minimum, and average values of the simulated runoff ratio for the three climate change models and scenarios are presented. The results indicate that the runoff ratio is expected to increase considerably between 2010 and 2100 in all three RCP scenarios, with an increase ranging from 20% to 25% for each RCP.

This highlights a significant change in the hydrological cycle of the basin, primarily driven by the rise in precipitation observed in Figure 5.9.b. The warming climate can hold more moisture in the atmosphere, resulting in increased precipitation, and warmer temperatures can cause earlier snowmelt and a shift from snow to rain, which ultimately increases streamflow.

5.5.5 Climate Scenarios: Hydrographs (With and Without Land Cover Change Transition)

To explore how land cover changes affect predicted streamflow under different climate scenarios, the Raven-UWFS model was used to compare simulated summer peak and summer volume of streamflow with and without considering a land cover change for BCC-CSM1.1 under three RCPs. For the case without land cover transitions, the land cover is held fixed at the 2010 land cover. Here, the Relative Difference Percentage (RDP) is used to estimate the impact of land cover transition on the simulated streamflow which can be calculated by:

$$RDP = \frac{F_{withLCC} - F_{withoutLCC}}{F_{withLCC}} \tag{5.5}$$

where $F_{withLCC}$ and $F_{withoutLCC}$ represent the simulated streamflow by the hydrological model with and without land cover evolution information as input. The estimated RDP values for summer peak streamflow range from 9% to 9.8% for RCP2.6, RCP4.5, and RCP8.5, respectively. Similarly, the RDP values for summer streamflow volume range from 10.5% to 11% under the same scenarios. This indicates that precipitation and temperature changes are significant factors contributing to the increase in streamflow. The

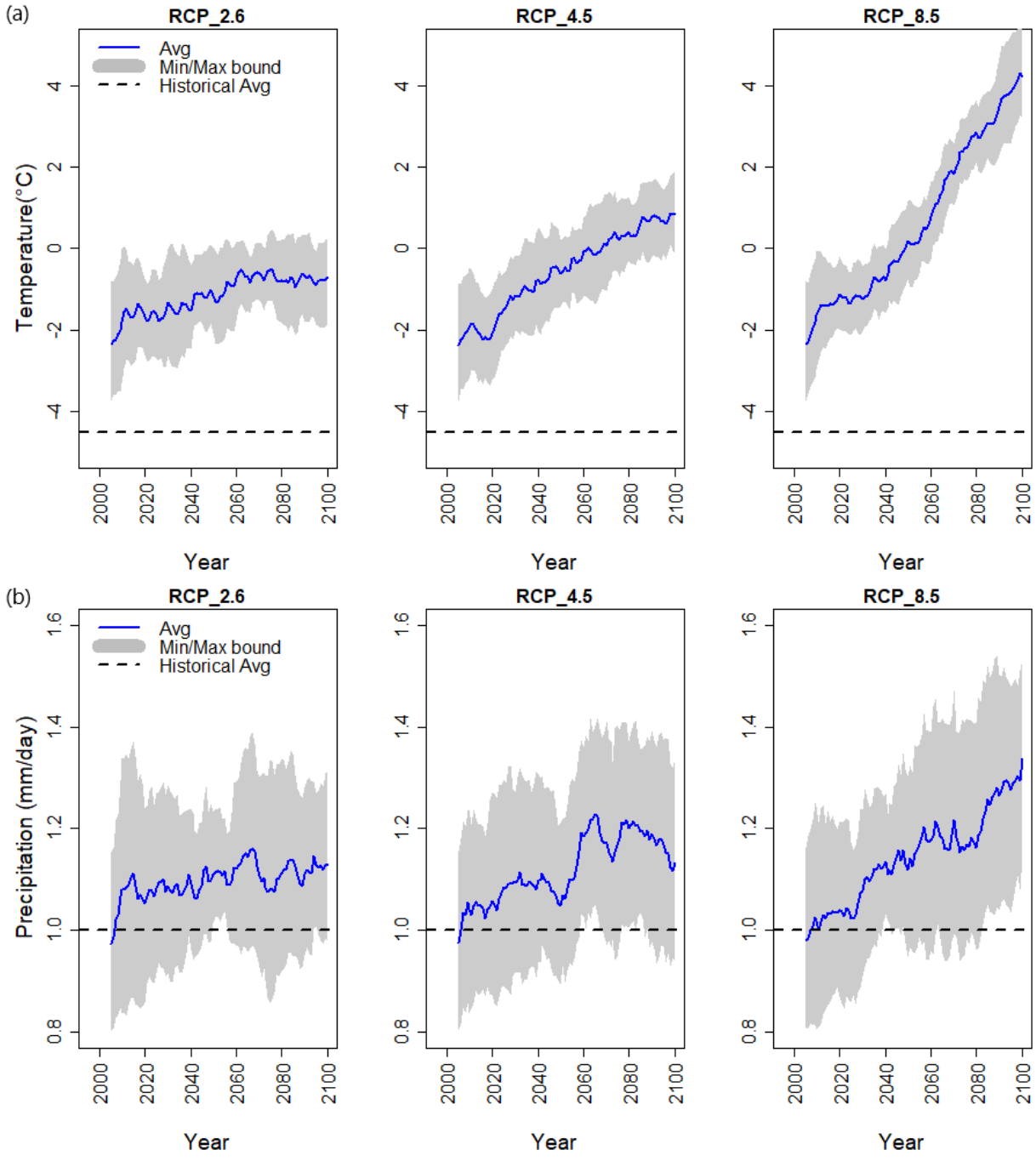

Figure 5.9: The 10-year moving average of the forecasted temperature and precipitation for three climate scenarios: (a) Air temperature; (b) Precipitation.

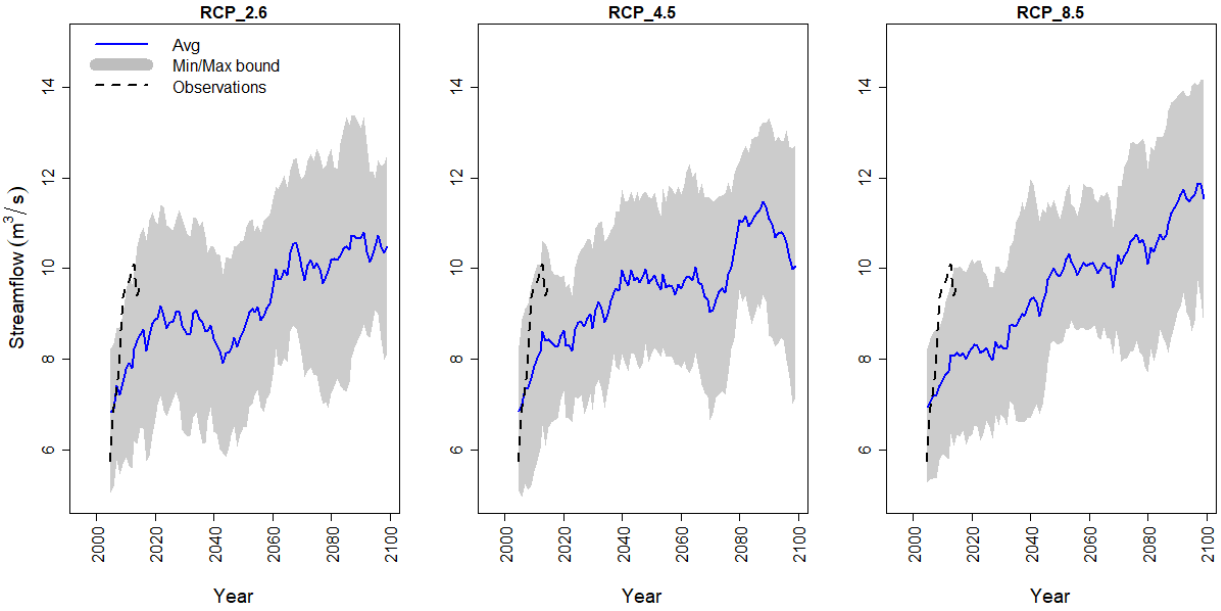

Figure 5.10: The 10-year moving average of the simulated annual peak from three climate scenarios and models [119].

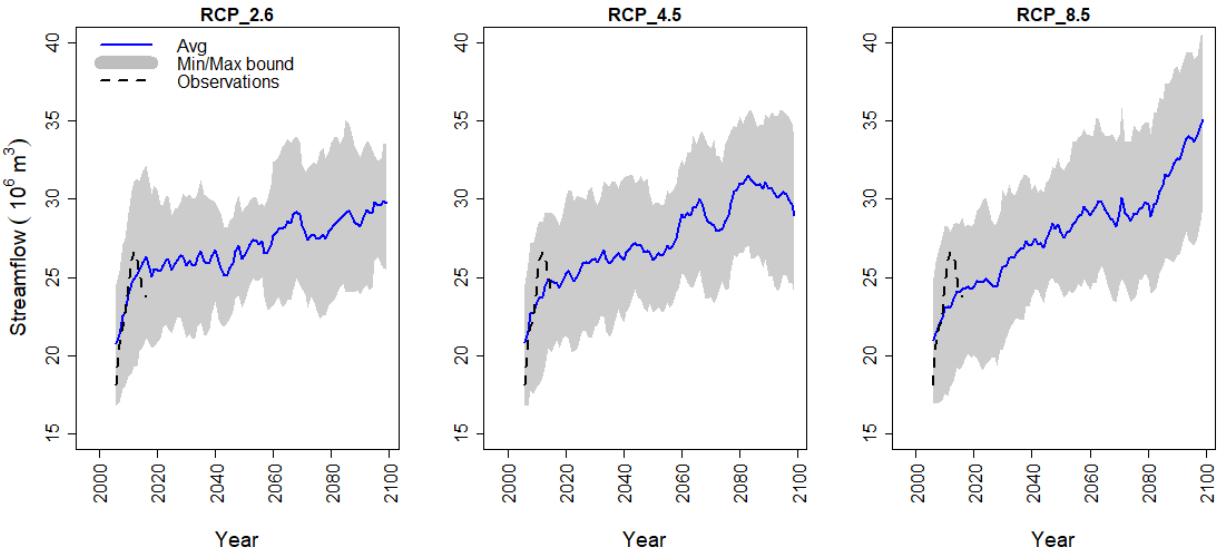

Figure 5.11: The 10-year moving average of the simulated annual runoff volume from the three climate scenarios and the models [119].

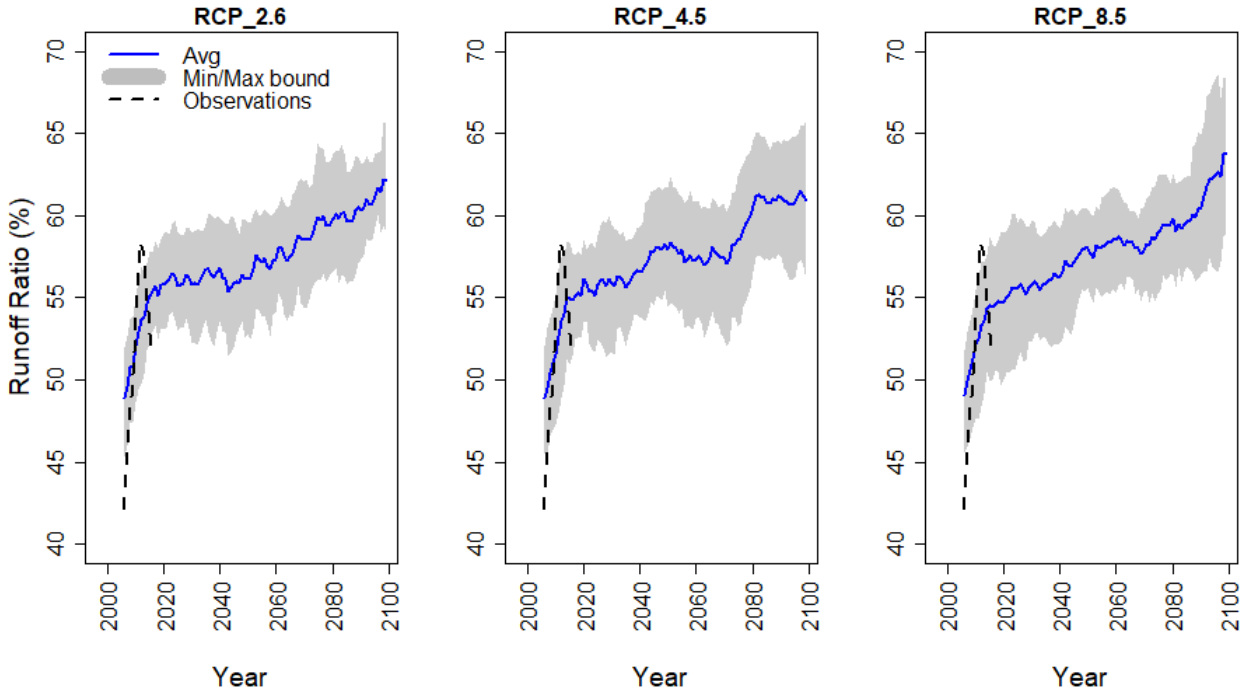

Figure 5.12: The 10-year moving average of the simulated annual runoff ratio from the three climate scenarios and the models [119].

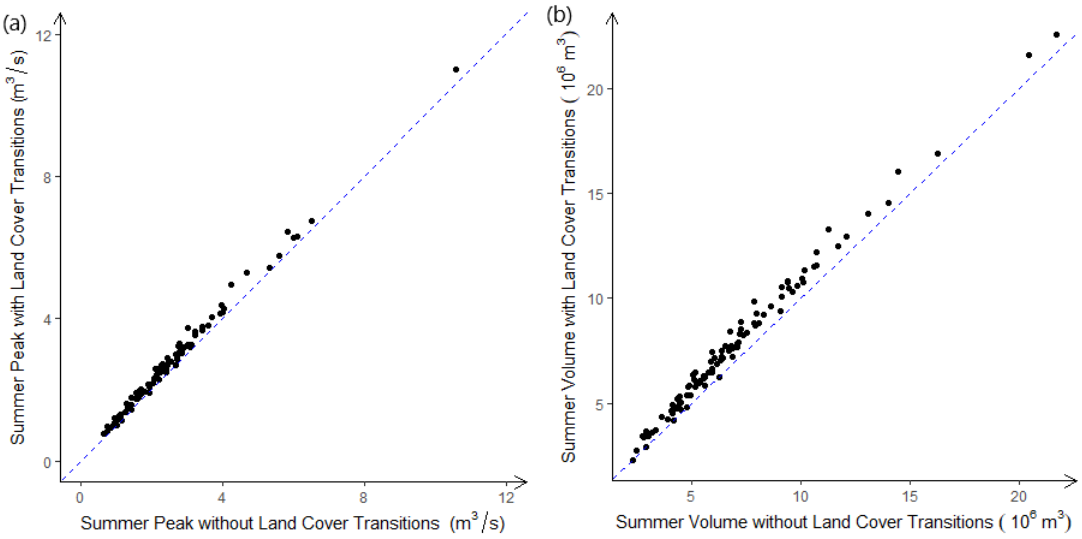

Figure 5.13: The comparison of simulated: (a) summer peak; (b) Summer volume of streamflow from the Scotty Creek basin with and without land cover change for RCP4.5 of the BCC-CSM1.1 climate model.

RDP value for annual peak and volume streamflow is estimated to be around 7% and 5.6%, respectively. These results suggest that the fill-and-spill process has a greater impact on the generation of runoff in the secondary area during the summer season.

In Figure 5.13, land cover transitions were examined in relation to predicted streamflow by comparing the simulated summer peak flow and summer volume with and without the incorporation of land cover transitions in the model for BCC-CSM1.1 under RCP4.5. The simulated streamflow when the land cover transition information is introduced to the hydrological model is higher, as the majority of land cover transitions are from secondary to primary runoff areas (Figure 5.13), meaning that less water is stored and lost as evaporation. Furthermore, as the basin's storage capacity decreases during this transition, the streamflow increases.

5.6 Conclusion

In the discontinuous permafrost zones of the Northwest Territories, lateral permafrost thaw is causing the redistribution of hydrologically important land cover types and modifying their hydrological function. Permafrost thaw has been found to increase hydrological con-

nectivity and streamflow magnitude in a basin, decrease secondary runoff area and storage capacity, accelerate the transition to primary runoff area, and reduce the extent of secondary runoff area.

A land cover change model, TSLCM, and a hydrological model, UWFS, were here coupled to examine the effects of thaw-induced land cover transitions on the hydrological response of a wetland-permafrost plateau complex. The TSLCM is used to estimate the long-term evolution of the hydrologically important land cover and simulate spatial patterns and pace of change. Based on an upscaled fill-and-spill process in wetlands, the probabilistic UWFS algorithm in Raven differentiates runoff generation processes in secondary and primary runoff areas.

Coupling the TSLCM land cover transition data with the UWFS model estimates the long-term effects of land cover evolution on streamflow generation. According to the simulated streamflow for the selected model and scenarios, there is a possibility of an earlier spring freshet occurring in the future due to the increasing temperatures. Based on the selected climate models and scenarios, it is predicted that basin runoff will increase by approximately 20 to 25% in the future. This corresponds to the expected rise in streamflow volume, which is due to an anticipated increase in rainfall within the basin, as well as an increase in bog capture primarily resulting from the conversion of secondary runoff areas to primary areas.

The study indicated that land cover transitions had an impact on predicted streamflow for the BCC-CSM1.1 model under different RCPs, resulting in an estimated increase of approximately 10% beyond that of meteorological changes alone. The fact that similar behavior was observed in other selected GCMs indicates a low level of uncertainty in the estimation of land cover's impact on streamflow. These findings align with those of Connon et al.(2014) [31], who found that ignoring connected bogs as dynamic transmission features in the landscape may lead to an underestimation of water available for streamflow by 5-15%.

This study suggests that while land cover transitions were a critical factor in increasing streamflow in the past, in the future, precipitation is expected to play a more dominant role due to the decrease in the extent of the secondary runoff area and the transitions to the primary runoff area.

The results of this study have made a contribution to our understanding of managing and monitoring hydrological responses to land cover evolution in Canadian wetlands. The presented machine learning-informed hydrologic model coupling framework provides a starting point for bridging the gap between hydrological models and machine learning-based land cover change models. Further application and evaluation of this framework

in other areas of interest would strengthen our understanding of the effects of permafrost thaw-induced land cover transitions on streamflow generation and are likely to improve the performance of hydrological models created for discontinuous permafrost zones.

However, it is important to acknowledge the limitations and potential sources of uncertainty associated with the presented methods that must be considered in future studies. One source of uncertainty is the limited selection of climate change models used to predict climate-related variables, which was done without following a systematic processs. Future studies could benefit from including a larger ensemble of climate models to improve the reliability of the presented approach.

Moreover, as mentioned in Chapter 4, the TSLCM used in this study is not able to capture the transition from wetlands to forest over time since this transition was not the main land cover change in the study area during the time presented in the input data. This could affect the runoff generation simulated by the hydrological model and should be addressed in future studies. By addressing these limitations, the presented approach could be further refined and applied to other regions, providing useful information for managing and monitoring hydrological responses to land cover evolution in Canadian wetlands and beyond.

Chapter 6

Conclusions

6.1 Summary

The aim of this research was to develop, test, and apply methods for simulating the thaw-induced evolution of dominant land covers in discontinuous permafrost zones and its hydrological effect. In Chapter 1, three objectives were presented; Chapter 3 through Chapter 5 documented the research required to achieve those objectives. Here, we summarize the key findings of each Chapter and their associated objectives:

- Objective 1) **Iteratively develop and test a machine learning geospatial model that can estimate the conversion between the three primary land cover types at SCRS and in other similar discontinuous permafrost regions of the discontinuous permafrost zones in the taiga plains:** Chapter 4 discusses the development of a spatio-temporal TSLCM for simulating the transition of dominant land covers in these discontinuous permafrost zones. This is the first land cover change model developed for thawing discontinuous permafrost landscapes that considers both spatial and temporal drivers of change. The TSLCM was demonstrated to reliably represent historical hydrologically-important land cover transitions and provide estimates of the long-term future climate impacts on the evolution of these unique landscapes. A novel data boosting strategy was presented in this work to solve the data limitation issues for training a machine learning model, specifically for infilling data in time when only a finite number of historically classified images are available for training. The boosting strategy was able to help simulate the long-term land cover changes by generating synthetic data from the existing data set and adding it to the training data set. It is possible that similar strategies may be deployed for other machine-learning models of the transient phenomenon in data-poor environments.

  Chapter 4 presents the performance of different machine learning methods for capturing land cover transition patterns and rates in discontinuous permafrost zones, identifies a preferred machine learning-based model to replicate historical data and extrapolate the change predictions into the future, and examines the role of different driving factors of change in informing an accurate land cover change model. The results proved that MLR's extrapolations into the future exhibit superior consistency with projected physical patterns compared to ensemble learning's time series land cover change projections, and the distance-based variables were the most important factors influencing the model's output. The developed model predicted a time series of land cover changes, indicating that permafrost plateaus are undergoing transformation into fens. Furthermore, the model predicted an increase in the proportion of

fen cover over time. This is consistent with historical observations and our current understanding of change mechanisms in these landscapes. Overall, the developed TSLCM is a valuable tool for predicting hydrologically-important land cover transitions and analyzing the long-term climate impacts on the hydrology of discontinuous permafrost regions.

- Objective 2) **Use historical remote sensing imagery products to evaluate long-term changes to the land cover characteristics of discontinuous permafrost zone's wetlands by incorporating deep learning-based algorithms:** This objective aims to enhance our understanding of the factors driving changes in discontinuous permafrost zones over time, specifically related to thaw-induced processes, and streamline the data preparation process for hydrological analysis, making it easier and more efficient to study the hydrological impacts of permafrost thaw.

  The TSLCM devised in Chapter 4 and hydrological analysis of the land cover evolution covered in Chapter 5 both require classified maps and the estimates of the delineated runoff areas of the wetlands. These classified maps can now be generated using the TWINN automatic solution presented in Chapter 3. The TWINN solution enables the automatic classification of high-resolution RGB imagery from discontinuous permafrost zones into forests, wetlands, and water. This allows for a more efficient and accurate analysis of land cover change in wetlands over time. In addition, TWINN's ability to delineate the local runoff area of individual wetlands is also critical for achieving the final goal of this thesis. The runoff area of wetlands is needed to estimate the contributing area of isolated and connected wetlands, which is essential for hydrological analysis and understanding the effects of climate change.

  The TWINN solution generated promising results for classifying wetlands, permafrost plateaus, and water using only RGB images. This study confirmed that CNN's deep architecture and machine learning methodologies are superior to previous pixel-based methods for classifying heterogeneous landscapes like wetlands.

- Objective 3) **Simulate the likely future hydrological impacts of thaw-induced landscape changes based on the predicted land cover evolution from the machine learning-based model using a hydrological model(UWFS method) implemented in the Raven hydrological framework:** Chapter 3, Chapter 4, and Chapter 5 aimed to reach this objective. Chapter 5 was focused on addressing this objective by coupling the developed TSLCM [4], the TWINN solution, and the hydrological model (the UWFS method), implemented in the Raven hydrological modeling framework [120].

To develop a hydrological model of the area, the UWFS model [120] needed to be informed by historical land cover maps and changes in the primary and secondary runoff areas of wetlands over time. The TWINN solution, presented in Chapter 3, was used to generate land cover distribution data that informs hydrological models like UWFS. Moreover, Chapter 5 outlines an approach to incorporate information on land cover changes due to climate change and permafrost thaw into the UWFS model, which is crucial for enhancing our understanding of the hydrological impacts in the region.

Then, the outputs of the land cover change model for different climate scenarios in the future and historical data were imported into the developed hydrological model to analyze the role of land cover evolution on the hydrology of the Scotty Creek basin. The amount of land cover change in the Scotty Creek basin that the TSLCM anticipated for future climatic scenarios demonstrated the model's applicability on a larger scale.

The study contributes to a better understanding of the historical role of landscape change on streamflow in the Scotty Creek basin. It provides an approach to incorporate information on land cover changes due to climate change and permafrost thaw directly into hydrological models. The findings of this study show that future application and assessment of the provided machine learning-informed hydrologic model coupling framework on other regions of interest can help to improve the understanding of the impacts of permafrost thaw-induced land cover changes on streamflow generation.

The land cover change model and classification model developed herein are thought to be helpful in further research used to improve our understanding of the poorly understood process of land cover change in discontinuous permafrost regions of the NWT and similar environments.

6.2 Thesis Limitations and Scope

The methods developed in this thesis represent a contribution to our understanding of how thaw-induced land cover changes affect the hydrological response of the unique Scotty Creek-like landscape type found in Northern Canada. However, there are several limitations related to each presented method in this work, especially with regard to the extension to other landscape types. Here, the most important drawbacks of the devised methods are listed:

- The semantic segmentation model was trained only on the data set representing the Scotty Creek Basin land covers, this leads to misclassifications when employing the TWINN solution on other taiga wetland environments.
- Only three types of lands—water, wetlands, and forests—can be identified using the classification approach in high-resolution images of any taiga wetlands region. This solution does not currently generate classified maps that incorporate uplands and permafrost plateaus.
- The TSLCM was developed using data collected at the SCRS; there may therefore be several limitations regarding the model's applicability to larger scales and to other discontinuous permafrost regions.
- The driving factors of change for developing the land cover change model were selected based on the characteristics of the dominant landscapes and pattern of land cover evolution in the SCRS. Other key drivers of change may affect how land types evolve in different cases, and it is likely that additional drivers could improve the performance of the existing model.
- The TSLCM makes the assumption that all bogs connected to fens transform into fens based on the 'bog capture' phenomenon; however, the nature of this transition may vary in other discontinuous permafrost landscapes.
- The hydrological simulations did not consider lateral heat transfer through permafrost underlying taliks or other complex local-scale phenomena.
- The selection of climate change models used to predict climate-related variables has been done without following a systematic process and only a limited number of models have been included in the analysis. It may be that alternate selection of climate models would lead to distinct results.

6.3 Future Works

The objective of this study is to enhance the effectiveness of current classification methods and develop a land cover change model of discontinuous permafrost regions of NWT for producing geospatial data used in the hydrological analysis of wetland systems. The study did not aim to create a flawless and unbiased representation of reality. Based on the limitations of the developed methods in this work, there are other pathways that can be pursued to improve upon and extend this work. Future work may involve:

- Including and assessing more candidate driving factors of change and/or training on more data sets, so the land cover change model will be able to take diverse transitions into account in any discontinuous permafrost zones, improving its effectiveness and transferability.
- Improving the performance of the TWINN solution by boosting the training dataset and including more land cover types covering the taiga wetlands discontinuous permafrost regions.
- Addressing the relative impacts of land cover evolution on the hydrology of the taiga plains via hydrological modelling using the simulated land cover as inputs for other discontinuous permafrost landscapes.
- Including a more comprehensive ensemble of climate change forecasts to inform simulation of the streamflow trends.

6.4 Publications and Presentations

6.4.1 Research Papers

Chapter 4 of this thesis is published in peer-reviewed journal and Chapter 3 of this thesis is under review in the International Journal of Applied Earth Observation and Geoinformation. The list of publications is as follows:

- Shaghayegh Akbarpour and James R. Craig. Simulating thaw-induced land cover change in discontinuous permafrost landscapes. Remote Sensing Applications: Society and Environment, 28:100829, 2022
- Shaghayegh Akbarpour, Laura Chasmer, and James R. Craig. Hydrological classification of isolated wetlands in discontinuous permafrost regions using RGB imagery. Under review in the International Journal of Applied Earth Observation and Geoinformation, 2023

6.4.2 Conference Presentations

- A computer vision-based wetland identification solution for discontinuous permafrost landscapes of northern Canada, Shaghayegh Akbarpour, James R. Craig, AGU Fall Meeting 2022, Chicago.

- Application of machine-learning to spatio-temporal modeling of land cover evolution in discontinuous permafrost regions, Shaghayegh Akbarpour, James R. Craig, CWRA June 2022, Canmore.
- A machine-learning model to predict uncertainty in permafrost thaw-induced land cover transition, Shaghayegh Akbarpour, James R. Craig, EGU May 2022, Vienna.
- Multinomial simulation of land cover evolution in discontinuous permafrost zones of Northwest Territories, Shaghayegh Akbarpour,James R. Craig , AGU Fall Meeting 2021.
- Semantic segmentation of Isolated wetland in discontinuous permafrost regions of the Northwest Territories using deep convolutional neural networks, Shaghayegh Akbarpour, James R. Craig, AGU Fall Meeting 2021.
- Impact of climate-induced land cover change on the hydrological response of discontinuous permafrost landscapes,Mahkameh Taheri, Shaghayegh Akbarpour, James R. Craig, ArcticNet ASM 2021.
- Modelling Evolution of Discontinuous Permafrost Landscapes and Hydrology, Shaghayegh Akbarpour, James R. Craig, AGU Fall Meeting 2020.
- Modeling the evolution of landcover in a lowland ecosystem of the NWT , Shaghayegh Akbarpour, James R. Craig, AC2020conferenc.

References

[1] Kjetil S Aas, Léo Martin, Jan Nitzbon, Moritz Langer, Julia Boike, Hanna Lee, Terje K Berntsen, and Sebastian Westermann. Thaw processes in ice-rich permafrost landscapes represented with laterally coupled tiles in a land surface model. *Cryosphere*, 13(2):591–609, 2019.

[2] Abu Yousuf Md Abdullah, Arif Masrur, Mohammed Sarfaraz Gani Adnan, Md Abdullah Al Baky, Quazi K. Hassan, and Ashraf Dewan. Spatio-temporal patterns of land use/land cover change in the heterogeneous coastal region of Bangladesh between 1990 and 2017. *Remote Sensing 2019, Vol. 11, Page 790*, 11(7):790, apr 2019.

[3] Shaghayegh Akbarpour, Laura Chasmer, and James R. Craig. Hydrological classification of isolated wetlands in discontinuous permafrost regions using rgb imagery. *Under review in International Journal of Applied Earth Observation and Geoinformation*, 2023.

[4] Shaghayegh Akbarpour and James R. Craig. Simulating thaw-induced land cover change in discontinuous permafrost landscapes. *Remote Sensing Applications: Society and Environment*, 28:100829, 2022.

[5] Husam A.H. Al-Najjar, Bahareh Kalantar, Biswajeet Pradhan, Vahideh Saeidi, Alfian Abdul Halin, Naonori Ueda, and Shattri Mansor. Land cover classification from fused DSM and UAV images using convolutional neural networks. *Remote Sensing 2019, Vol. 11, Page 1461*, 11(12):1461, jun 2019.

[6] Meisam Amani, Sahel Mahdavi, Majid Afshar, Brian Brisco, Weimin Huang, Sayyed Mohammad Javad Mirzadeh, Lori White, Sarah Banks, Joshua Montgomery, and Christopher Hopkinson. Canadian Wetland Inventory using Google Earth Engine: The First Map and Preliminary Results. *Remote Sensing 2019, Vol. 11, Page 842*, 11(7):842, apr 2019.

[7] Meisam Amani, Bahram Salehi, Sahel Mahdavi, Jean Granger, and Brian Brisco. Wetland classification in Newfoundland and Labrador using multi-source SAR and optical data integration. *https://doi.org/10.1080/15481603.2017.1331510*, 54(6):779–796, nov 2017.

[8] Meisam Amani, Bahram Salehi, Sahel Mahdavi, Jean Granger, and Brian Brisco. Wetland classification in Newfoundland and Labrador using multi-source SAR and optical data integration. *https://doi.org/10.1080/15481603.2017.1331510*, 54(6):779–796, nov 2017.

[9] Erfan A Amiri and James R. Craig. Effect of soil thermal heterogeneity on permafrost evolution. In *Cold Regions Engineering 2019*, pages 492–499. American Society of Civil Engineers Reston, VA, 2019.

[10] Erfan A Amiri, James R. Craig, and Barret L Kurylyk. A theoretical extension of the soil freezing curve paradigm. *Advances in Water Resources*, 2018.

[11] Jamal Jokar Arsanjani, Marco Helbich, Wolfgang Kainz, and Ali Darvishi Boloorani. Integration of logistic regression, Markov chain and cellular automata models to simulate urban expansion. *International Journal of Applied Earth Observation and Geoinformation*, 21(1):265–275, 2012.

[12] Jennifer L. Baltzer, Tyler Veness, Laura E. Chasmer, Anastasia E. Sniderhan, and William Quinton. Forests on thawing permafrost: Fragmentation, edge effects, and net forest loss. *Global Change Biology*, 20(3):824–834, mar 2014.

[13] Thiago M. Barros, Plácido A. Souza Neto, Ivanovitch Silva, and Luiz Affonso Guedes. Predictive models for imbalanced data: A school dropout perspective. *Education Sciences 2019, Vol. 9, Page 275*, 9(4):275, nov 2019.

[14] David W. Beilman and Stephen Robinson. Peatland permafrost thaw and landform type along a climatic gradient. *Proceedings of the 8th International Conference on Permafrost*, pages 61–65, 2003.

[15] Tedros M. Berhane, Charles R. Lane, Qiusheng Wu, Oleg A. Anenkhonov, Victor V. Chepinoga, Bradley C. Autrey, and Hongxing Liu. Comparing pixel- and object-based approaches in effectively classifying wetland-dominated landscapes. *Remote Sensing 2018, Vol. 10, Page 46*, 10(1):46, dec 2017.

[16] Md Abul Ehsan Bhuiyan, Chandi Witharana, and Anna K Liljedahl. Use of very high spatial resolution commercial satellite imagery and deep learning to automatically map ice-wedge polygons across tundra vegetation types. *Journal of Imaging*, 6(12):137, 2020.

[17] Leo Breiman. Random Forests. *Machine Learning 2001 45:1*, 45(1):5–32, oct 2001.

[18] Daniel G. Brown, Bryan C. Pijanowski, and Jiunn-Der Duh. Modeling the relationships between land use and land cover on private lands in the Upper Midwest, USA. *Journal of Environmental Management*, 59(4):247–263, 2000.

[19] Olivia Carpino, Kristine Haynes, Ryan Connon, James Craig, Élise Devoie, and William Quinton. Long-term climate-influenced land cover change in discontinuous permafrost peatland complexes. *Hydrology and Earth System Sciences*, 25(6):3301–3317, 2021.

[20] Olivia A. Carpino, Aaron A. Berg, William Quinton, and Justin R. Adams. Climate change and permafrost thaw-induced boreal forest loss in northwestern Canada. *Environmental Research Letters*, 13(8), 2018.

[21] Laura Chasmer, Danielle Cobbaert, Craig Mahoney, Koreen Millard, Daniel Peters, Kevin Devito, Brian Brisco, Chris Hopkinson, Michael Merchant, Joshua Montgomery, Kailyn Nelson, and Olaf Niemann. Remote sensing of boreal wetlands 1: Data use for policy and management, 2020.

[22] Laura Chasmer and Chris Hopkinson. Threshold loss of discontinuous permafrost and landscape evolution. *Global Change Biology*, 23(7):2672–2686, 2017.

[23] Laura Chasmer, Chris Hopkinson, and William Quinton. Quantifying errors in discontinuous permafrost plateau change from optical data, Northwest Territories, Canada: 1947–2008. *Canadian Journal of Remote Sensing*, 36(sup2):S211–S223, jan 2010.

[24] Laura Chasmer, Chris Hopkinson, Tyler Veness, William Quinton, and Jennifer L. Baltzer. A decision-tree classification for low-lying complex land cover types within the zone of discontinuous permafrost. *Remote Sensing of Environment*, 143:73–84, 2014.

[25] Laura Chasmer, Christopher Hopkinson, Joshua Montgomery, and Richard Petrone. A physically based terrain morphology and vegetation structural classification for wetlands of the boreal plains, Alberta, Canada. *https://doi.org/10.1080/07038992.2016.1196583*, 42(5):521–540, sep 2016.

[26] Laura Chasmer, Craig Mahoney, Koreen Millard, Kailyn Nelson, Daniel Peters, Michael Merchant, Chris Hopkinson, Brian Brisco, Olaf Niemann, Joshua Montgomery, Kevin Devito, and Danielle Cobbaert. Remote sensing of boreal wetlands 2: Methods for evaluating boreal wetland ecosystem state and drivers of change. *Remote Sensing*, 12(8):1321, 2020.

[27] Laura Chasmer, William Quinton, Chris Hopkinson, Richard Petrone, and Pete Whittington. Vegetation canopy and radiation controls on permafrost plateau evolution within the discontinuous permafrost zone, Northwest Territories, Canada. *Permafrost and Periglacial Processes*, 22(3):199–213, jul 2011.

[28] Meng Chen, Xiaohui Yu, and Yang Liu. Mining moving patterns for predicting next location. *Information Systems*, 54:156–168, 2015.

[29] Torben R. Christensen, Torbjörn Johansson, H. Jonas Åkerman, Mihail Mastepanov, Nils Malmer, Thomas Friborg, Patrick Crill, and Bo H. Svensson. Thawing sub-arctic permafrost: Effects on vegetation and methane emissions. *Geophysical Research Letters*, 31(4), 2004.

[30] Ryan F. Connon, William Quinton, James R. Craig, and Masaki Hayashi. Changing hydrologic connectivity due to permafrost thaw in the lower Liard River valley, NWT, Canada. *Hydrological Processes*, 28(14):4163–4178, jul 2014.

[31] Ryan F. Connon, William Quinton, James.R Craig, Justin Hanisch, and Oiver Sonnentag. The hydrology of interconnected bog complexes in discontinuous permafrost terrains. *Hydrological Processes*, 29(18):3831–3847, 2015.

[32] James R. Craig, Genevieve Brown, Robert Chlumsky, R Wayne Jenkinson, Georg Jost, Konhee Lee, Juliane Mai, Martin Serrer, Nicholas Sgro, Mahyar Shafii, et al. Flexible watershed simulation with the raven hydrological modelling framework. *Environmental Modelling & Software*, 129:104728, 2020.

[33] Evan R. DeLancey, John F. Simms, Masoud Mahdianpari, Brian Brisco, Craig Mahoney, and Jahan Kariyeva. Comparing deep learning and shallow learning for large-scale wetland classification in Alberta, Canada. *Remote Sensing 2020, Vol. 12, Page 2*, 12(1):2, dec 2019.

[34] Élise G. Devoie, James R. Craig, Ryan F. Connon, and William Quinton. Taliks: a tipping point in discontinuous permafrost degradation in peatlands. *Water Resources Research*, 55(11):9838–9857, nov 2019.

[35] Élise G. Devoie, James R. Craig, Mason Dominico, Olivia Carpino, Ryan F. Connon, Ashley C.A. Rudy, and William Quinton. Mechanisms of discontinuous permafrost thaw in peatlands. *Journal of Geophysical Research: Earth Surface*, 126(11):e2021JF006204, nov 2021.

[36] Dimitre D. Dimitrov, Jagtar S. Bhatti, and Robert F. Grant. The transition zones (ecotone) between boreal forests and peatlands: Ecological controls on ecosystem productivity along a transition zone between upland black spruce forest and a poor forested fen in central Saskatchewan. *Ecological Modelling*, 291:96–108, nov 2014.

[37] Guan Dongjie, Gao Weijun, Watari Kazuyuki, and Fukahori Hidetoshi. Foundation: Sasakawa scientific foundation of Japan, No.20-238; National Basic Research Program of China (973 Pro-gram). *No*, 18:455–468, 2008.

[38] Caroline Duchesne, John Frederick Wright, and Mark Ednie. High-resolution numerical modeling of climate change impacts on permafrost in the vicinities of inuvik, norman wells, and fort simpson, nt, canada. In *Proceedings of the Ninth International Conference on Permafrost*, volume 29, pages 385–390. Institute of Northern Engineering, University of Alaska at Fairbanks, 2008.

[39] Claude Duguay, Guido Grosse, and Alfred Wegener. Remote sensing of the cryosphere alpine tundra view project glob temperature view project. 2017.

[40] ECCC. Meteorological Data for Fort Simpson. Retrieved from https://climate.weather.gc.ca/climate_data/daily_data_e.html?StationID=52780, accessed 2020-10-10, 2020.

[41] Andres Etter, Clive McAlpine, David Pullar, and Hugh Possingham. Modelling the conversion of Colombian lowland ecosystems since 1940: Drivers, patterns and rates. *Journal of Environmental Management*, 79(1):74–87, 2006.

[42] Robert C. Frohn, Molly Reif, Charles Lane, and Brad Autrey. Satellite remote sensing of isolated wetlands using object-oriented classification of Landsat-7 data. *Wetlands 2009 29:3*, 29(3):931–941, sep 2009.

[43] Saman Ghaffarian, João Valente, Mariska van der Voort, and Bedir Tekinerdogan. Effect of attention mechanism in deep learning-based remote sensing image processing: A systematic literature review. *Remote Sensing*, 13(15):2965, 2021.

[44] Carolyn M. Gibson, Karl. Cottenie, Tristan. Gingras-Hill, Steve. V. Kokelj, Jennifer L. Baltzer, Laura Chasmer, and Merritt. R. Turetsky. Mapping and understanding the vulnerability of northern peatlands to permafrost thaw at scales relevant to community adaptation planning. *Environmental Research Letters*, 16(5):055022, may 2021.

[45] Sonia Hachem, Michel Allard, and Claude Duguay. Using the modis land surface temperature product for mapping permafrost: An application to northern Québec and Labrador, Canada. *Permafrost and Periglacial Processes*, 20(4):407–416, 2009.

[46] Karen A Harper, S Ellen Macdonald, Philip J Burton, Jiquan Chen, Kimberley D Brosofske, Sari C Saunders, Eugenie S Euskirchen, DAR Roberts, Malanding S Jaiteh, and Per-Anders Esseen. Edge influence on forest structure and composition in fragmented landscapes. *Conservation biology*, 19(3):768–782, 2005.

[47] Masaki Hayashi, William Quinton, Alain Pietroniro, and John J Gibson. Hydrologic functions of wetlands in a discontinuous permafrost basin indicated by isotopic and chemical signatures. *Journal of Hydrology*, 296(1-4):81–97, 2004.

[48] Kristine M. Haynes, Ryan F. Connon, and William Quinton. Permafrost thaw induced drying of wetlands at Scotty Creek, NWT, Canada. *Environmental Research Letters*, 13(11), 2018.

[49] Kaiming He, Xiangyu Zhang, Shaoqing Ren, and Jian Sun. Deep residual learning for image recognition. *Proceedings of the IEEE Computer Society Conference on Computer Vision and Pattern Recognition*, 2016-Decem:770–778, dec 2015.

[50] Thorsten Hoeser and Claudia Kuenzer. Object detection and image segmentation with deep learning on earth observation data: A review-part I: Evolution and recent trends. *Remote Sensing 2020, Vol. 12, Page 1667*, 12(10):1667, may 2020.

[51] Jeremy Howard and Sylvain Gugger. Fastai: A layered api for deep learning. *Information*, 11(2):108, 2020.

[52] Ziyu Jiang, Kate Von Ness, Julie Loisel, and Zhangyang Wang. ArcticNet: A deep learning solution to classify arctic wetlands, 2019.

[53] Shahab Eddin Jozdani, Brian Alan Johnson, and Dongmei Chen. Comparing deep neural networks, ensemble classifiers, and support vector machine algorithms for object-based urban land use/land cover classification. *Remote Sensing*, 11(14):1713, jul 2019.

[54] Abdulla Al Kafy, Abdullah Al Faisal, Ragib Mahmood Shuvo, Md Nazmul Huda Naim, Md Soumik Sikdar, Radwan Rahman Chowdhury, Md Arshadul Islam, Md Hasnan Sakin Sarker, Md Hasib Hasan Khan, and Marium Akter Kona. Remote sensing approach to simulate the land use/land cover and seasonal land surface temperature change using machine learning algorithms in a fastest-growing megacity of Bangladesh. *Remote Sensing Applications: Society and Environment*, 21:100463, jan 2021.

[55] Mikhail Kanevski, Alexei Pozdnukhov, and Ville Timonin. Machine learning algorithms for geospatial data. applications and software tools. 2008.

[56] Sultan Daud Khan, Louai Alarabi, and Saleh Basalamah. Deep hybrid network for land cover semantic segmentation in high-spatial resolution satellite images. *Information*, 12(6):230, 2021.

[57] Iman Khosravi, Abdolreza Safari, Saeid Homayouni, and Heather McNairn. Enhanced decision tree ensembles for land-cover mapping from fully polarimetric SAR data. *https://doi.org/10.1080/01431161.2017.1372863*, 38(23):7138–7160, dec 2017.

[58] Diederik P Kingma and Jimmy Ba. Adam: A method for stochastic optimization. *arXiv preprint arXiv:1412.6980*, 2014.

[59] Lene Kristensen and Hanne H Christiansen. Arctic rockwall retreat rates estimated using laboratory-calibrated ERT measurements of talus cones in Longyeardalen, Svalbard View project FrostInSAR: Upscaling the investigation of periglacial landforms in the Norwegian Arctic using Synthetic Aperture R. Technical report, 2012.

[60] Max Kuhn. Building predictive models in R using the caret package. *Journal of Statistical Software*, 28(5):1–26, 2008.

[61] Max Kuhn, Jed Wing, Steve Weston, Andre Williams, Chris Keefer, Allan Engelhardt, Tony Cooper, Zachary Mayer, Michael Benesty, Reynald Lescarbeau, et al. Package "caret" classification and regression training description misc functions for training and plotting classification and regression models, 2017.

[62] Sathees Kumar, Nisha Radhakrishnan, and Samson Mathew. Land use change modelling using a Markov model and remote sensing. *Geomatics, Natural Hazards and Risk*, 5(2):145–156, 2014.

[63] Barret L. Kurylyk, Masaki Hayashi, William Quinton, Jeffrey M. McKenzie, and Clifford I. Voss. Influence of vertical and lateral heat transfer on permafrost thaw,

peatland landscape transition, and groundwater flow. *Water Resources Research*, 52(2):1286–1305, feb 2016.

[64] Barret L Kurylyk, Masaki Hayashi, William L Quinton, Jeffrey M McKenzie, and Clifford I Voss. Influence of vertical and lateral heat transfer on permafrost thaw, peatland landscape transition, and groundwater flow. *Water Resources Research*, 52(2):1286–1305, 2016.

[65] Naresh KG Lakku and Manasa R Behera. Skill and inter-model comparison of regional and global climate models in simulating wind speed over south asian domain. *Climate*, 10(6):85, 2022.

[66] NASA Landsat. Science data users handbook. *Availabe online http//landsathandbook. gsfc. nasa. gov/inst_cal/prog_sect8_2. html (7)(accessed 11 March 2011), 7AD*, 7.

[67] Trevor C. Lantz and Steven V. Kokelj. Increasing rates of retrogressive thaw slump activity in the Mackenzie Delta region, N.W.T., Canada. *Geophysical Research Letters*, 35(6), mar 2008.

[68] Angus Lang Sun Lee, Curtis Chun Kit To, Alfred Lok Hang Lee, Joshua Jing Xi Li, and Ronald Cheong Kin Chan. Model architecture and tile size selection for convolutional neural network training for non-small cell lung cancer detection on whole slide images. *Informatics in Medicine Unlocked*, 28:100850, jan 2022.

[69] Sahel Mahdavi, Bahram Salehi, Meisam Amani, Jean Elizabeth Granger, Brian Brisco, Weimin Huang, and Alan Hanson. Object-based classification of wetlands in Newfoundland and labrador using multi-temporal PolSAR data. *https://doi.org/10.1080/07038992.2017.1342206*, 43(5):432–450, sep 2017.

[70] Masoud Mahdianpari, Brian Brisco, Jean Granger, Fariba Mohammadimanesh, Bahram Salehi, Saeid Homayouni, and Laura Bourgeau-Chavez. The third generation of pan-canadian wetland map at 10 m resolution using multisource earth observation data on cloud computing platform. *IEEE Journal of Selected Topics in Applied Earth Observations and Remote Sensing*, 14:8789–8803, 2021.

[71] Masoud Mahdianpari, Brian Brisco, Jean Elizabeth Granger, Fariba Mohammadimanesh, Bahram Salehi, Sarah Banks, Saeid Homayouni, Laura Bourgeau-Chavez, and Qihao Weng. The second generation Canadian wetland inventory map at 10 meters resolution using Google Earth Engine. *https://doi.org/10.1080/07038992.2020.1802584*, 46(3):360–375, may 2020.

[72] Masoud Mahdianpari, Bahram Salehi, Fariba Mohammadimanesh, Brian Brisco, Saeid Homayouni, Eric Gill, Evan R. DeLancey, and Laura Bourgeau-Chavez. Big Data for a Big Country: The first generation of Canadian wetland inventory map at a spatial resolution of 10-m using Sentinel-1 and Sentinel-2 data on the Google Earth Engine cloud computing platform. *https://doi.org/10.1080/07038992.2019.1711366*, 46(1):15–33, jan 2020.

[73] Javed Mallick, Vijay P. Singh, Mohammed K. Almesfer, Swapan Talukdar, Majed Alsubhi, Mohd Ahmed, and Roohul Abad Khan. Spatio-temporal analysis and simulation of land cover changes and their impacts on land surface temperature in urban agglomeration of Bisha Watershed, Saudi Arabia. *https://doi.org/10.1080/10106049.2021.1980616*, 2021.

[74] L. Shawn Matott. OSTRICH: an optimization software tool, documentation and user's guide, version 17.12.19. 79 pages, University at Buffalo Center for Computational Research, 2017.

[75] Lysha M Matsunobu, Hugo TC Pedro, and Carlos FM Coimbra. Cloud detection using convolutional neural networks on remote sensing images. *Solar Energy*, 230:1020–1032, 2021.

[76] Aaron E. Maxwell, Timothy A. Warner, and Luis Andrés Guillén. Accuracy assessment in convolutional neural network-based deep learning remote sensing studies—part 2: Recommendations and best practices. *Remote Sensing 2021, Vol. 13, Page 2591*, 13(13):2591, jul 2021.

[77] Chris McColl and Graeme Aggett. Land-use forecasting and hydrologic model integration for improved land-use decision support. *Journal of Environmental Management*, 84(4):494–512, sep 2007.

[78] Jeffrey M McKenzie, Clifford I Voss, and Donald I Siegel. Groundwater flow with energy transport and water-ice phase change: Numerical simulations, benchmarks, and application to freezing in peat bogs. *Advances in Water Resources*, 30(4):966–983, 2007.

[79] Sarah K McMenamin, Elizabeth A Hadly, and Christopher K Wright. Climatic change and wetland desiccation cause amphibian decline in Yellowstone National Park. *Proceedings of the National Academy of Sciences of the United States of America*, 105(44):16988–16993, 2008.

[80] Michael A Merchant. Classifying open water features using optical satellite imagery and an object-oriented convolutional neural network. *Remote Sensing Letters*, 11(12):1127–1136, 2020.

[81] Hanna Meyer, Christoph Reudenbach, Stephan Wöllauer, and Thomas Nauss. Importance of spatial predictor variable selection in machine learning applications–moving from data reproduction to spatial prediction. *Ecological Modelling*, 411:108815, 2019.

[82] Koreen Millard and Murray Richardson. On the importance of training data sample selection in random forest image classification: A case study in peatland ecosystem mapping. *Remote Sensing 2015, Vol. 7, Pages 8489-8515*, 7(7):8489–8515, jul 2015.

[83] Shervin Minaee, Yuri Y Boykov, Fatih Porikli, Antonio J Plaza, Nasser Kehtarnavaz, and Demetri Terzopoulos. Image segmentation using deep learning: A survey. *IEEE transactions on pattern analysis and machine intelligence*, 2021.

[84] Fariba Mohammadimanesh, Bahram Salehi, Masoud Mahdianpari, and Mahdi Motagh. A new hierarchical object-based classification algorithm for wetland mapping in Newfoundland, Canada. *International Geoscience and Remote Sensing Symposium (IGARSS)*, 2018-July:9233–9236, oct 2018.

[85] Joshua Montgomery, Brian Brisco, Laura Chasmer, Kevin Devito, Danielle Cobbaert, and Chris Hopkinson. SAR and Lidar temporal data fusion approaches to boreal wetland ecosystem monitoring. *Remote Sensing 2019, Vol. 11, Page 161*, 11(2):161, jan 2019.

[86] Daniel N Moriasi, Jeffrey G Arnold, Michael W Van Liew, Ronald L Bingner, R Daren Harmel, and Tamie L Veith. Model evaluation guidelines for systematic quantification of accuracy in watershed simulations. *Transactions of the ASABE*, 50(3):885–900, 2007.

[87] Leah M. Mungai, Joseph P. Messina, Leo C. Zulu, Jiaguo Qi, and Sieglinde Snapp. Modeling spatiotemporal patterns of land use/land cover change in central Malawi using a neural network model. *Remote Sensing 2022, Vol. 14, Page 3477*, 14(14):3477, jul 2022.

[88] Talat Munshi, Mark Zuidgeest, Mark Brussel, and Martin van Maarseveen. Logistic regression and cellular automata-based modelling of retail, commercial and residential development in the city of Ahmedabad, India. *Cities*, 39:68–86, 2014.

[89] Ahmed Mustafa, Andreas Rienow, Ismaïl Saadi, Mario Cools, and Jacques Teller. Comparing support vector machines with logistic regression for calibrating cellular automata land use change models. *European Journal of Remote Sensing*, 51(1):391–401, 2018.

[90] Mahmoud K Okasha, Haroun M Bhar, and Mohammed A M Shehada. Related papers modeling violence against women in Palestinian society. *International Journal of Advanced Research*, 49(2):560–573, 2016.

[91] Stacy L. Ozesmi and Marvin E. Bauer. Satellite remote sensing of wetlands. *Wetlands Ecology and Management*, 10(5):381–402, oct 2002.

[92] Pacific Climate Impacts Consortium. Canadian downscaled climate scenarios - univariate (CMIP5). Retrieved from https://data.pacificclimate.org/portal/downscaled_gcms/map/, accessed 2022-12-01, 2022.

[93] Scott L. Painter, David Moulton, and Cathy J. Wilson. Modeling challenges for predicting hydrologic response to degrading permafrost. *Hydrogeology Journal*, 21:221–224, 2013.

[94] Serge Payette, Ann Delwaide, Marco Caccianiga, and Michel Beauchemin. Accelerated thawing of subarctic peatland permafrost over the last 50 years. *Geophysical Research Letters*, 31(18):1–4, 2004.

[95] Bryan C Pijanowski and David Hyndman. Using neural networks and GIS to forecast land use changes: A Land Transformation Model. *Computers, Environment and Urban Systems*, 26(6):553–575, 2002.

[96] Stefan. Pohl, Philip Marsh, Cuyler. Onclin, and Mark. Russell. The summer hydrology of a small upland tundra thaw lake: Implications to lake drainage. In *Hydrological Processes*, number 17, pages 2536–2546, aug 2009.

[97] Vasilis Pollatos, Loukas Kouvaras, and Eleni Charou. Land cover semantic segmentation using resunet. *arXiv preprint arXiv:2010.06285*, 2020.

[98] John W. Pomeroy, Donald M. Gray, Tim Brown, Nick R. Hedstrom, William Quinton, Richard J. Granger, and Sean K. Carey. The cold regions hydrological model: a platform for basing process representation and model structure on physical evidence. *Hydrological Processes: An International Journal*, 21(19):2650–2667, 2007.

[99] Darren Pouliot, Rasim Latifovic, Jon Pasher, Jason Duffe, Jon Pasher@canada, (J P Ca, Jason Duffe@canada, and (J D Ca. Assessment of convolution neural networks for wetland mapping with Landsat in the central Canadian boreal forest region. *Remote Sensing 2019, Vol. 11, Page 772*, 11(7):772, mar 2019.

[100] Biswajeet Pradhan. A comparative study on the predictive ability of the decision tree, support vector machine and neuro-fuzzy models in landslide susceptibility mapping using GIS. *Computers and Geosciences*, 51:350–365, 2013.

[101] Alden M Provost and Clifford I Voss. Sutra, a model for saturated-unsaturated, variable-density groundwater flow with solute or energy transport—documentation of generalized boundary conditions, a modified implementation of specified pressures and concentrations or temperatures, and the lake capability. Technical report, US Geological Survey, 2019.

[102] William Quinton, Justin R. Adams, Jennifer L. Baltzer, Aaron A. Berg, James R. Craig, and E. A. Johnson. Consortium for Permafrost Ecosystems in Transition: traversing the southern margin of discontinuous permafrost with hydrological, ecological and remote sensing research, northeastern British Columbia and southwestern Northwest Territories. *Geoscience BC*, 1:79–86, 2017.

[103] William Quinton, Aaron Berg, Michael Braverman, Olivia Carpino, Laura Chasmer, Ryan Connon, James R. Craig, Elise Devoie, Masaki Hayashi, Kristine Haynes, David Olefeldt, Alain Pietroniro, Fereidoun Rezanezhad, Robert Schincariol, and Oliver Sonnentag. A synthesis of three decades of hydrological research at Scotty Creek, NWT, Canada. *Hydrology and Earth System Sciences*, 23(4):2015–2039, apr 2019.

[104] William Quinton, Masaki Hayashi, and Laura Chasmer. Peatland hydrology of discontinuous permafrost in the northwest territories: overview and synthesis. *Canadian Water Resources Journal*, 34(4):311–328, 2009.

[105] William Quinton, Masaki Hayashi, and Laura Chasmer. Permafrost-thaw-induced land-cover change in the Canadian subarctic: Implications for water resources. *Hydrological Processes*, 25(1):152–158, 2011.

[106] William Quinton, Masaki Hayashi, and Alain Pietroniro. Connectivity and storage functions of channel fens and flat bogs in northern basins. *Hydrological Processes*, 17(18):3665–3684, 2003.

[107] Mohammad Rezaee, Masoud Mahdianpari, Yun Zhang, and Bahram Salehi. Deep convolutional neural network for complex wetland classification using optical remote

sensing imagery. *IEEE Journal of Selected Topics in Applied Earth Observations and Remote Sensing*, 11(9):3030–3039, sep 2018.

[108] Daniel Riseborough, Nikolay Shiklomanov, Bernd Etzelmüller, Stephan Gruber, and Sergei Marchenko. Recent advances in permafrost modelling. *Permafrost and Periglacial Processes*, 19(2):137–156, 2008.

[109] Olaf Ronneberger, Philipp Fischer, and Thomas Brox. U-net: Convolutional networks for biomedical image segmentation. In *Medical image computing and computer-assisted intervention–MICCAI 2015: 18th International Conference, Munich, Germany, October 5-9, 2015, Proceedings, Part III 18*, pages 234–241. Springer, 2015.

[110] Majid Shadman Roodposhti, Jagannath Aryal, and Brett A Bryan. A novel algorithm for calculating transition potential in cellular automata models of land-use/cover change. *Environmental Modelling and Software*, 2019.

[111] Edward A G Schuur, James R. Bockheim, Josep G Canadell, Eugenie Euskirchen, Christopher B Field, Sergey V Goryachkin, Stefan Hagemann, Peter Kuhry, Peter M Lafleur, Hanna Lee, Galina Mazhitova, Frederick E Nelson, Annette Rinke, Vladimir E Romanovsky, Nikolay Shiklomanov, Charles Tarnocai, Sergey Venevsky, Jason G Vogel, and Sergei A Zimov. Vulnerability of Permafrost Carbon to Climate Change: Implications for the Global Carbon Cycle. *BioScience*, 58(8):701–714, 2008.

[112] Michal Segal-Rozenhaimer, Alan Li, Kamalika Das, and Ved Chirayath. Cloud detection algorithm for multi-modal satellite imagery using convolutional neural-networks (cnn). *Remote Sensing of Environment*, 237:111446, 2020.

[113] Leonardo Pereira e. Silva, Ana Paula Campos Xavier, Richarde Marques da Silva, and Celso Augusto Guimarães Santos. Modeling land cover change based on an artificial neural network for a semiarid river basin in northeastern Brazil. *Global Ecology and Conservation*, 21:e00811, mar 2020.

[114] Sharon L Smith, Margo M Burgess, Dan Riseborough, and F Mark Nixon. Recent trends from canadian permafrost thermal monitoring network sites. *Permafrost and periglacial processes*, 16(1):19–30, 2005.

[115] Tricia. Stadnyk, Natalie A. St. Amour, Nicholas. Kouwen, Thomas. W.D. Edwards, Alain Pietroniro, and John. J. Gibson. A groundwater separation study in boreal wetland terrain: the WATFLOOD hydrological model compared with stable isotope tracers. *http://dx.doi.org/10.1080/10256010500053730*, 41(1):49–68, mar 2007.

[116] Lindsay Elena Stone. The role of channel fens in permafrost degradation induced changes in peatland discharge at scotty creek, nt. 2018.

[117] Dmitry Streletskiy, Nikolay Shiklomanov, and Frederick Nelson. Permafrost, infrastructure, and climate change: A gis-based landscape approach to geotechnical modeling. *Arctic, Antarctic, and Alpine Research*, 44(3):368–380, 2012.

[118] Bo Sun and Derek T Robinson. Comparison of statistical approaches for modelling land-use change. *Land*, 7(4), 2018.

[119] Mahkameh Taheri. *Upscaling Fill-and-Spill Hydrologic Processes*. University of Waterloo, 2023.

[120] Mahkameh Taheri, Mark Ranjram, and James R. Craig. An upscaled model of fill-and-spill hydrological response. *Under review in Water Resources Research*, 2023.

[121] Karl E Taylor, Ronald J Stouffer, and Gerald A Meehl. An overview of cmip5 and the experiment design. *Bulletin of the American meteorological Society*, 93(4):485–498, 2012.

[122] Amir Hossein Tayyebi, Amin Tayyebi, and Nitin Khanna. Assessing uncertainty dimensions in land-use change models: using swap and multiplicative error models for injecting attribute and positional errors in spatial data. *International Journal of Remote Sensing*, 35(1):149–170, 2013.

[123] Bryan A Tolson and Christine A Shoemaker. Dynamically dimensioned search algorithm for computationally efficient watershed model calibration. *Water Resources Research*, 43(1), 2007.

[124] Priit Ulmas and Innar Liiv. Segmentation of satellite imagery using U-Net models for land cover classification. *arXiv preprint arXiv:2003.02899*, 2020.

[125] Diego Valbuena, Peter H Verburg, Arnold K Bregt, and Arend Ligtenberg. An agent-based approach to model land-use change at a regional scale. *Landscape Ecology*, 25(2):185–199, 2010.

[126] Nathan D. Van Schmidt, Tamara S. Wilson, and Ruth Langridge. Linkages between land-use change and groundwater management foster long-term resilience of water supply in California. *Journal of Hydrology: Regional Studies*, 40:101056, apr 2022.

[127] Detlef P Van Vuuren, Jae Edmonds, Mikiko Kainuma, Keywan Riahi, Allison Thomson, Kathy Hibbard, George C Hurtt, Tom Kram, Volker Krey, Jean-Francois Lamarque, et al. The representative concentration pathways: an overview. *Climatic change*, 109:5–31, 2011.

[128] Warwick F Vincent, Mickaël Lemay, and Michel Allard. Arctic permafrost landscapes in transition: towards an integrated Earth system approach. *Arctic Science*, 3(2):39–64, 2017.

[129] Dale H. Vitt, Linda A. Halsey, and Susan C. Zoltai. The bog landforms of continental western Canada in relation to climate and permafrost patterns. *Arctic & Alpine Research*, 26(1):1–13, 1994.

[130] Michelle A Walvoord and Barret L Kurylyk. Hydrologic impacts of thawing permafrost—a review. *Vadose Zone Journal*, 15(6), 2016.

[131] Lei Wang, Yao Lu, and Yunlong Yao. Comparison of three algorithms for the retrieval of land surface temperature from landsat 8 images. *Sensors (Switzerland)*, 19(22), 2019.

[132] Li Wen and Michael Hughes. Coastal wetland mapping using ensemble learning algorithms: A comparative study of bagging, boosting and stacking techniques. *Remote Sensing*, 12(10):1683, 2020.

[133] Ming Ko Woo. *Permafrost hydrology*, volume 9783642234. Springer, 2012.

[134] WSC. Hydrometric data for Mackenzie river at Fort Simpson. Retrieved from https://wateroffice.ec.gc.ca/report/real_time_e.html?stn=10GC001, accessed 2020-10-10, 2020.

[135] Xiaoling Xia, Qinyang Lu, and Xin Gu. Exploring an easy way for imbalanced data sets in semantic image segmentation. page 22003, 2019.

[136] Zhiyong Xu, Weicun Zhang, Tianxiang Zhang, and Jiangyun Li. HRCNet: High-resolution context extraction network for semantic segmentation of remote sensing images. *Remote Sensing 2021, Vol. 13, Page 71*, 13(1):71, dec 2020.

[137] Xiaohui Yuan, Jianfang Shi, and Lichuan Gu. A review of deep learning methods for semantic segmentation of remote sensing imagery. *Expert Systems with Applications*, 169:114417, 2021.

[138] Marvin Zelen. Multinomial response models. *Computational statistics & data analysis*, 12(2):249–254, 1991.

[139] Tingjun Zhang, Roger G Barry, K Knowles, JA Heginbottom, and J Brown. Statistics and characteristics of permafrost and ground-ice distribution in the northern hemisphere. *Polar Geography*, 23(2):132–154, 1999.

[140] Weixing Zhang, Chandi Witharana, Anna K. Liljedahl, and Mikhail Kanevskiy. Deep convolutional neural networks for automated characterization of arctic ice-wedge polygons in very high spatial resolution aerial imagery. *Remote Sensing*, 10(9):1487, sep 2018.

[141] Yingtong Zhang, Curtis E. Woodcock, Shijuan Chen, Jonathan A. Wang, Damien Sulla-Menashe, Zhenpeng Zuo, Pontus Olofsson, Yetianjian Wang, and Mark A. Friedl. Mapping causal agents of disturbance in boreal and arctic ecosystems of North America using time series of Landsat data. *Remote Sensing of Environment*, 272:112935, apr 2022.

[142] Yu Zhang, Rudy Slingerland, and Christopher Duffy. Fully-coupled hydrologic processes for modeling landscape evolution. *Environmental Modelling & Software*, 82:89–107, aug 2016.

[143] Zhong Qiu Zhao, Peng Zheng, Shou Tao Xu, and Xindong Wu. Object detection with deep learning: A review. *IEEE Transactions on Neural Networks and Learning Systems*, 30(11):3212–3232, nov 2019.

APPENDICES

Appendix A

Repositories of data and Code

A.1 Data

The remote sensing data used in this work which helped in achieving the goals of this research is available in the Scotty Creek Data Archive. This archive is hosted at Wilfrid Laurier University and can be requested by contacting Dr. William Quinton (wquinton@wlu.ca) who heads this research station.

A.2 Model

The TSLCM code model discussed in Chapter 3 is available here:

Transition-of-Landcovers-SCRS.